STUDIA
UNIVERSITATIS BABEȘ-BOLYAI

PHYSICA

1
1979

CLUJ-NAPOCA

STUDIA
UNIVERSITATIS BABEȘ-BOLYAI

PHYSICA

1

SUMAR — CONTENTS — SOMMAIRE

2

RESISTIVE ANOMALIES AT MAGNETIC CRITICAL POINTS. EFFECT OF NAMBU-GOLDSTONE MODES ON THE LONGITUDINAL CORRELATION FUNCTIONS

D. DĂDÂRLAT, AL. ANGHEL

1. Introduction. At the second-order phase transition point of a magnetic system, various transport coefficients such as the electrical and thermal conductivity have a singular behaviour and anomalies. This is the result of the so-called critical scattering of the charge and thermal carriers on the fluctuations of the order parameter.

Much theoretical effort has been devoted to understand the origins of these singularities and many theoretical methods have been developed accordingly. For a review of the experimental and theoretical situation as of 1971, the reader is to refer to P a r k s [1]. Some more recent references may be found in A l e x a n d e r et al. [2].

There are two ways of approaching the critical region i.e. $T > T_c$ and $T < T_c$ and the theoretical works are to include this appropriately.

In a theory developed for $T < T_c$ one must take into account the breaking-of-symmetry effect. Indeed, the phase transition is always accompanied by a breaking of a continuous or discret symmetry. The system's reaction to this mechanism is expressed via Nambu — Goldstone modes, which act as symmetry restoring forces.

In this paper we are going to study the critical behaviour of the magnetic part of the electrical resistivity for $T < T_c$, taking into account the effect of Nambu-Goldstone modes on the correlation function. We limit our analysis to the case of a ferromagnetic system. The effect of Nambu-Goldstone modes on the transverse and longitudinal (to the direction of ordering) correlation functions have been extensively studied [3] taking into account the couplings between the longitudinal and Nambu-Goldstone modes. Although this effect is not really a critical phenomenon, as was suggested by M a z e n k o [4], we expect it to produce a strong enhancement of the magnetic part of the electrical resistivity.

The second section of the paper is devoted to the calculation of the magnetic part of the electrical resistivity. In the third section, the influence of the Nambu-Goldstone modes on the correlation function is considered. At the end of the paper we present some discussions and conclusions.

2. The electrical resistivity near the critical point. Following de G e n n e s and F r i e d e l [5] we assume a contact interaction between the charge carriers and the magnetic moment $\vec{S}$ which contribute to the magnetic ordering

$$H_{e-s} = - \int d^3rg \sum_{lk} \delta(\vec{r} - \vec{R}(lk)) \, \vec{S}(lk)) \, \Psi_s^+(\vec{r}) \, \vec{\sigma}_{ss'} \Psi_{s'}(\vec{r}) \tag{2.1}$$

where g is a coupling constant and 1k — labels the unit cells and the sublatices of the system.

Following B i n d e r et al. [6] we express the differential cross-section as:

$$\frac{d\sigma}{d\Omega} = \left(\frac{m}{2\pi\hbar^2}\right)^2 g^2 \sum_{lk} [\langle \vec{S}(0,0)\, \vec{S}(lk)\rangle - \langle \vec{S}(0,0)\rangle\langle \vec{S}(lk)\rangle]\, e^{i\vec{q}\cdot\vec{R}(lk)} \tag{2.2}$$

From eq. (2.2) we calculate the magnetic part of the alectrical resistivity [4], [7] as:

$$\rho_{crit}^m \sim n_{eff}^{-1} \int d^d q \cdot q [\langle \vec{S}(\vec{q})\, \vec{S}(-\vec{q})\rangle - M^2 \delta(\vec{q} - \vec{q}_0)] \tag{2.3}$$

where d is the dimension of the space. When $T < T_c$, M — the magnetization, is non-zero.

3. **Influence of Nambu-Goldstone modes on the correlation function.** The magnetic part of the electrical resistivity, in the critical region, below T_c, is determined by the correlation function

$$\chi(q) = \langle \vec{S}(\vec{q}) \cdot \vec{S}(-\vec{q})\rangle \tag{3.1}$$

which may be split into transversal and longitudinal modes

$$\chi(q) = (N - 1)\, \chi_T(q) + \chi_L(q) \tag{3.2}$$

where a N-component order parameter has been considered.

To order $0(\varepsilon)$ χ_L and χ_T have been calculated by M a z e n k o [4] and their expressions are:

$$\chi_L^{-1}(q) = q^2 - \frac{9\varepsilon UM^2}{N+8}\left(1 + \frac{(x^2+4)^{\frac{1}{2}}}{x}\, ln\, \frac{1}{2}\left[(x^2+4)^{\frac{1}{2}} - x\right]\right) +$$

$$+ \lambda^2\left(\frac{UM^2}{\lambda^2}\right)^{1+\frac{\varepsilon}{2}} \frac{N+8+\frac{1}{2}(10-N)\,\varepsilon}{9+(N-1)x^{-\varepsilon}} \tag{3.3}$$

and

$$\chi_T^{-1}(q) \sim q^2 \tag{3.4}$$

with $\varepsilon = 4 - d$ and

$$U = \frac{2\varepsilon}{(N+8)K_4} + 0(\varepsilon^2) \tag{3.5 a}$$

$$x^2 = \frac{q^2}{UM^2} \tag{3.5 b}$$

$$\xi^{-2} = \lambda^2\left(\frac{UM^2}{\lambda^2}\right)^{1+\frac{\varepsilon}{2}} \tag{3.5 c}$$

The parameter λ is the usual cutoff. It will appear in our final result as a non-universl parameter.

We have chosen two ways of approaching the critical region i.e. $x \ll 1$ and $x \gg 1$. The first *asymptotic* limit gives

$$\chi(q) \sim x^{-2} + ax^{-\epsilon} \qquad x \ll 1 \tag{3.6}$$

with

$$a = \frac{1}{N + 8}\left(1 + \frac{2N - 19}{4(N + 8)}\epsilon\right) \tag{3.7}$$

and the second one

$$\chi(q) = Nq^2 + \frac{9\epsilon UM^2}{q^4(N + 8)}\left[\frac{1}{x} - \frac{1}{x^2} + \frac{2}{x^3}\right] -$$

$$- \lambda^2\left(\frac{UM^2}{\lambda^2}\right)^{1 + \frac{\epsilon}{2}}\frac{1}{q^4}\left[\frac{N + 8 + \frac{1}{2}(10 - N)\epsilon}{9}\right] \qquad x \gg 1 \tag{3.8}$$

From eq. (3.6) and (3.8) we get:

$$\rho_{crit}^m \sim n_{eff}^{-1} M^{\frac{3}{2}}\left[1 + C(\lambda)\, M^{\frac{3}{2}}\right] \tag{3.9}$$

in the asymptotic limit $x \ll 1$ and

$$\rho_{crit}^m \sim n_{eff}^{-1} M^3 \tag{3.10}$$

for $x \gg 1$, where $C(\lambda)$ is a constant depending on the ultraviolet cutoff.

Using the well-known behaviour of M as a function of $T - T_c$, in the critical region

$$M \sim \left(\frac{T - T_c}{T_c}\right)^\beta \tag{3.11}$$

the eq. (3.9) and (3.10) become:

$$\rho_{crit}^m \sim n_{eff}^{-1}\left(\frac{T - T_c}{T_c}\right)^{\frac{3\beta}{2}}\left[1 + C(\lambda)\left(\frac{T - T_c}{T_c}\right)^{\frac{3\beta}{2}}\right] \qquad x \ll 1 \tag{3.12}$$

and

$$\rho_{crit}^m \sim n_{eff}^{-1}\left(\frac{T - T_c}{T_c}\right)^{3\beta} \qquad x \gg 1 \tag{3.13}$$

4. **Discussions and conclusions.** We have obtained scaling laws for the magnetic part of the electrical resistivity in the critical region, below T_c. For a regular behaviour of n_{eff}, the critical exponents determined are $3\beta/2$ for $x \ll 1$ and 3β for $x \gg 1$. If the critical behaviour of the effective number of charge carriers is expressed as

$$n_{eff}^{-1} \sim \left(\frac{T - T_c}{T_c}\right)^\omega \tag{4.1}$$

then the corresponding critical exponents would be corrected to : $3\beta/2 + \omega$ and $3\beta + \omega$ and $3\beta + \omega$. The calculation of the new critical exponent ω will be presented in a following paper. In the present analysis we have neglected tacitly the possible cross-over behaviour from Wilson to Gaussian fixed point.

REFERENCES

1. L. D. P a r k s, *Proceedings of the Twelfth International Conference on Low Temperature Physics*, edited by E. Kanda, Keigaku, Tokyo, p. 217, 1971.
2. S. A l e x a n d e r, J. S. H e l m a n, I. B a l b e r g, Phys. Rev., **B 13**, 304(1976).
3. D. F o r s t e r, *Hydrodynamic Fluctuations, Broken Symmetry and Correlation Functions*, Benjamin, New York, 1975.
4. G. F. M a z e n k o, Phys. Rev. **B. 14**, 3933 (1976).
5. P. G. G e n n e s and J. F r i e d e l, J. Phys. Chem. Solids, **4**, 71 (1958).
6. K. B i n d e r, G. M e i s s n e r, H. M a i s, Phys. Rev., **B 13**, 4890 (1976).
7. Y. S u e z a k i, H. M o r i, Prog. Theor. Phys., **41**, 1117 (1969).

ANOMALIA REZISTENŢEI ELECTRICE ÎN APROPIEREA TEMPERATURII CRITICE. EFECTUL MODURILOR NAMBU-GOLDSTONE ASUPRA FUNCŢIILOR DE CORELARE LONGITUDINALE

(R e z u m a t)

Se studiază anomalia rezistenţei electrice în regiunea critică $(T < T_c)$ pentru substanţe feromagnetice, luîndu-se în considerare efectul modurilor Nambu-Goldstone asupra funcţiei de corelare. Se găsesc legi de scaling pentru comportarea critică a rezistenţei electrice, în cele două limite $q \xi \ll 1$ şi $q \xi \gg 1$.

SOLITON'S WIDTH DEPENDENCE ON THE IONIC TEMPERATURE

MARIA CRISTEA

In a previous paper [1] we have investigated the effect of ionic temperature on the amplitude of solitons in a two ion species plasma with finite ion temperature.

In the present paper we shall examine the variation of soliton's width with the temperature of light ions, assuming unequal ion temperatures.

For a plasma consisting of hot isothermal electrons and two ion species with unequal temperatures, using a reductive perturbation method [2] — [4], the following Korteweg — de Vries equation can be derived

$$\frac{\partial n_e^{(1)}}{\partial \tau} + S n_e^{(1)} \frac{\partial n_e^{(1)}}{\partial \xi} + R \frac{\partial^3 n_e^{(1)}}{\partial \xi^3} = 0, \tag{1}$$

where $n_e^{(1)}$ is the dimensionless perturbation of electron density, and the stretched variables ξ and τ are connected with the spatial and temporal dimensionless coordinates x and t by the relations

$$\xi = \varepsilon^{1/2}(x - \lambda t), \quad \tau = \varepsilon^{3/2} t \quad (0 < \varepsilon \ll 1).$$

λ is the phase velocity of the ion acoustic wave and has the value

$$\lambda^2 = \frac{1}{2(1 - \alpha + \mu\alpha)} \Big\{ [1 - \alpha + \sigma_2) + \mu(\alpha + \sigma_1)] \pm$$

$$\pm \sqrt{[(1 - \alpha + \sigma_2) - \mu(\alpha + \sigma_1)]^2 + 4\mu\alpha(1 - \alpha)} \Big\} \tag{2}$$

where $\alpha = n_1/(n_1 + n_2)$ is the concentration of light ions, $\mu = m_2/m_1$ is the mass ratio, and the quantities σ_1 and σ_2 are given by

$$\sigma_1 = \gamma_1 T_1/T_e, \quad \sigma_2 = \gamma_2 T_2/T_e \tag{3}$$

T_1, T_2 and T_e being the temperatures of light ions, heavy ions and electrons respectively. The constants γ_1 and γ_2 have the values 3 or 1, depending on the equations of state: $\gamma = 3$ if the ion fluid is governed by an adiabatic equation of state and $\gamma = 1$ in the case of isothermal ions.

We consider the particular case $\lambda = 1$ (velocities being normalized to the ion sound speed $c_s = \lambda_D \omega_p$, where λ_D is the electron Debye length and ω_p the ion plasma frequency). In this case it follows that the temperature of light and heavy ions are not independent. Taking $\lambda = 1$ in (2), one obtains

$$\sigma_2 = \frac{\mu^2 \alpha \sigma_1}{\mu \sigma_1 - 1 + \alpha}. \tag{4}$$

Then, the quantities S and R from (1) have the following expressions

$$S = \frac{\alpha(1 - \alpha)(A - \sigma_1)(A - 1 - \sigma_1)^2 + 2A[\alpha(1 - \alpha)^2 + \mu(A - \alpha - \sigma_1)^3]}{2A(1 - \alpha)(A - \sigma_1)[\alpha(1 - \alpha) + \mu(A - \alpha - \sigma_1)^2]} \tag{5}$$

$$R = \frac{(1 - \alpha)(A - \sigma_1)^2}{2A[\alpha(1 - \alpha) + \mu(A - \alpha - \sigma_1)^3]} \tag{6}$$

with $A = (1 - \alpha + \mu\alpha)/\mu$.

Imposing appropriate boundary conditions, we can get the usual solitary-wave solution of equation (1), in a frame moving with the velocity $M = 1 + \varepsilon U$:

$$n_e^{(1)} = \frac{3U}{S} \operatorname{sech}^2\left\{\sqrt{\frac{U}{2R}} [\xi - \xi_0 - U(\tau - \tau_0)]\right\}. \tag{7}$$

For a prescribed velocity U, the soliton's amplitude is proportional to S^{-1}, while the soliton's width is proportional to $\sqrt{2R}$. As it can be seen from (5) and (6), both amplitude and width depend on α, μ and σ_1. We are interested in their dependence on σ_1. The variation of S^{-1} with temperature has been analysed in [1] where we have imposed the much more restrictive condition $\sigma_1 = \sigma_2$. Now we examine the dependence of $\sqrt{2R}$ on the temperature of light ions. Figures 1 and 2 represent $\sqrt{2R}$ as a function of σ_1 for two values of the mass ratio: $\mu = 10$ and $\mu = 40$, and for various values of light ion concentration α.

It can be shown that if $\sigma_1 < A$ the light ions follow an adiabatic equation of state, and if $\sigma_1 > A$, they are isothermal. These temperature ranges are separated by a narrow domain with $\sigma_1 \simeq A$, where the thermal velocity of light ions is almost equal to the phase velocity of the wave. For $\sigma_1 = A$ the quantity R vanishes as it follows from (6). Thus, in figs. 1 and 2 the points $\sqrt{2R} = 0$ separate each curve into two branches. The branch situated on the left corresponds to ions described by an adiabatic equation of state, while the branch situated on the right corresponds to isothermal light ions. The behaviour of the soliton's width is quite different for the two cases.
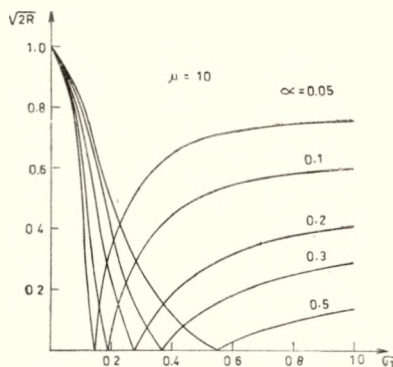
F i g. 1.
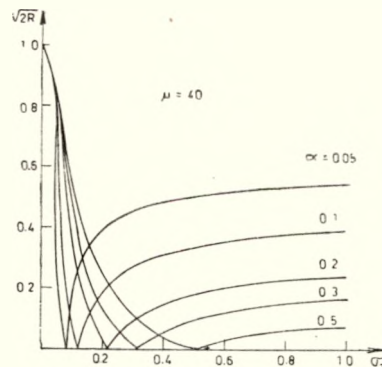
F i g. 2.

In the first case $(\sigma_1 > A)$, all curves start from the point $\sqrt{2R} = 1$. This point corresponds to a cold ion plasma $(\sigma_1 = \sigma_2 = 0)$. It is well-known [2] that for a two ion species plasma with cold ions, the soliton's width does not depend on α and μ, having a constant value $(R = 1/2)$. As the temperature increases, the quantity R decreases, tending to zero. For a given temperature, R increases with increasing light ion concentration α.

In the second case $(\sigma_1 > A)$, the quantity R increases from zero to an almost constant value, as the temperature increases. For all concentrations, these constant values of $\sqrt{2R}$ are smaller than the value corresponding to the case of cold ions. For a prescribed value of the light ion temperature, the width of soliton decreases as the concentration α increases.

In conclusion, in a plasma with two ion species with unequal temperatures related by (4), the soliton's width is strongly affected by the ionic temperature. The soliton's width reaches its maximum value in the case of a cold ion plasma, and it vanishes when the thermal velocity of light ions becomes equal to the linear phase velocity of the ion acoustic wave.

REFERENCES

1. M. C r i s t e a, Studia Univ. Babeş-Bolyai, Phys., 1, 35 (1978).
2. M. Q. T r a n, P. J. H i r t, Plasma Phys., **16,** 617 (1974).
3. M. Q. T r a n, Plasma Phys., **16,** 1167 (1974).
4. M. W a s h i m i, T. T a n i u t i, Phys. Rev. Lett., **17,** 996 (1966).

DEPENDENȚA LĂRGIMII SOLITONULUI DE TEMPERATURA IONILOR

(R e z u m a t)

Se examinează dependența de temperatură a lărgimii solitonilor iono-acustici, într-o plasmă cu două specii de ioni, cu temperaturi diferite. Se arată că lărgimea solitonului are valoarea maximă în cazul unei plasme cu ioni reci și se anulează cind viteza termică a ionilor ușori devine egală cu viteza liniară de fază a undei iono-acustice.

ANIZOTROPIA CONDUCȚIEI TERMICE ÎN CAZUL
MONOCRISTALULUI BaO.6(Fe₂O₃)

A. NÉDA

Ferita de bariu, datorită posibilităților largi de aplicare, din punct de vedere al proprietăților magnetice a fost mult studiată. M. R o s e n b e r g și colab. [1] au studiat structura domeniilor de magnetizare spontană, stabilind că magnetizarea acestora este orientată după axa hexagonală. Anizotropia magnetică a fost studiată de C. T ă n ă s o i u [2], stabilind totodată și valoarea temperaturii Curie, 730 K. Măsurătorile lui K. Z a v e t a [3], efectuate în cazul unei probe monocristaline, au arătat că conductibilitatea electrică prezintă o puternică anizotropie. Rezistivitatea măsurată în direcția axei c este aproximativ cu un ordin de mărime mai mare decît cea măsurată în planul bazal, însă în acest plan nu s-a obținut o dependență în funcție de direcție. Pe de altă parte, aceste măsurători au demonstrat că această ferită are proprietăți semiconductoare, fiind de tip n, iar conductibilitatea se datorește prezenței ionilor Fe^{2+}.

Date experimentale. Ferita studiată a fost un monocristal de compoziție stochiometrică, avînd dimensiuni : 3,12 mm (după axa c), 5,24 mm și 5,86 mm, obținută prin metoda Verneuille. Coeficientul de difuzivitate termică a fost determinată cu metoda dinamică, denumită metoda impulsului de căldură, descrisă în [4]. Măsurătorile au fost efectuate în domeniul de temperatură 100 K—850 K, după două direcții cristalografice : după axa $c(a_{||})$ și perpendicular pe această axă $(a_⊥)$, adică în planul bazal. Măsurătorile efectuate după cele două direcții din planul bazal au arătat că în limita erorilor de determinare valorile obținute se suprapun.

Datele experimentale, referitoare la variația coeficientului de difuzivitate termică în funcție de temperatură, sînt reprezentate în figura 1. Conform figurii, rezultă că mărimea studiată prezintă o anizotropie puternică, cea măsurată după o direcție din planul bazal (curba 1) fiind mai mare pe întregul interval de temperatură studiat. Anizotropia semnalată se micșorează cu creșterea temperaturii, astfel la 100 K raportul difuzivității termice $a_⊥/a_{||} = 5,1$ iar la 400 K $a_⊥/a_{||} = 2,25$. Pe lîngă anizotropia semnalată se mai constată că și caracterul de variație al difuzivității termice în funcție de temperatură este diferit. Urmărind variația acestei mărimi măsurată după axa c, se constată că ea descrește slab cu creșterea temperaturii, variație care este caracteristică substanțelor amorfe, sau a acelor substanțe cristaline la care drumul
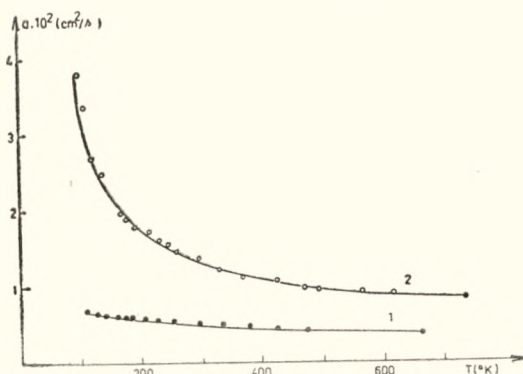
F i g. 1.

liber mijlociu al fononilor se poate considera constant.

Reprezentînd grafic coeficientul de difuzivitate termică, măsurată după o direcție din planul bazal (a⊥), în funcție de valoarea inversă a temperaturii (fig. 2), pe grafic se pot deosebi trei domenii distincte care corespund intervalelor de temperatură 100—155 K, 155—728 K și peste 728 K. Peste temperatura de 155 K mărimea studiată scade liniar cu $1/T$. Pentru a elucida natura conducției, a fost determinată la temperatura camerei conductibilitatea electrică specifică a probei după cele două direcții cristalografice ($\sigma_{\parallel} = 5{,}5 \cdot 10^{-3}\ \Omega^{-1}\cdot cm^{-1}$

F i g. 2.

și $\sigma_{\perp} = 3{,}08.10^{-2}\ \Omega^{-1}\cdot cm^{-1}$). Din aceste valori rezultă că aportul purtătorilor de sarcină la realizarea fluxului termic este neglijabil, adică în cazul de față transportul energiei termice este asigurat de către fononi. În cazul conducției pur fononice, variația liniară a coeficientului de difuzivitate termică în funcție de $1/T$ apare deasupra temperaturii Debye (θ_D), astfel pentru valoarea acestei temperaturi se poate considera 155 K.

A doua schimbare în panta variației difuzivității termice în funcție de $1/T$ apare la 728 K, valoare care este foarte apropiată de temperatura transformării de fază, de 730 K, determinat de către C. T ă n ă s o i u [2] în cazul eșantionului folosit și la măsurătorile noastre. Cauza acestei schimbări este trecerea substanței din starea magnetică ordonată în cea dezordonată. Coeficientul de difuzivitate termică, în funcție de drumul liber mijlociu al fononilor ($\bar{l}$) și viteza lor ($\bar{v}$), se poate exprima cu relația

$$a = \frac{1}{3} \cdot \bar{l} \cdot \bar{v}. \tag{1}$$

Drumul liber mijlociu al purtătorilor energiei termice este determinat de procesele trifononice — U, de împrăștierea acestora pe defectele rețelei cristaline, respectiv de interacțiunea ce apare între fononi și magnoni, conform relației

$$\bar{l}_{fm} = \bar{l}_{ofm}\left[1 - \frac{M(T)}{M(0)}\right] \tag{2}$$

dată de G. A. S l a c k [5], unde $M(T)$ și $M(0)$ reprezintă magnetizarea probei la temperatura* T, respectiv la O K, iar $\bar{l}_{ofm}$ drumul liber mijlociu determinat de interacțiunea magnon-fonon în starea paramagnetică, care poate fi considerată constantă. Din (2) rezultă că, cu cît temperatura este mai apropiată de temperatura transformării de fază, numărul magnonilor și împrăștierea fononilor pe magnoni crește și în felul acesta $\bar{l}_{fm}$, determinat numai de interacțiunea magnon-fonon scade. Astfel se poate aștepta ca în vecinătatea temperaturii Curie, în
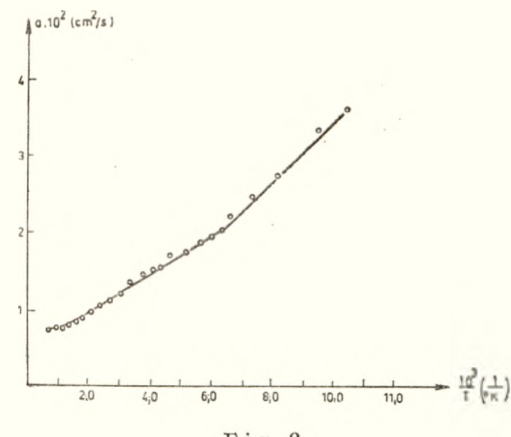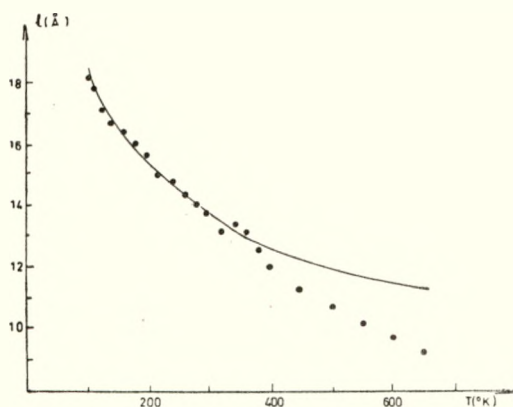
Fig. 3.

domeniul ferimagnetic, să apară o micșorare mai accentuată a difuzivității termice în funcție de temperatură, decît în starea paramagnetică.

Considerînd pentru temperatura Debye valoarea de 155 K și utilizînd pentru constantele celulei elementare valorile $c = 23,2$ Å, $a = b = 5,88$ Å [6], cu relația

$$v = \frac{k \cdot \theta_D}{\hbar} \cdot \left(\frac{V}{6\pi}\right)^{1/3}, \qquad (3)$$

în care V este volumul celulei elementare, pentru viteza sunetului se obține $v = 1,14 \cdot 10^{-3}$ m/s. În funcție de această viteză cu (1) se poate evalua drumul liber mijlociu al fononilor.

Anizotropia conducției termice se poate explica în funcție de drumul liber mijlociu. În acest scop considerăm ipoteza lui A m i r h a n o v și colab. [7]. După autorii citați rezistența termică în cazul fluxului îndreptat după o direcție din planul bazal este determinată în primul rînd de interacțiunea trifononică — U. În cazul fluxului termic avînd direcția perpendiculară pe acest plan, fononii suferă împrăștieri în urma proceselor U și pe straturile cristaline. Acest ultim tip de împrăștiere apare, deoarece legătura dintre ioni în interiorul stratului este mult mai puternică decît între straturi. Autorii citați nu au verificat această ipoteză în mod cantitativ.

Rezistența termică determinată de interacțiunea trifononică —U caracteristică conducției după o direcție din planul bazal, se poate da :

$$W_{ff} = \frac{3}{C_v \cdot \bar{l}_\perp \cdot \bar{v}} \qquad (4)$$

În cazul conducției după axa c rezistența termică se compune aditiv din cea cauzată de interacțiunea dintre fononi și împrăștierea lor pe straturile hexagonale. Ultimul proces de împrăștiere se caracterizează prin drumul liber mijlociu egal tocmai cu grosimea stratului ($\bar{l}_c = c$). Rezistența termică a probei după această direcție va fi

$$W = W_{ff} + W_{fc} = \frac{3}{c_v \cdot \bar{l}_\perp \cdot \bar{v}} + \frac{3}{c_v \cdot \bar{l}_c \cdot \bar{v}} = \frac{3}{c_v \cdot \bar{l}_\parallel \cdot \bar{v}} \qquad (5)$$

Din (5) pentru drumul liber mijlociu al fononilor în cazul conducției după axa c rezultă :

$$\bar{l}_\parallel = \frac{\bar{l}_\perp \cdot \bar{l}_c}{\bar{l}_\perp + \bar{l}_c} \qquad (6)$$

Utilizînd pentru $\bar{l}_\perp$ valoarea drumului liber mijlociu obținut din măsurători de difuzivitate termică după o direcție din planul bazal, cu relația (6) s-a calculat drumul liber mijlociu ($\bar{l}_\parallel$) pentru conducția după axa c. Această valoare teoretică s-a reprezentat cu linie continuă pe figura 3. Cu relația (1) s-a calculat același

drum liber mijlociu din datele experimentale ale coeficientului de difuzivitate termică, valori care pe figura 3 sînt reprezentate prin puncte. Concordanța dintre cele două valori este bună atît timp cît drumul liber mijlociu determinat de procesele de împrăștiere în urma proceselor trifononice — U nu devin aproximativ egale cu dimensiunea celulei elementare după direcția c. Aceasta apare aproximativ la $380-400$ K. Peste această temperatură apare o discordanță, deoarece aditivitatea rezistențelor termice nu mai este valabilă, datorită faptului că rezistențele termice cauzate de cele două tipuri de împrăștiere au valori comparabile.

Concluzii. 1. S-a constatat că conducția termică este pur fononică.

2. S-a pus în evidență anizotropia conducției, anizotropia care a fost explicată pe baza împrăștierii fononilor în urma proceselor trifononice — U și pe straturile hexagonale.

3. S-a demonstrat că variația coeficientului de difuzivitate termică în funcție de temperatură este corespunzătoare pentru studiul transformărilor de stare magnetică.

BIBLIOGRAFIE

1. M. R o s e m b e r g, C. T ă n ă s o i u. Rev. Phys. (Roum), **8**, 383 (1963).
2. C. T ă n ă s o i u, Stud. Cerc. Fiz., **23**, 1163 (1971).
3. K. Z a v e t a, Phys. Stat. Sol., **3**, 2111, (1963).
4. F. K e l e m e n și A. N é d a, Studia Univ. Babeș-Bolyai, ser. Phys., 2, 107 (1962).
5. G. A. S l a c k, Phys. Rev., **122**, 1451 (1961).
6. J. S m i t and H. P. W i j n, *Ferrites*, Netherlands, Philips Tehnical Library, 1959, p. 163.
7. H. U. A m i r h a n o v, B. G. B o g d u e v, M. A. K a j l a e v, Dokl. A.N. SSSR, **124**, 554 (1959) .

THERMAL CONDUCTION ANISOTROPY OF BaO·6(Fe₂O₃) MONOCRYSTAL

(S u m m a r y)

The thermal difusivity measurements are carried out in a single crystal of BaO·6(Fe₂O₃) as a function of temperature and direction. The temperature dependence of the thermal difusivity may be explained by U processes. The anisotropy of the thermal conduction has been pointed out, which was explained with the scattering of the phonons by U processes and on hexagonal layers.

THE SCATTERING OF SLOW POSITRONS BY RARE GASES

R. I. CÂMPEANU

The importance of the study of positrons interactions for the atomic collisions theory was perhaps first emphasized by M a s s e y and M o h r [1]. In the electron-atom scattering problem the effective static potential, the polarization and the electron exchange are all attractive, while in the positron-atom calculations the mean static field of the atom is repulsive and the polarization and the positron-electron correlation are attractive. This is why the positron-atom calculations are expected to be a more severe test on the different theoretical approximations than the electron-atom calculations.

Until recently the theoretical results on positron-rare gases scattering were tested only against the swarm measurements, which give the positron lifetime before annihilation with the gas electrons. After their emission from a radioactive source, the probability that the positrons will be annihilated at a given time t is closely related to the annihilation effective charge of the atom averaged over the positron velocity distribution $y(k, t)$:

$$\bar{Z}_{eff} = \int Z_{eff}(k)\, y(k, t)\, \mathrm{d}t \Big/ \int y(k, t)\, \mathrm{d}t \tag{1}$$

where k is the positronic wave number. The most significant part of the lifetime spectrum corresponds to the elastically scattered positrons and it is known as „the schoulder''. In this case the positron distribution $y(k, t)$ is the solution of a diffusion equation [2, 3] which contains the temperature, the external electric field strength, the dependences $Z_{eff}(k)$ and $\sigma_{mt}(k)$, σ_{mt} being the momentum transfer cross section, which is responsible for the slowing down process in the elastic energy range and is related to the scattering phase shifts η_e through the expression :

$$\sigma_{mt}(k) = \frac{4\pi}{k^2} \sum_{l=0}^{\infty} (l+1)\ sin^2\ (\eta_l - \eta_{l+1}) \tag{2}$$

The information about the scattering phase shifts obtained in the swarm experiments was consequently indirect and rather ambiguous. From 1972 the use of the positronic beams allowed the direct measurements of elastic cross sections, which are directly related to the phase shifts :

$$\sigma_t(k) = \frac{4\pi}{k^2} \sum_{l=0}^{\infty} (2l+1)\ sin^2\ \eta_l \tag{3}$$

Unfortunately there are still a few technical problems [3] which make the precision of the beam experiments to be poorer than the precision of the swarm experiments. On the other hand, the theoretical swarm results depend more heavily on the approximation used and therefore we can consider the annihilation spectra as being the decisive test on the theory.
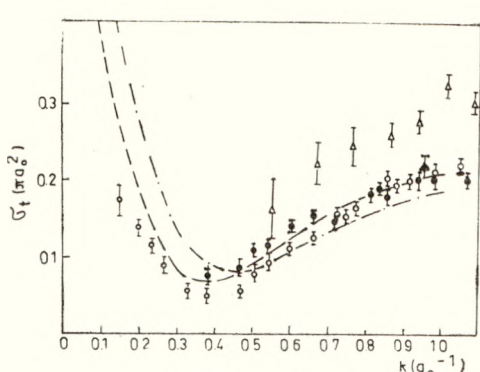
F i g. 1. Positron — helium elastic cross secti-
ons. Theoretical results : — — model H5 [3],
— . — model Hl [3]. Experimental results :
o [7], △ [8], ● [9], ▲ [10].
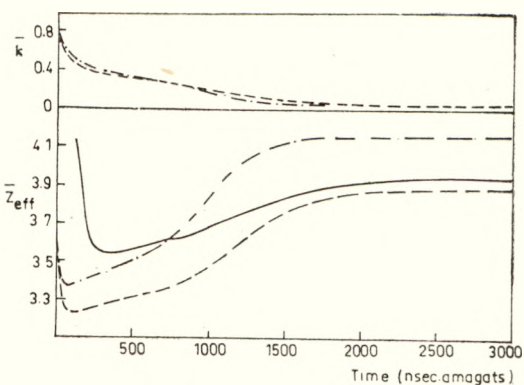
F i g. 2. The time dependence of $\overline{Z}_{eff}$ and $\overline{k}$ at
zero electric field strength and room temperature
in helium. Theoretical results : — — model H5 [3],
— . — model Hl [3]. Experimental results: — [12].

Experimentally only the positron scattering on rare gases was studied
and theoretically most work was done on the positron hydrogen and positron-
helium systems where sophisticated approximations can be employed. It is the
purpose of this paper to show the state of agreement between theory and expe-
riment for the scattering of slow positrons by He, Ne, Ar. The results for He
[2, 3] and the beam state of agreement for Ne and Ar [9, 13] have been published
already, but we shall enclose them for completeness.

For positron-helium elastic scattering the most elaborate calculation to
date uses the Kohn variational method [4,5,3]. S, p and d-wave phase shifts were
calculated with trial functions containing 70, 83 and 70 short range Hylleraas
terms respectively. The elastic cross sections obtained with these phase shifts
are given in figure 1 together with the experimental results. Curve H5 corresponds
to a 5-terms Hylleraas helium model wave function and Hl to a simple exponential
helium wave function. Model H5 was shown [6] to be sufficiently accurate and
it agrees best with the measurements of C a n t e r et al [7]. The inclusion in
the d-wave calculation of more short range terms of higher symmetries is likely
to lift only slightly the theoretical H5 curve to become probably in better agre-
ement with the experimental result of B r e n t o n et al [10]. The agreement
between curve Hl and the experiment is worse than the agreement for curve H5.

Figure 2 shows the theoretical and the experimental helium ,,shoulders''
$\overline{Z}_{eff}$(t), together with the variation with time of the averaged positronic wave
number $\overline{k}(t)$, which is obtained with an equation similar to (1). The momentum
transfer cross section σ_{mt} (k) is calculated from (2) with the variational phase
shifts and $Z_{eff}(k)$ is given by :

$$Z_{eff}(k) = Z \sum_{l=0}^{\infty} \int |\Psi_l(\overline{r}_1 = \overline{r}_2, \ \overline{r}_2, \ \dots \ \overline{r}_N)|^2 \, d\overline{r}_2 \dots d\overline{r}_N \qquad (4)$$

where Ψ_i is the partial wave variational wave function of the scattering system, $\bar{r}_1$ the positron vector and $\bar{r}_i (i = 2 \ldots N)$ the electron vectors. All the theoretical swarm results given in this paper were obtained with a k^2 initial positronic distribution, but a different choice would give very similar results [2]. Model H5 is in good agreement with the experimental result of C o l e m a n et al [12] However, it was recently shown [11] that the same measurements performed with a purer helium sample can give $\bar{Z}_{eff}(t)$ values very close to the H5 curve. The slight differences which probably still persist are explained by the fact that Z_{eff}, a nonvariational result, is slowly convergent and the H5 curve corresponds to a finite number of short range terms. Figure 2 also shows the complete failure of the simple model H1, which cannot reproduce the lifetime spectrum.

The elaborate variational methods become impracticable for heavier atoms and one must look for simpler approximations. All the calculations on e^+ Ne and e^+ Ar to date neglect the virtual positronium formation (the positron-electron correlation), but consider the mean atomic field and the target polarization. Figure 3 shows the elastic cross sections obtained for e^+ Ne. The calculation of M c E a c h r a n et al [13] is the most elaborate adiabatic calculation and it appears to be in good agreement with the higher energy measurements of C a n - t e r et al [7] and with the lower energy results of K a u p p i l a et al [9]. The adiabatic method overestimates the attractive polarization effect and for some energies this can compensate the lack of positron-electron correlation. The result of C â m p e a n u and D u b a u [16] is obtained with a close coupling nonadiabatic calculation and although without positron-electron correlation it agrees over a wide range of energies with the experiment of K a u p p i l a et al. [9]. This is due to the fact that, although all the phase shifts are underestimated, for most energies the opposite sign of η_0 and $\eta_l \ (l \geqslant 1)$ masks the incompleteness of the calculation.

We have further used the phase shifts which gave elastic cross sections in best agreement with the beam experiment, in the diffusion program used in the
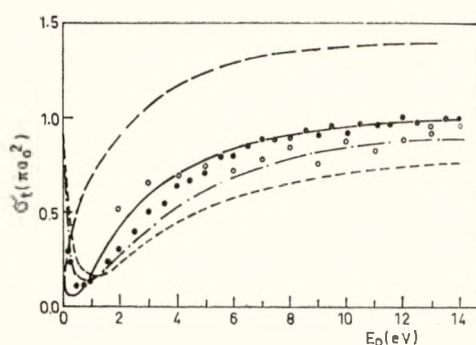
F i g. 3. Positron — neon elastic cross sections. Theoretical results: — . — [13], —— —— [14], — — — [15], —— [16]. Experimental results: o [7], ● [9].
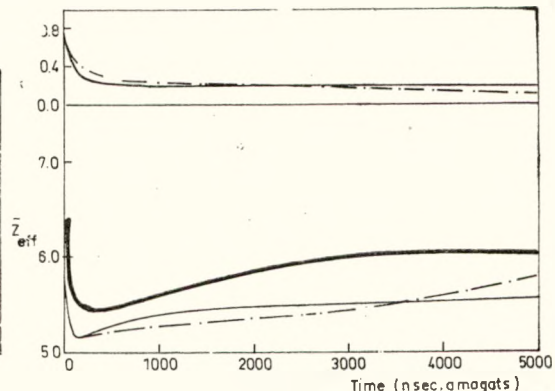
F i g. 4. The time dependence of $\bar{Z}_{eff}$ and $\bar{k}$ at zero electric field strength and room temperature in neon. Theoretical results: — . — [13], —— [16]. Experimental results: ▬▬ [17].
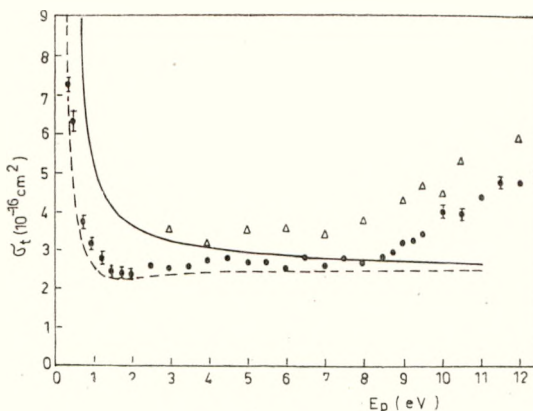
F i g. 5. Positron — argon elastic cross sections. Theoretical results : —— [13], — — [15]. Experimental results : ▲ [7], ● [9].
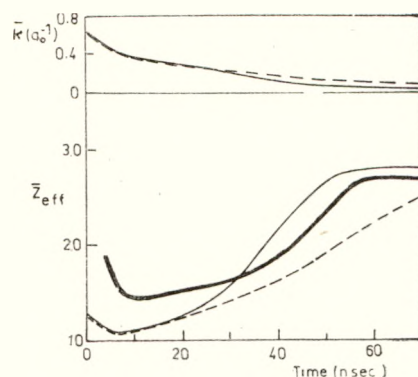
F i g. 6. The time dependence of $\overline{Z}_{eff}$ and $\overline{k}$ at zero electric field strength and room temperature in argon. Theoretical results:—— [13], — — [15]. Experimental results : ━━ [17].

helium case. We employed Z_{eff} (k) calculated by Mc E a c h r a n et al [13] without the inclusion of higher multipoles in the adiabatic potential. Their Z_{eff} for thermal positronic energy was 6.1 in best agreement with the experimental 6.0 [17]. Figure 4 compares, in a manner similar to figure 2, theory and swarm experiment. It is found that, although in relative agreement with the beam experiment, no theoretical approximation can reproduce the experimental shoulder length, the calculated slowing down process not being fast enough. As the annihilation term in the diffusion equation is not important it appears that only the values of $\sigma_{mt}(k)$ below $k = 0.3$ are responsible for the too long shoulder. In this energy range too small values for $\sigma_{mt}(k)$ imply too low $\sigma_t(k)$ as well. We can conclude that for $k \geqslant 0.3$ the experimental elastic cross sections of K a u p p i l a et al [9] are too low. This observation was already made in the helium case [6].

Figure 5 gives the adiabatic elastic cross sections [13,15] and the best beam experimental results [7, 9] for the argon case. The calculation of M c E a c h r a n at al [13] is again the best and it also gives a very good thermal energy value for Z_{eff}. In figure 6 we give the theoretical ,,shoulders" corresponding to the two adiabatic calculations. As the values for the annihilation effective charge obtained by M o n t g o m e r y and L a B a h n [15] were in very bad agreement with the experimental observations, we employed in both ,,shoulder" calculations Z_{eff}(k) of M c E a c h r a n et al [13]. The shoulder length obtained with the phase shifts of M c E a c h r a n et al [13] is in good agreement with the experimental one [17] and this implies that $\sigma_t(k \geqslant 0.3)$ given by [13] is also correct. It appears again that the experimental elastic cross sections of K a u p p i l a et al [9] are too small in the low energy range and this is consistent with the observation that the calculation of M o n t g o m e r y and L a B a h n [15], which is in good agreement with [9], gives a too long shoulder.

REFERENCES

1. H. S. W. Massey and C.B.O. Mohr, Proc. Phys. Soc. (London), **54,** 695 (1954).
2. R. I. Câmpeanu and J. W. Humberston, J. Phys., **B 10,** 239 (1977).
3. R. I. Câmpeanu, PhD Thesis, University of London, 1977.
4. J. W. Humberston, J. Phys., **B 6,** L305 (1973).
5. R. I. Câmpeanu and J. W. Humberston, J. Phys., **B 8,** L244 (1975).
6. R. I. Câmpeanu and J. W. Humberston, J. Phys. **B 10,** L153 (1977),
7. K. F. Canter, P. G. Coleman, T. C. Griffith and G. R. Heyland, J. Phys. **B 6,** L201 (1973).
8. B. Jaduszliwer and D. A. L. Paul, Can. J. Phys. **51, 1565** (1973).
9. W. A. Kauppila, T. S. Stein, V. Pol and G. Jesion, Proc. 4 th Int. Conf. on Positron Annihilation (Helsingőr), A4, A5 (1976).
10. A. G. Brenton, J. Dutton and F. M. Harris, Proc. 4 th. Int. Conf. on Positron Annihilation (Helsingőr), A16 (1976).
11. G.R. Heyland, private communication, 1977.
12. P. G. Coleman, T. C. Griffith, G. R. Heyland and T. L. Killeen J. Phys., **B 8,** L454 (1975)
13. R. P. McEachran, A. G. Ryman and A.D. Stauffer, Proc. 10 th ICPEAC (Paris) Abstracts p. 820 and to appear in J. Phys, B.
14. H. S. W. Massey, J. Lawson and D. G. Thompson, *Quantum Theory of Atoms, Molecules and Solid State* (Acad. NY) p. 203, 1966.
15. R. E. Montgomery and R. W. La Bahn, Can. J. Phys., **48,** 1288 (1970).
16. R. I. Câmpeanu and J. Dubau, to be published.
17. T. L. Killeen, PhD Thesis, University of London, 1975.

ÎMPRĂŞTIEREA POZITRONILOR LENŢI PE GAZE NOBILE

(Rezumat)

Cele mai bune rezultate teoretice în împrăştierea elastică a pozitronilor pe gaze nobile sînt comparate cu rezultatele măsurătorilor de transmisie de flux de pozitroni şi cu spectrele de timp de viaţă ale pozitronilor în gaz. Pentru heliu aproximaţia variaţională Kohn poate da rezultate în perfect acord cu ambele tipuri de experienţe. În cazul neonului şi argonului corelaţiilor la distanţă mică nu pot fi incluse explicit şi se foloseşte în principal metoda adiabatică. Se arată că această aproximaţie poate fi în acord cu experienţele de flux, dar numai pentru argon ea poate reproduce şi spectrul experimental de timp de viaţă.

CONSIDÉRATIONS SUR LA MODÉLATION NUMÉRIQUE D'UN MÉLANGE TURBULENT DANS L'ESPACE DES NOMBRES D'ONDE

STELIANA CODREANU

L'étude du comportement d'un champ scalaire turbulent (concentration, température) superposé à un champ turbulent de vitesse, est un problème essential pour un mélange turbulent. Les méthodes utilisées en ce cas sont des extensions des méthodes proposées pour l'analyse même du champ turbulent de vitesse [1—5].

On sait que la turbulence, comme ensemble statistique, est caractérisée par la coexistence d'un nombre infini de moments multidimensionnels et c'est pourquoi le système des équations médiées, décrivant le mouvement turbulent, contient un nombre infini d'équations. Pratiquement, ce système est limité habituellement aux équations pour les moments de deuxième et troisième ordre. En ce cas le système d'équations décrivant la turbulence reste ouvert : en effet l'équation pour le moment d'ordre N contient le moment d'ordre $N + 1$, comme inconnue. Afin de fermer le système il est nécessaire, en utilisant une hypothèse de fermeture, d'exprimer le moment d'ordre $N + 1$ par des moments d'ordre inférieur. Les résultats ainsi obtenus chaque fois doivent être vérifiés expérimentalement. Par conséquent toute théorie statistique de la turbulence devient sémiempirique.

L'équation décrivant la variation temporelle de la densité spectrale de l'énergie turbulente $F_{ii}(\vec{k},t)$ du moment de deuxième ordre (l'équation spectrale) :

$$\frac{\partial F_{ii}(\vec{k}, t)}{\partial t} = \Gamma_{ii}(\vec{k}, t) - 2\nu k^2 F_{ii}(\vec{k}, t) - \Pi_{ii}(\vec{k}, t) \tag{1}$$

contient des moments de troisième ordre : $\Gamma_{ii}(\vec{k}, t)$ — le transport d'énergie dans le spectre et $\Pi_{ii}(\vec{k}, t)$ — l'échange énergetique, entre les trois composantes de la vitesse, du aux pulsations de la pression. Dans le cas d'une turbulence isotrope le terme $\Pi_{ii}(\vec{k}, t)$ s'annule et, pour fermer l'équation spectrale, il faut une hypothèse permettant d'exprimer $\Gamma_{ii}(\vec{k}, t)$ par la densité spectrale $F_{ii}(\vec{k}, t)$. De telles hypothèses de fermeture sont données en [6].

Le problème d'une telle fermeture se pose aussi dans le cas d'un mélange turbulent.

L'équation spectrale

$$\frac{\partial E_{\theta\theta}(\vec{k}, t)}{\partial t} = T_{\theta\theta}(\vec{k}, t) - 2\chi k^2 E_{\theta\theta}(\vec{k}, t) \tag{2}$$

qui représente la variation temporelle du spectre de la quantité scalaire θ contient le moment de troisième ordre $T_{\theta\theta}(\vec{k}, t)$ — le terme du transfert responsable de la redistribution de θ, grandeur fluctuante, dans le spectre des nombres d'onde.

Afin d'exprimer les moments de troisième ordre en fonction de ceux de deuxième ordre dans les équations (1) et (2), on a besoin d'hypothèses auxiliaires. Du fait que le nombre d'hypothèses est important, la vérification expérimentale de chacune est rendue difficile. D'autre part, l'absence d'une telle vérification expérimentale induit une certaine incertitude à l'égard des résultats théoriques.

Le développement des computers ouvre une nouvelle voie dans l'étude de la turbulence ; à savoir le calcul de la dynamique des différentes réalisations de la turbulence à partir directement de l'équation Navier—Stokes [7].

Ces calculs n'exigent aucune hypothèse supplémentaire du fait qu'essentiellement elles sont des modélations numériques des écoulements turbulents. Le plus convenable est d'effectuer la modélation numérique dans l'espace des nombres d'onde.

Dans cet ouvrage on présente, brièvement, la déduction des équations des amplitudes, nécessaires afin d'effectuer la modélation numérique du mélange turbulent dans l'espace des nombres d'onde. En réalité les équations des amplitudes sont les transformations Fourier de l'équation Navier—Stokes et de l'équation de la thermoconductibilité.

On considère une turbulence nonlimitée, qui dégénère (il n'y a pas un apport énergétique de l'extérieur) et sur laquelle on superpose le champ scalaire de la température. Le système d'équations, décrivant une telle turbulence, est :

$$\frac{\partial u_i}{\partial t} + u_l \frac{\partial u_i}{\partial x_l} = -\frac{1}{\rho}\frac{\partial p}{\partial x_i} + \nu \frac{\partial^2 u_i}{\partial x_l \partial x_l} \tag{3}$$

$$\frac{\partial \theta}{\partial t} + u_l \frac{\partial \theta}{\partial x_l} = \chi \frac{\partial^2 \theta}{d x_l d x_l} \tag{4}$$

$$\frac{\partial u_l}{\partial x_l} = 0 \tag{5}$$

Délimittons spatiellement un parallélipipède rectangle, de dimensions suffisamment grandes, L_i, dans un système de coordonnées arbitrairement choisi. Représentons la distribution des grandeurs physiques dans ce parallélipipède à chaque instant, sous la forme d'une superposition d'ondes planes :

$$u_i(\vec{x}, t) = \sum_{\vec{k}} A_i(\vec{k}, t) \, e^{i\vec{k}\cdot\vec{x}} \tag{6}$$

$$p(\vec{x}, t) = \sum_{\vec{k}} C(\vec{k}, t) e^{i\vec{k}\cdot\vec{x}} \tag{7}$$

$$\theta(\vec{x}, t) = \sum_{\vec{k}} D(\vec{k}, t) e^{i\vec{k}\cdot\vec{x}} \tag{8}$$

où $A_i(\vec{k}, t)$, $C(\vec{k}, t)$, $D(\vec{k}, t)$ sont les amplitudes respectives. En effectuant la divergence de l'équation du mouvement, on obtient :

$$-\frac{1}{\rho}\frac{\partial^2 p}{\partial x_i \partial x_i} = \frac{\partial u_l}{\partial x_i}\frac{\partial u_i}{\partial x_l} \tag{9}$$

En introduisant les expressions (6) et (7) dans cette équation, on obtient la relation suivante, permettant l'élimination de l'amplitude $C(\vec{k}, t)$:

$$\frac{k^2}{\rho} C(\vec{k}, t) = - k_l k_m \sum_{\vec{k'}} A_l(\vec{k'}, t) A_m(\vec{k} - \vec{k'}, t) \tag{10}$$

En tenant compte de cette relation et introduisant en (3) et (4) les expressions (6)—(8), on obtient les équations des amplitudes :

$$\frac{\partial}{\partial t} A_i(\vec{k}, t) = i \left[-k_l \sum_{\vec{k'}} A_i(\vec{k'}, t) A_l(\vec{k} - \vec{k'}, t) + \frac{k_i k_l k_m}{\rho} \sum_{\vec{k'}} A_l(\vec{k'}, t) A_m(\vec{k} - \vec{k'}, t) \right] - $$
$$ - \nu k^2 A_i(\vec{k}, t). \tag{11}$$

$$\frac{\partial}{\partial t} D(\vec{k}, t) = ik_l \sum_{\vec{k'}} D(\vec{k'}, t) A_l(\vec{k} - \vec{k'}, t) - \chi k^2 D(\vec{k}, t) \tag{12}$$

Ces équations permettent d'effectuer le calcul de la variation temporelle de n'importe quelle réalisation isolée du mélange turbulent, déterminé initiellement par $A_i(\vec{k}, o)$ et $D(\vec{k}, o)$.

La méthode proposée peut être utilisée aussi dans l'étude de l'influence du champ magnétique sur le mélange turbulent. On peut penser que l'influence d'un tel champ sur les différentes réalisations de la turbulence sera la même que sur l'ensemble turbulent comme entier. Par conséquent, le calcul d'une ou de plusieurs réalisations turbulentes à l'aide des équations des amplitudes permet la clarification du caractère de l'influence du champ magnétique sur une turbulence nonlimitée, généralement, et sur un mélange turbulent, particulièrement.

BIBLIOGRAPHIE

1. S. C o r r s i n, J. Appl. Phys., **22**, 469 (1951).
2. E. E. O' B r i e n, G. C. F r a n c i s, J. Fluid. Mech., **13**, 369 (1962).
3. P. C. J a i n, Proc. Nat. Inst. of India **A 28**, 401 (1962).
4. S. C o d r e a n u, Studia Univ. Babeş-Bolyai, Ser. Phys., 2, 69 (1973).
5. H i m a d r i P a i M a z u m d a r, Appl. Sci. Res. **32**, 571 (1976).
6. A. S. M o n i n, A. M. I a g l o m, *Statisticeskaia ghidrodinamica*, I—II, Izd. Nauka, Moskva, 1965.
7. L. G. G h e n i n, S. P. M a n g h a, Magnitnaia ghidrodinamica, **1**, 89 (1976).

CONSIDERAŢII PRIVIND MODELAREA NUMERICĂ A AMESTECULUI TURBULENT ÎN SPAŢIUL NUMERELOR DE UNDĂ

(R e z u m a t)

Se prezintă succint deducerea ecuaţiilor amplitudinilor cu ajutorul cărora se poate efectua modelarea numerică a amestecului turbulent în spaţiul numerelor de undă.

THE METACHROMATIC EFFECT PRODUCED BY THE NEGATIVE IONS PRESENT IN THE AQUEOUS SOLUTION OF THE DRUG ETHIDIUM BROMIDE

HOREA PORUMB*, TUDOR PORUMB

Introduction. The object of the present investigation is the trypanocidal drug ethidium bromide. This molecule belongs to a class of chemical compounds which all possess extended, aromatic chromophores. The absorption bands of these chromophores lie in the visible region of the spectrum and usually there is a shift in the wavelength of the maximum absorption peak following the interaction of these molecules with polyelectrolytes such as proteins and nucleic acids (metachromatic effect).

It is now known that ethidium bromide ows its biological activity to the intercalation of its flat chromophore in between adjacent base pairs of the DNA double helix, in common with other drugs of biological or medical importance, such as daunomycin, actinomycin D, proflavine [1]. There is mounting evidence, especially from relaxation kinetics studies, that besides the intercalative mode of binding the ethidium bromide molecule may also attach electrostatically to the exterior of the DNA helix, like many dyes with tissue-staining properties, such as acridine orange or toluidine blue [2].

The difficulty in characterizing the second mode of binding is due to the fact that both the intercalated and the externally bound phases display spectra of similar appearance, namely a visible band which is red shifted and hypochromic with respect to that of the free drug [3]. The aim of this paper is to provide a rationale for the similarity of the absorption spectra of the two bound species.

Experimental Results. Upon increasing the ionic strength of an aqueous solution of ethidium bromide there is hypochromism and a red shift in the wavelength of the visible absorption peak of the drug. The magnitude of this effect is directly proportional to the size of the negative ion of the electrolyte (fig. 1).
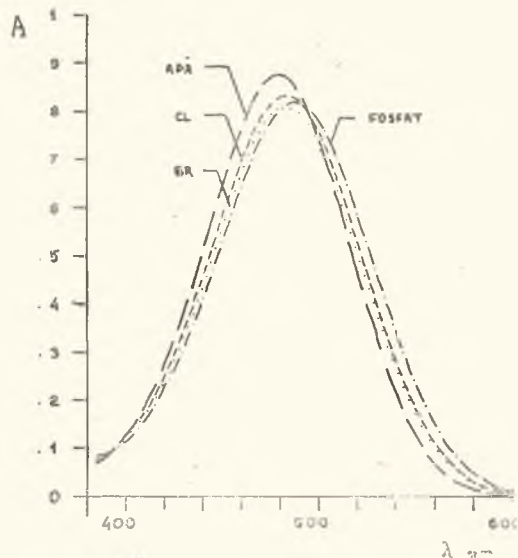
F i g. 1. Visible absorption spectra of ethidium bromide ($8 < 10^{-4}$ M) in water and in the presence of sodium salts (NaCl, NaBr, Na$_2$HPO$_4$) at 2M concentration.

* Departament of Biophysics, Medical and Pharmaceutical Institute, Cluj-Napoca.

Indeed, along the sodium halide series (NaCl, NaBr, NaI) the greatest effect was encountered with NaI. (In the presence of 2M NaI, a 3mM ethidium bromide solution precipitated in the form of a violet crystalline deposit.) An even larger spectral effect was obtained in the presence of the sodium phosphate, which reminds us of the interaction between the drug and the phosphate groups of the DNA backbone.

It should be mentioned that a similar red shift and hypochromism was achieved by Thomas and Roques as a result of increasing the concentration of a pure ethidium bromide solution. These authors proved by proton magnetic resonance that the aromatic cationic drug chromophores aggregated in concentrated aqueous solutions in the form of stacked dimers [4].

Significance of Results. In order to explain the red shift encountered upon aggregation, it is suggested that the bromide counterion, freely dissociated in a dilute ethidium bromide solution, is offered the possibility to attach specifically to a site on the ethidium dimer, created as a result of aggregation. The presence of the negative ion in the close proximity of the chromophore as, in general, the presence of any substituent with electron donating powers (auxochrome) is equivalent to enlarging the territory available to the pi-electron system, with the consequence that the wavelength of the electronic transition is red shifted. It is alledged that the large negative ions of the electrolyte, besides causing non-specific electrostatic screening which promotes aggregation up to the point of precipitation, are also able to replace the bromide ion from its suggested site and act as more powerful donors of electrons, with the consequence of a larger spectral red shift.

The significance of these findings to the spectroscopy of the drug-nucleic acid interactions lies in the fact that they provide a rationale for the observed indistinguishability of the intercalated and outside bound forms of the drugs to DNA. Whereas intercalation results in spectral red shift due to exciton interactions [5], a similar red shift is caused in the case of the outside bound drug by charge donation to the drug chromophore from the phosphate backbone of the DNA.

It is reckoned that the red shift encountered upon the binding of ethidium bromide to RNA, single stranded polynucleotides and polyelectrolytes such as polyphosphate, polyvynil alcohol, polystiren sulphonic acid and proteins [6] may also be explained by the charge donation mechanism.

(Received March 14, 1978)

REFERENCES

1. W. F u l l e r, M. J. W a r i n g, Ber Bunsenges. Phys. Chem, **68**, 805—808 (1967).
2. J. L. B r e s l o f f, D. M. C r o t r e r s, J. Mol. Biol., **95**, 103—123 (1975).
3. H. J. L i, D. M. C r o t h e r s, Biopolymers, **8**, 217—235 (1969).
4. G. T h o m a s, B. R o q u e s, FEBS Lett., **26**, 169—175 (1972).
5. M. R. P h i l i p o t t, J. Chem. Phys., **53**, 968 (1970).
6. M. J. W a r i n g, Biochim. Biophys. Acta, **114**, 234—244 (1966).

EFECTUL METACROMATIC PRODUS DE IONII NEGATIVI PREZENȚI ÎN SOLUȚIILE APOASE ALE ANTIBIOTICULUI BROMURĂ DE ETHIDIU

(R e z u m a t)

Deplasarea spre roșu a benzii de absorbție a antibioticului bromură de ethidiu în soluție apoasă se datorește donării de sarcină electronică de la ionii negativi ai electrolitului către moleculele agregate.

A RELATIONSHIP WHICH ENABLES THE ESTIMATION OF THE AMOUNT OF LIPID BOUND TO PROTEIN IN BIO-MEMBRANES FROM SPIN LABEL DATA

T. PORUMB, H. PORUMB*

1. Introduction. Electron spin resonance studies performed on membrane and model membrane systems spin labeled with fatty acid and phospholipid spin labels [1, 2] have revealed the existence in a membrane of two lipid phases, of distinct mobilities: a ,,mobile" phase, corresponding to the bilayer lipids, and an ,,immobile" phase, customarily referred to as ,,the boundary" lipid, corresponding to the lipid molecules which are tightly attached to the membrane proteins. The fact that the lipid label molecules added to the system distribute themselves to both the mobile and immobile phases inferres the existence of an exchange of lipid molecules between the two phases.

In the present paper it is assumed that the number of ,,boundary" lipid molecules in a membrane system is a constant, independent of the type of lipid molecules which fill the boundary phase (i.e. membrane lipids or lipid labels). The existence of a linear relationship is demonstrated between the reciprocal of the fraction of immobilized lipid label molecules and the total amount of lipid label added to the system, which enables one to determine the absolute magnitude of the boundary domain in a membrane system on the basis of spin label data.

2. Theory. The partition of the lipid label molecules between the mobile and immobile phases will reflect, after equilibrium, both the sizes of the two domains and the different affinities of the label for the two phases. The difference in affinity mentioned above could arise, for example, because a lipid label molecule might experience difficulty in replacing an immobilized lipid molecule from the boundary, or, because only a fraction of the lipid ,,binding" sites from the boundary might be accessible to the lipid labels. Quantitatively, these statements may be expressed in the form of the proportions (1):

$$n_m^* = a_m \cdot (n + n^* - b) \tag{1}$$

$$n_i^* = a_i \cdot b$$

where n_m^* and n_i^* are the number of lipid label molecules in the mobile and immobile phases, $n^* = n_m^* + n_i^*$ is the total number of lipid label molecules, n is the number of lipid molecules of the membrane, b is the number of boundary lipid molecules and a_m and a_i are the affinities (under given conditions, such as the hydration or temperature) of the lipid label for the mobile and immobile phases, respectively.

In the above proportions the factors which specify the magnitude of the two phases contain both the membrane lipids and the lipids introduced to

---

* Biophysics Department, Medical and Pharmaceutical Institute, Cluj-Napoca,

the system as spin label. Provided they are expressed in the same kind of units, the n's and b may be numbers of molecules, of moles, or concentrations. If one takes the ratio of the proportions (1) and defines a partition coefficient a as the ratio a_i/a_m (a is less than one for the situation mentioned above), one is led, after suitable rearrangements, to the relationship (2):

$$\frac{n^*}{n_i^*} = \frac{n^*}{ab} + \frac{n - (1 - a)\,b}{ab} \tag{2}$$

3. Discussion. According to relationship (2), the reciprocal of the fraction of immobilized lipid label molecules increases linearly with the amount of spin label added to the sample.

The extrapolation to zero label concentration in a plot of n^*/n_i^* versus n^* is expected to provide the image of the membrane system as seen by the spin label under conditions of minimum interference from the spin label itself. The examination of the expression for the intercept of the plot,

$$\frac{n - (1 - a)\,b}{ab}$$

shows that the system behaves as if only a fraction of the immobilized (boundary) lipid, ab, is seen by the spin label, the total number of lipid molecules of the membrane system appearing to be reduced from n by the number of boundary lipid molecules $(1-a)\,b$ that cannot be ,,seen''. This provides an alternative definition of the coefficient a, as the fraction of the magnitude of the boundary phase that is seen by the spin label; a quantity which is proportional to the fraction of lipid ,,binding sites'' on the protein boundary that are available to the lipid label by exchange, and is also dependent on the difference in affinity, in the usual chemical sense, manifested by the lipid label for the two phases.

Relationship (2) enables one to determine quantitatively both the absolute magnitude of the boundary phase (b) and the value of the coefficient a, from the slope and the intercept of the plot. The system is fully determined, as the fraction of immobilized lipid spin label molecules (n_i^*/n^*) can be obtained from the analysis of the ESR spectra by spectral titration procedures [1], the amount of lipid spin label added to the sample (n^*) is known and the lipid content of the sample (n) can be determined by chemical analysis.

REFERENCES

1. O. H. Griffith, P. C. Jost, R. A. Capaldi, G. Vanderkooi, Ann. N. Y. Acad. Sci., **222**, 561—72 (1973).
2. Gh. Benga, D. Chapman, Anal. Chem., **28**, 1756—58 (1976).

O RELAŢIE CARE PERMITE ESTIMAREA CANTITĂŢII DE LIPIDE IMOBILIZATE PE PROTEINE ÎN BIO-MEMBRANE, FOLOSIND DATE DE MARCARE CU SPIN

(Rezumat)

Între lipidele bio-membranelor din faza fluidă şi cele imobilizate de către proteine (numărul acestora este o constantă, b) se execută schimburi permanente. Adăugînd sistemului lipide marcate cu spin (n^*), acestea se vor regăsi distribuite în ambele aceste faze. Panta şi ordonata la origine a graficului bazat pe relaţia (2) furnizează mărimea stratului imobilizat, b, şi coeficientul de partiţie al lipidelor marcate, a, fracţia de molecule de marker imobilizate putînd fi determinată prin analiza spectrelor RES.

DETERMINAREA ULTRASONICĂ A UNOR PARAMETRI STRUCTURALI PENTRU TOLUEN ŞI m-XILEN

C. ŞTEŢIU şi **M. ILUŢIU**

1. Introducere. Este binecunoscut faptul că propagarea undelor sonore într-un mediu elastic depinde de structura acestui mediu. În literatura de specialitate există o serie de relaţii ce descriu dependenţa vitezei de propagare a sunetelor atît de volumul molecular, cît şi de forţele de interacţiune moleculară [1, 2, 3].

Folosindu-se un raţionament termodinamic şi aproximaţia „volumului liber", în cazul lichidelor ce prezintă o simetrie sferică, se ajunge [2] la următoarea dependenţă a vitezei de propagare v de volumul molecular V al unui lichid

$$v = \left(\frac{RT}{M}\right)^{1/2} \frac{1}{1 - \left(\frac{V_0}{V}\right)^{1/3}} \left[\frac{5}{3} - \frac{2}{3}\left(\frac{V_0}{V}\right)^{1/3}\right]^{1/2} \tag{1}$$

unde V_0 reprezintă volumul propriu al moleculelor dintr-un mol de lichid, R — constanta universală a gazelor, T — temperatura în K, iar M — masa molară.

Pe de altă parte, între viteza de propagare şi bariera de potenţial ε_0 a lichidului studiat s-a stabilit [3] relaţia

$$\varepsilon_0 = \frac{1}{nm}\left(\frac{M}{\gamma} v^2 - TR\right) \tag{2}$$

unde m şi n sînt exponenţii potenţialului Lennard-Jones, iar γ exponentul adiabatic.

Din relaţiile (1) şi (2) rezultă posibilitatea de evaluare din date asupra vitezei de propagare atît a volumului molecular, cît şi a barierei de potenţial.

2. Prelucrarea datelor experimentale. Pornind de la ecuaţia (1), s-a calculat volumul propriu V_0 al moleculelor, obţinîndu-se relaţia

$$V_0 = \frac{M}{\rho N_A}\left[1 - \frac{1 - \sqrt{3\left(\frac{3v^2 M}{RT}\right) + 1}}{\frac{3v^2 M}{RT}}\right]^3 \tag{3}$$

unde ρ reprezintă densitatea lichidului studiat, iar N_A numărul lui Avogadro.

Pe baza datelor asupra vitezei de propagare şi densitate, s-a evaluat din relaţia (3) volumul propriu al moleculelor de toluen şi m-xilen. Rezultatele obţinute sînt prezentate în fig. 1, studiindu-se dependenţa volumului propriu de temperatură. Schimbarea de pantă care se observă indică temperatura schimbării fazei lichide în faza gazoasă. Se observă de asemenea o creştere a volu-
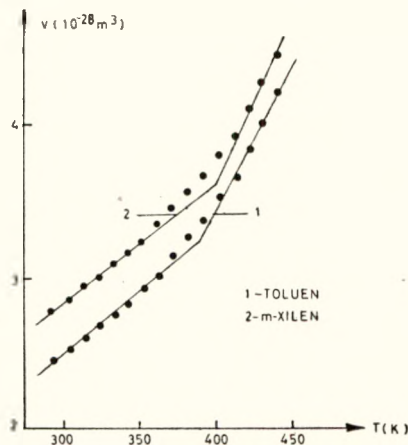
F i g. 1. Dependenţa de temperatură a
volumului molecular.
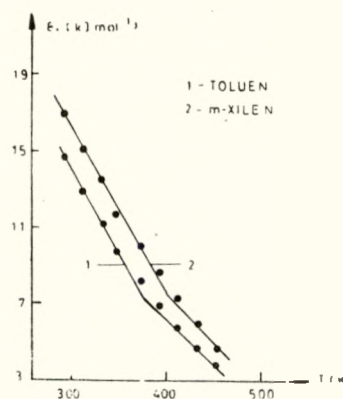
F i g. 2. Variaţia cu temperatura a
barierei de potenţial.

mului molecular la creşterea temperaturii. Astfel, la o creştere a temperaturii
cu 10 K, volumul molecular al stării lichide variază pentru toluen cu 9%,
iar pentru xilen cu 8%; în stare gazoasă, la aceeaşi variaţie de temperatură,
corespunde o creştere a volumului molecular cu 24% pentru toluen şi cu
20% pentru xilen.

Datele obţinute pentru volumul molecular propriu al substanţelor în
studiu, au fost comparate cu cele existente în literatură [4] pentru covolum,
valori obţinute din date critice. Pentru toluen, tabelele indică un covolum
de $2,4107 \cdot 10^{-28} m^3$, iar pentru xilen, de $2,9199 \cdot 10^{-28} m^3$, date ce concordă
cu cele obţinute în studiul de faţă.

Din relaţia (2) s-a evaluat bariera de potenţial pentru toluen şi m-xilen,
în intervalul de temperatură $20-190 °C$. Exponentul adiabatic s-a luat din
tabele [4].

Variaţia cu temperatura a barierei de potenţial este reprezentată în fig. 2.
Se observă o scădere lineară a barierei de potenţial la creştere a temperaturii.
Schimbarea de pantă apare la temperatura de transformare a stării lichide
în stare de vapori.

Cunoscînd bariera de potenţial (care reprezintă potenţialul lichidului ce
ocupă la o temperatură dată volumul de echilibru) şi faptul că în cazul poten-
ţialului (12—6) abscisa ce corespunde lui ε_0 este $r_0 = 2^{1/6}\sigma_0$, unde σ_0 este
diametrul de ciocnire, se poate evalua potenţialul de interacţiune Lennard-
Jones,

$$\Phi(r) = 4\varepsilon_0 \left[\left(\frac{\sigma_0}{r} \right)^{12} - \left(\frac{\sigma_0}{r} \right)^6 \right] \qquad (4)$$

σ_0 calculîndu-se din datele obţinute pentru volumul molecular.

Folosind relaţia (4), s-a calculat $\Phi(r)$ pentru diferite valori ale raportului
σ_0/r, la temperaturi diferite. Fig. 3 respectiv 4 prezintă potenţialul de inter-
acţiune Lennard-Jones pentru toluen şi m-xilen.
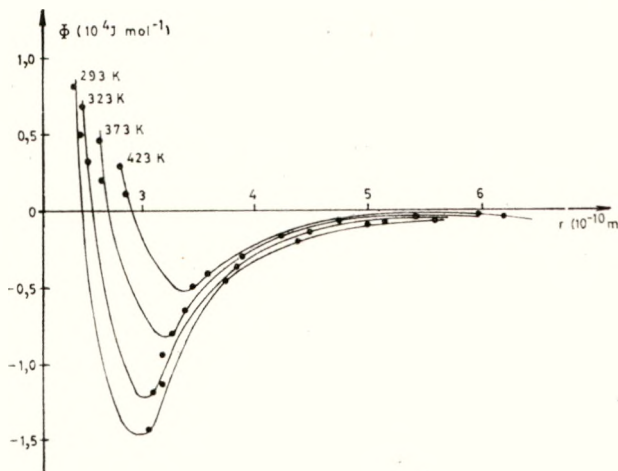
F i g. 3. Variaţia cu temperatura a potenţialului de inter-
acţiune molecular pentru toluen.
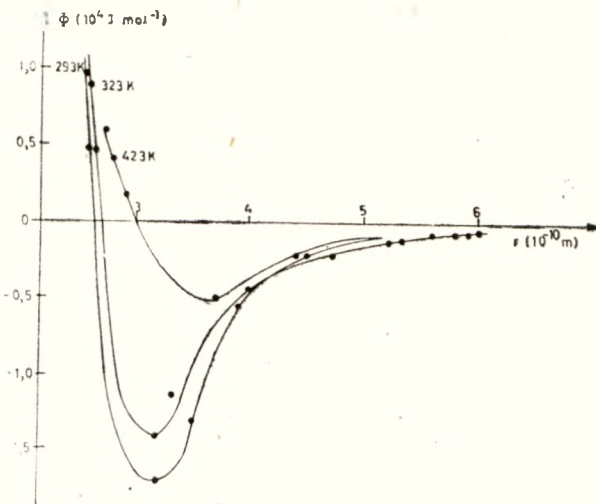
F i g. 4. Variaţia cu temperatura a potenţialului de inter-
acţiune molecular pentru m-xilen.

3. **Concluzii.** Cunoscînd din măsurători directe densitatea unui lichid, viteza de propagare a undelor sonore în acel lichid şi raportul capacităţilor calorice, se pot evalua unii parametri structurali ai lichidului, cum sînt volumul molecular şi potenţialul de interacţiune molecular.

B I B L I O G R A F I E

1. I. G. M i c h a i l o v, V. A. S o l o v i e v, I. P. S î r n i c o v, *Osnovî molekuljarnoi akustiki* Izd. Nauka, Moskva, 1964.
2. W. V a n D a e l, A. V a n I t t e r b e c k, *Physics of high Pressures and the Condessed Phase,* Ed. A. Van Itterbeck, North Holland Publ. Co., Amsterdam, 1965.
3. C. S t e ț i u, Studia Univ. Babeș-Bolyai, Phys., 11, 1976.
4. *Manualul chimistului*, Ed. Agir, București, 1948.

ULTRASONIC DETERMINATION OF SOME STRUCTURAL PARAMETERS OF
TOLUOL AND m-XYLOL

(S u m m a r y)

It was shown that there is the possibility of building up the Lennard-Jones potential of a li-quid, knowing its density, sound velocity and the ratio of specific heats.

STUDIUL R.E.S. AL UNOR CIANAȚI COMPLECȘI DE Cu(II) ÎN SOLUȚII

O. COZAR și **R. SEMENIUC**

În lucrarea de față sînt prezentate rezultatele RES cu privire la comportarea complecșilor $[Cu(\beta\text{-picolină})_2(NCO)_2]$ și $[Cu(\gamma\text{-picolină})_2(NCO)_2]$ în cloroform și amestecuri de cloroform + piridină. Probele folosite au avut o concentrație de $\simeq 1-2$ mg/cm³ pentru compusul cu β-picolină și respectiv 0,7 mg/cm³ pentru cel cu γ-picolină. S-a lucrat la temperatura camerei și 77 K în banda X, cu o instalație JES—3B, avînd modulația cîmpului magnetic de 100 kHz. Comportarea celor doi complecși este similară, neapărînd diferențe remarcabile.

Spectrele RES obținute la temperatura camerei în cloroform prezintă o slabă asimetrie, iar structura hiperfină nu este clar rezolvată. Aceasta devine mai bine rezolvată în amestecurile de cloroform + piridină, conținînd 20— —50% piridină (fig. 1). Adaosul de piridină contribuie la rezolvarea structurii hiperfine prin faptul că au loc coordinări ale moleculelor de piridină la ionii Cu^{2+}, ceea ce duce la creșterea timpului de corelare $\tau = \dfrac{4\pi r^3 \eta}{3KT}$ prin mărirea razei efective (r) a complexului și totodată conform teoriilor lui W i l s o n - K i v e l s o n [1] precum și A l t ș u l e r - V a l i e v [2] la o îngustare a liniilor de structură hiperfină, mai ales a celor corespunzătoare pentru $m_I = -3/2$ și $-1/2$, din partea înaltă a cîmpului magnetic. Parametrii izotropici găsiți pentru complexul cu β-picolină sînt: $g_0 = 2,135$ și $A_0 = 57,2 \cdot 10^{-4} cm^{-1}$.

La 77 K s-au obținut spectre în care pe lîngă semnalele de la $B \simeq 3\,000$ gauss, mai apare un semnal slab la $B \simeq 1560$ gauss (fig. 2). Prezența acestui semnal la cîmpuri joase indică formarea unor „aglomerări" ale
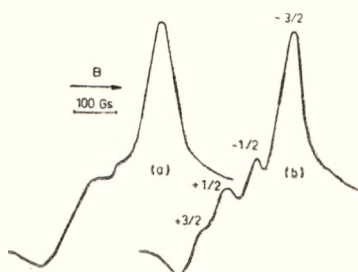
F i g. 1. Spectrele R.E.S. ale complexului $[Cu(\beta - pic.)_2 (NCO)_2]$ la temperatura camerei în cloroform (a) și 50% cloroform +50% piridină (b).
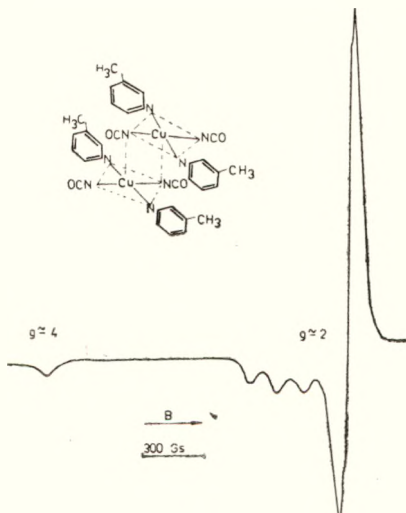
F i g. 2. Spectrul R.E.S. al complexului $[Cu(\beta\text{-pic.})_2(NCO)_2]$ la 77 K în 80% cloroform +20% piridină și structura dimeră posibilă.
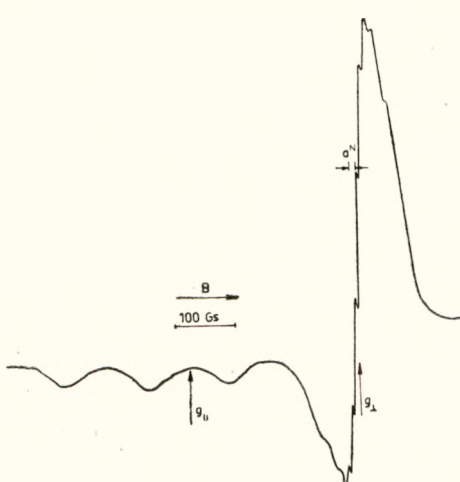
F i g. 3. Spectrul R.E.S. de la g $\simeq$ 2, pentru o viteză de înregistrare de 3 ori mai mare.

moleculelor de complex în anumite zone ale soluției înghețate [3]. Este posibilă totodată formarea unor dimeri de tipul azotatului de bis(piridin N-oxid)–Cu(II) [4].

După cum se știe, în cazul compleșilor dimeri de Cu(II) apare un cuplaj dipol-dipol între ionii de cupru cu spin 1/2, combinația celor doi spini dînd o stare de singlet (S=0) și una de triplet (S=1) [5—7]. În starea de triplet sînt permise tranzițiile $\Delta M = \pm 1$ ce dau semnale RES la g $\simeq$ 2 ($B \simeq 3\,000$ gauss) și de asemenea apar tranziții „interzise" la $\Delta M = \pm 2$ ce dau un semnal slab la g $\simeq$ 4 ($B \simeq 1500$ gauss).

În fig. 3 este prezentat spectrul de la g $\simeq$ 2, care este tipic unei molecule de complex „izolate", structura hiperfină din banda paralelă fiind clar rezolvată. Totuși interacțiile dipolare cu ionii de cupru vecini se manifestă printr-o lărgime mare a liniilor hiperfine. Forma spectrelor și faptul că $g_{\parallel} < g_{\perp}$, indică pentru acești compleși o simetrie de tip D_{4h} cu orbitalul $d_{x^2-y^2}$ ca stare fundamentală pentru electronul paramagnetic. În regiunea absorbției perpendiculare apar rezolvate liniile de structură superhiperfină datorate interacțiilor cu nucleele ^{14}N. S-au pus în evidență nouă semnale hiperfine de ligand ce pot fi atribuite celor patru atomi de azot echivalenți din planul moleculei. Parametrii RES obținuți din acest spectru sînt :

$$g_{\parallel} = 2{,}259 \quad g_{\perp} = 2{,}045 \quad A_{\parallel} = 148 \cdot 10^{-4}\,\text{cm}^{-1} \quad a^N = 12{,}8 \cdot 10^{-4}\,\text{cm}^{-1}$$

Valoarea mai mică a constantei de structură hiperfină $A_{\parallel}$ decît în cazul altor compleși de cupru(II) cu liganzi conținînd atomi de azot considerați planar-pătratici unde $A_{\parallel} \simeq 200 \cdot 10^{-4}\,\text{cm}^{-1}$ [8, 9], poate fi explicată prin prezența în cazul compleșilor de față a unei distorsii T_d. Aceasta favorizează mixtarea orbitalului $4p_z$ în starea fundamentală, ceea ce determină o reducere a constantei de structură hiperfină [10, 11].

Coeficienții MO caracteristici stării fundamentale (α^2) și primelor stări excitate (β^2, δ^2) s-au evaluat după Y o k o i și I s o b e [8], folosind relațiile :

$$\alpha^2 = \frac{A_{\parallel}}{P} + (g_{\parallel} - 2{,}002) + \frac{3}{7}(g_{\perp} - 2{,}002) + 0{,}04 \tag{1}$$

$$g_{\parallel} = 2{,}002 - 0{,}96\frac{8\lambda}{\Delta E_{xy}}\alpha^2\beta^2 \tag{2}$$

$$g_{\perp} = 2{,}002 - 0{,}96\frac{2\lambda}{\Delta E_{xz}}\alpha^2\delta^2 \tag{3}$$

Densitatea de spin la atomii de azot în starea fundamentală s-a calculat din despicările superhiperfine, după relația [12]:

$$a^N = \frac{8\pi}{9}\, g_e\beta_e g_n\beta_n\, |\,\psi_{2s}(0)\,|^2 \left(\frac{\alpha'^2}{4}\right) \tag{4}$$

Pentru evaluarea coeficienților β^2 și δ^2 este nevoie de valorile tranzițiilor ΔE_{xy} și ΔE_{xz}. Spectrele electronice ale acestor complecși în cloroform constau dintr-o bandă de absorbție la 14 500 cm^{-1} și una la 30 500 cm^{-1}. Studiile optice efectuate asupra unor complecși similari cu atomi donori de azot au indicat faptul că tranzițiile d au loc în domeniul (14—18) 10^3 cm^{-1}, iar spre 30 000 cm^{-1} apar benzi atribuite transferului de sarcină [13—15]. Ținînd cont de acestea am considerat pentru calcularea coeficienților β^2 și δ^2 că $\Delta E_{xy} = \Delta E_{xz} = 14\,500$ cm^{-1}. Valorile astfel obținute pentru coeficienții MO sînt:

$$\alpha^2 = 0{,}73 \qquad \alpha'^2 = 0{,}28 \qquad \beta^2 = 0{,}80 \qquad \delta^2 = 0{,}53$$

Din acestea se poate observa o covalență apreciabilă pentru legătura σ din planul moleculei, precum și o puternică covalență a legăturii π în afara planului ($\delta^2 = 0{,}53$), fapt întîlnit și la complecșii amoniacali de Cu(II) [8, 16].

(Intrat în redacție la 18 mai 1978)

BIBLIOGRAFIE

1. R. Wilson, D. Kivelson, J. Chem. Phys., **44**, 4445 (1966).
2. S. A. Altșuler, K. A. Valiev, Jurn. Exp. Toer. Fiz., **35**, 947 (1958).
3. S. Fujiwara, S. Katsumata, T. Seki, J. Phys. Chem., **71**, 115 (1967).
4. W. E. Hatfield, J. A. Barnes, D.Y. Jeter, R. Whyman, E.R. Jones, J. Am. Chem. Soc., **92**, 4982 (1970).
5. J. F. Boas, R. H. Dunhill, J. R. Pilbrow, R.C. Srivastava, T. D. Smith, J. Chem. Soc. A, 94 (1969).
6. P. D.W. Boyd, T. D. Smith, J. H. Price, J. R. Pilbrow, J. Chem. Phys., **56**, 1253 (1972).
7. K. T. McGregor, W. E. Hatfield, J. Chem. Phys., **65**, 4155 (1976).
8. H. Yokoi, T. Isobe, Bull. Chem. Soc. Japan, **41**, 2835 (1968).
9. G. Formicka-Kozlowska, H. Kozlowski, B. Jezowska-Trzebiatowska, Inorg. Chim. Acta, **24**, 1(1977).
10. C. A. Bates, W. S. Moore, K. J. Standley, K. W. H. Steven, Proc. Phys. Soc., **79**, 73(1962).
11. M. Sharnoff, J. Chem. Phys., **42**, 3383 (1965).
12. D. Rehorek, Ph. Thomas, E. Uhlemann, Z. Anorg. Allg. Chem., **396**, 59 (1973).
13. I. M. Prokter, B. J. Hathaway, P. Nicholls, J. Chem. Soc. A, 1678 (1968).
14. A. A. G. Thomlinson, B. J. Hathaway, J. Chem. Soc. A, 1685 (1968).
15. D. E. Billing, B. J. Hathaway, P. Nicholls, J. Chem Soc. A, 316 (1969).
16. O. Cozar, Thesis, Univ. of Cluj-Napoca, 1978.

E.S.R. INVESTIGATION OF SOME Cu(II) COMPLEX CYANATES IN SOLUTIONS

(S u m m a r y)

E.S.R. results obtained on the complex compounds [Cu(β-pic.)₂ (NCO)₂] and [Cu(γ-pic.)₂(NCO)₂] in chloroform and chloroform+pyridine mixtures are presented. The g $\simeq$ 4 signal proves that these complexes exist in a dimeric form too.

POUND WATKINS AUTODYNE ADAPTATION FROM JEOL-NMR INSTALATION TO THE NUCLEAR RESONANCE MEASUREMENTS IN ZERO FIELD

F. DÉNES, E. TĂTARU, V. SIMON and M. COLDEA

The existence in the magnetic ordered solids of a very large local magnetic field gives the possibility to obtain the NMR spectra in zero external magnetic field [1].

For local magnetic fields of the order 10^4 to 10^5 Gs, founded in such substances with 3d transition elements, the resonance condition $\omega = \gamma H_{loc.}$ gives for the resonance frequency values between 20 and 700 MHz [2, 3].

At a given temperature $H_{loc.}$ is constant, so for the registration of NMR spectra in zero field it is necessary to scan the frequency around the resonance value. After the first results reported on Co^{59}, Fe^{57} and Ni^{51} nuclei, the application area of this method has been very much extended, as a result of the information which can be obtained about the internal magnetic fields and about the nature and magnitude of different magnetic interactions.

The description of the NMR detector used in these experiments is to be found elsewhere [4—7]. The autodyne achieves at the threshold of oscillation a large sensitivity by the quality factor Q variations. In addition, in order to avoid the saturation phenomenon one can work with very small radiofrequency levels, while the modulation degree may be large enough.

Because the JEOL spectrometer autodyne is able to generate the radiofrequency fields in a large frequency range, we propose the adaptation to this autodyne of an electronic equipment which allows the continuous scanning of the frequency around a certain value.

With that end in view we realised the equipment given in fig. 1.

The resonance signal modulation and the slowly frequency scanning were realised by the adequate polarisation of two varicaps inserted parallel with the oscillant circuit of the autodyne. The capacities C_1 and C_2 have small values in order not to affect the quality factor Q and not to alter too much the frequency stability at the temperature fluctuations. The modulation frequency was 1 KHz and the deviation of the carrier frequency was 20 KHz.

The varicap D_2, which realises the modulation function, was removed from conduction range with an inverse dc voltage and transformed in a time variable capacitance with an AF signal. The varicap D_1 is biased with a slowly
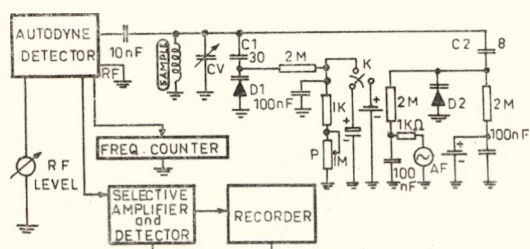
Fig. 1
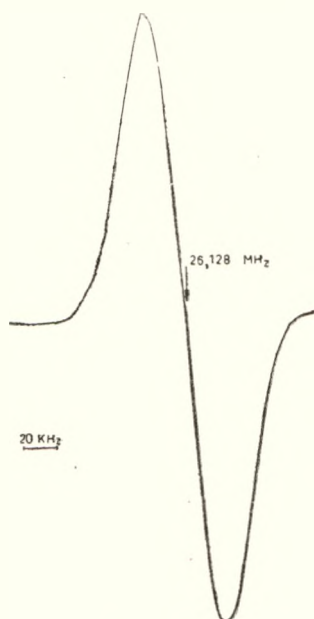
F i g. 2.
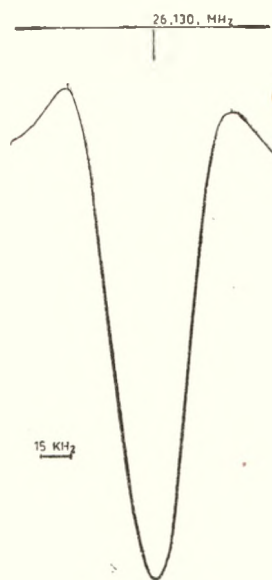
F i g. 3.

variable voltage, taken from the terminals of a condenser. The discharge time was regulated with the variable resistor P; in this way the frequency scanning range was 30—0.5 KHz/s. On a certain portion, this discharge provides practically a linear scanning in a suitable frequency range. The resistors have been so chosen that the capacities D_1 and D_2 were very small shunted. We used dc battery in order to avoid the noises due to the instability of the current source.

The commutator K allows the electrostatic charge of the condenser at the beginning of every recording.

In order to verify our equipment, we have made NMR measurements in zero field of Ni^{61} nuclei on Ni metallic powder, with 99.99% purity and dimensions less than 1 000 Å. The obtained results are compared with those reported by S t r e e v e r on a similar sample [8]. Figures 2 and 3 show our spectra on the first and second harmonics, from where one can see an excellent signal to noise ratio. The resonance frequency and the line width are as follows: 26.128 ± 0.002 MHz and 60 ± 15 KHz, in comparison with $26.127 \pm \pm 0,01$ MHz and 40 ± 10 KHz, obtained by S t r e e v e r [8] and A u b r u n [9]. One can see a very good agreement in resonance frequencies and a difference in the line width. The disagreement in the line widths may be assigned to a difference in the particle dimensions and thermal treatments.

NMR spectra are also recorded in external magnetic fields on this sample and our data reproduce the dependence $\nu(H_{ext})$ obtained by A u b r u n [9].

Our results confirm the adaptation possibility of the autodyne from a commercial spectrometer to the NMR measurements in zero field.

Since the parameters of autodyne oscillation circuit can be changed, it is also possible to obtain the signals from other nuclei in different magnetic ordered matrices.

On the other hand, our equipment may be used for pure quadrupolar resonance in those solids in which there is a very strong quadrupolar interaction (quadrupolar moment eQ and the gradient of electric field at the nuclei eq large enough).

REFERENCES

1. A. C. Gossard, A. M. Portis, Phys. Rev. Lett., **3**, 4, 164 (1959).
2. E. A. A. Turov, M. P. Petrov, *Ia. N. R. v fero i antiferomagnetikah*, Ed. Nauka, Moskva, 1969.
3. R. E. Watson, A. J. Freeman, Phys. Rev., **123**, 6, 2027 (1961).
4. H. Klever, D. Berschader, Rev. Sci. Instr., **44**, 1, 25 (1973).
5. I. Aslam, W. Weyhmann, Rev. Sci. Instr., **44**, 1, 71 (1973).
6. F. K. Davies, B, C. Mannig, Rev. Sci. Instr., **44**, 10, 1513 (1973).
7. W. R. Wampler, Rev. Sci. Instr., **46**, 1, 58 (1975) .
8. R. L. Streever, L. H. Bennett, Phys. Rev., **131**, 5, 2000 (1963).
9. J. N. Aubrun, Le Dang Khoi, CR, **263**, 3, B—249 (1966).

ADAPTAREA AUTODINEI DE LA INSTALAȚIA RMN-JEOL, PENTRU MĂSURĂTORI DE REZONANȚĂ ÎN CÎMP NUL

(Rezumat)

Se descrie adaptarea unui dispozitiv electronic la autodina Pound-Watkins din spectrometrul RMN-JEOL, care să permită înregistrarea rezonanței nucleare în cîmp nul.

ELECTRON SPIN RESONANCE OF Gd³⁺ IN B₂O₃—Li₂O—SiO₂ GLASS SYSTEM

S. SIMON, F. TOLEA, I. DUCA, AL. NICULA

I. **Introduction.** Since 1955, when for the first time S a n d s [1] studying the electron spin resonance of some transition metal ions in glassy hosts has evidenced in resonance spectra the presence of transitions at large values for $g_{eff} = \dfrac{h\nu}{\beta B}$, the number of works which present such results and the possibilities of their theoretical explanation has increased considerably.

The presence of resonances at large g_{eff} values was explained initially by C a s t n e r et al. [2], who assumed crystal field effects to be dominant in comparison with Zeeman term from the spin Hamiltonian, and the last one was treated as a perturbation. It was used the spin Hamiltonian

$$H = g_0 \beta \vec{B} \cdot \vec{S} + D\left[S_z^2 - \frac{1}{3} S(S+1)\right] + E(S_x^2 - S_y^2)$$

The Gd³⁺ ion was still studied (3—5) in various chalcogenide and silicate glasses, the resonance spectra presenting transitions at g_{eff} 2, 2.7 and 5.9. These large values for the g factors were explained considering that the Gd³⁺ ions are distributed in the glassy matrix in three types of sites characterized by crystal fields of different intensities and symmetries.

In order to explain the existence of large g_{eff} factors in the resonance spectra of Gd³⁺ ion in zeolites, T r i f and N i c u l a [6] presented theoretically all the possible transitions for the case of Gd³⁺ ion in strong crystal fields of different symmetries.

The purpose of the present paper is to give the results obtained by employing the electron spin resonance technique for Gd³⁺ ion included in B₂O₃—Li₂O—SiO₂ glass system, with the Gd₂O₃ concentration varying between 0.01 and 0.2 wt %.

The spectra are interpreted using the theory developed in the above mentioned papers.

II. **Experimental results.** In ESR spectra for the Gd³⁺ ion in a glassy matrix with the composition 80B₂O₃, 15Li₂O, 5SiO₂ (wt %), the Gd₂O₃ content for the different four samples being: I — 0.01%, II — 0.05%, III — 0.1% and IV — 0.2% (wt %), were recorded at room temperature, using a standard JEOL equipment, at 9.4 GHz.

In order to obtain the four samples with different Gd₂O₃ contents, the glassy matrix with the above given composition was first prepared and then this glass was very fine grinded and mixed in the wished proportion with Gd₂O₃.

The resulting powder was introduced into a furnace in Pt-crucibles, and maintained for five hours at 1200°C. At this temperature the melting was moved several times with a Pt-stick in order to obtain an homogeneous mass.
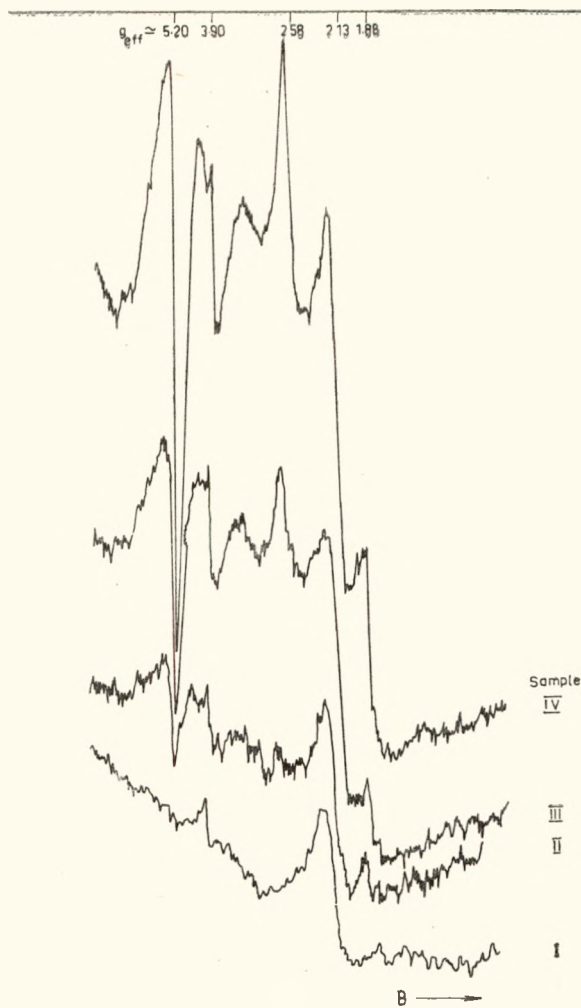
F i g. 1. Effect on ESR spectra of Gd_2O_3 content
in B_2O_3-Li_2O — SiO_2 glass system.

All the samples were quenched in air, at room temperature and the X-rays
spectra showed that they are in glassy phase.

Although Gd_2O_3 used contained as impurity 200 ppm Eu_2O_3 because
of the oxidizing medium where it lies, there was not Eu in S state which
could influence the resonance spectra. Also, the host-glass does not exhibit
paramagnetic resonant absorbtion.

The recorded spectra for the four samples are shown in fig. 1. One re-
marks that three resonance signals appear for the first sample at g = 2,1,
g = 2.7 and g = 3.9. In the limits of experimental errors one can estimate

that beginning with the sample II in addition to these three resonance transitions occur two more transitions at $g \simeq 1.88$ and $g \simeq 5.2$. The values of g-factors for the four samples are given in table 1.

Table 1

The g values of the Gd³⁺ spectra listed as a function of sample composition

Sample	Effective g values				
I	—	2.06	2.79	3.9	—
II	1.88	2.12	2.6	3.9	5.3
III	1.88	2.12	2.6	3.9	5.2
IV	1.88	2.13	2.58	3.9	5.2

III. **Discussion and conclusions.** While the interpretation case of resonance spectra of other paramagnetic ions (Fe^{3+}, Mn^{2+}, etc.) which are in different glassy matrices one starts from the assumption that these ions exist both in network forming sites and in network modifying sites the possibility to find Gd^{3+} in network forming site is eliminated because of its ionic radius much larger than that of the B^{3+} ion.

If Gd^{3+} ion would be considered only network modifier in a homogeneous random network, occupying similar sites without prefering certain symmetries, then the resonance spectra would be produced to a single large line. On the other hand, it is difficult to imagine the existence of several different sites for the Gd^{3+} ion in a homogeneous matrix. In view of a lot of other papers which evidence in this type of glasses the existence of at least two phases, one high in Li_2O content and other high in B_2O_3 content, it is to suppose that the glasses are not homogeneous first due to the inhomogeneous distribution of alkaline metal ions.

Such phases were observed by electronic microscopy on our samples too, making evident at the same time the existence of some transition regions between the two phases. The Gd^{3+} ion prefers the 6-or 8-fold coordination, which is easier to achieve rather by its arrangement in these transition regions than within the two phases.

From the g-factor values, given in table 1 and taking into account the theory developed to expound such values one can affirm that Gd^{3+} ions are placed in five independent sites.

Those corresponding to g-factors of 1.88 and 2.1 are cubic or rhombic-symmetry sites, the intensity of crystal field being small. The peak from $g = 2.7$ is due to the presence of Gd^{3+} ions in the transition regions wherein they are under the influence of an intermediate crystal field. The other two peaks from $g = 3.9$ and $g = 5.2$ are due to the Gd^{3+} ions placed in strong distorted sites, perhaps inside the two phases, with large values for the crystal field.

REFERENCES

1. R. H. Sands, Phys. Rev., **99**, 1222 (1955).
2. T. Castner, G. S. Newell, W. C. Holton, C. P. Slichter, J. Chem. Phys.. **32**, 668 (1960).
3. N. S. Garif'yanov and M. M. Zaripov, Sov. Phys. Solid State, **6**, 1209 (1964).
4. I.V. Chepeleva, V. N. Lazukin, S. A. Dembovski, Sov. Phys. Dokl., **11**, 864 (1967)
5. R. C. Niclin, J. K. Johnstone, R. G. Barnes, D. R. Wilder, J. Chem. Phys., **59**, 4, 1652 (1973).
6. E. Trif, Al. Nicula, Studia Univ. Babeş-Bolyai, ser. Phys., 1, 43 (1974).

REZONANŢĂ ELECTRONICĂ DE SPIN A Gd^{3+} ÎN SISTEMUL DE STICLĂ $B_2O_3 - Li_2O - SiO_2$

(R e z u m a t)

Sînt prezentate rezultatele obţinute prin studiul RES a Gd^{3+} într-o sticlă din sistemul $B_2O_3 -$ $- Li_2 O - SiO_2$, cu concentraţia Gd_2O_3 variind între 0,01 şi 0,2%. Se ajunge la concluzia că în această matrice ionul Gd^{3+}, atunci cînd concentraţia Gd_2O_3 este mai mare decît 0,05%, se distribuie în cinci poziţii independente caracterizate de cîmpuri cristaline de simetrie şi intensităţi diferite.

STUDIUL R.E.S. AL [Cu(trien)SCN]SCN ÎN APĂ ADSORBITĂ PE SiO₂

O. COZAR şi **V. ZNAMIROVSCHI**

1. Introducere. Cunoaşterea comportării cationilor metalici şi a complecşilor acestora pe suprafeţe, prezintă o deosebită importanţă datorită aplicaţiilor pe care le au în cataliză [1]. În general s-a urmărit determinarea poziţiilor ocupate de aceştia pe suprafaţa suport, precum şi obţinerea unor informaţii referitoare la simetria complecşilor şi influenţa moleculelor adsorbite asupra identităţii acestora [2—5]. S-a ajuns la concluzia că activitatea catalitică este puternic influenţată de gradul de dispersie al ionilor metalici [6], precum şi de gradul de ionicitate al legăturii metal-ligand [7].

În continuare ne propunem o extindere a acestor investigaţii analizînd comportarea complexului [Cu(trien)SCN]SCN în apă adsorbită pe SiO₂. Acesta are o configuraţie rombică D_{2h}, avînd ca stare fundamentală pentru electronul paramagnetic orbitalul d_{xy} [8].

Silicagelul folosit este fabricat de Mallinchrodt Chemical Works şi notat prin ARCC — 4/100—200. Suprafaţa sa specifică a fost măsurată prin adsorbţie de kripton şi este de 600 m²/g. Probele s-au obţinut prin impregnarea timp de o oră a pulberii de silicagel în soluţie apoasă de [Cu(trien)SCN]SCN, avînd concentraţia de 3 mg/cm³. După uscare ele au fost introduse în tuburi de sticlă şi închise. Conţinutul de apă s-a determinat gravimetric.

Măsurătorile RES s-au făcut cu un spectrometru JES—3B, lucrînd în banda X cu o modulaţie a cîmpului magnetic de 100 KHz.

2. Rezultate experimentale. Spectrele RES obţinute la temperatura camerei în apă prezintă rezolvate cele patru componente de structură hiperfină ale ionului Cu²⁺ (fig. 1). Parametrii acestui spectru sînt $g_0 = 2,077$ şi $A_0 = 72,5$ gauss. Scăzînd temperatura se observă o dispariţie a structurii hiperfine, obţinîndu-se la —15°C o singură linie largă, relativ simetrică, cu $g_0 = 2,075$, valoare aproape egală cu cea anterioară.

Situaţia se modifică în cazul apei adsorbite pe SiO₂. Pentru probe A cu apă în exces (peste 10 monostraturi de apă), la temperatura camerei se obţine un spectru similar cu cel din apa pură (fig. 2). Scăzînd însă temperatura la —15°C spectrul RES devine asemănător cu cel din soluţiile apă etanol la 77 K conţinînd peste 10% C₂H₅OH [8], unde structura hiperfină din banda paralelă ($g_{||}$) este bine rezolvată (fig. 2).

Micşorînd apoi conţinutul de apă pînă la 2—3 monostraturi (probe B), apare la temperatura camerei un spectru (fig. 3a) diferit de cele obţinute pînă acuma, care este rezultatul suprapunerii unui spectru caracteristic fazei lichide, parţial mediat datorită
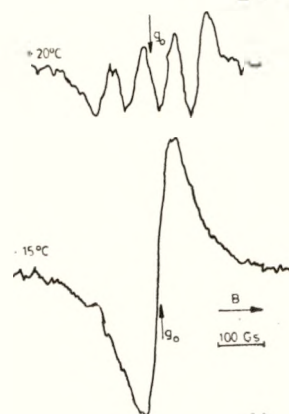

F i g. 1. Spectrele RES ale [Cu (trien) SCN]⁺ în apă, la concentraţia de 3 mg/cm³.
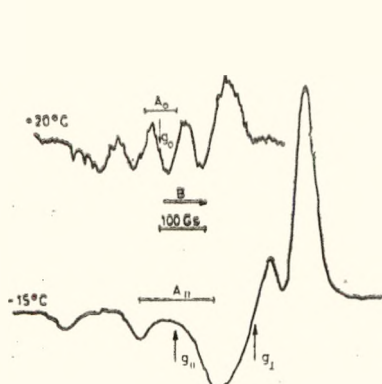
Fig. 2. Spectrele RES ale [Cu (trien) SCN]+ adsorbit pe SiO₂ (probă A — cu apă în exces).
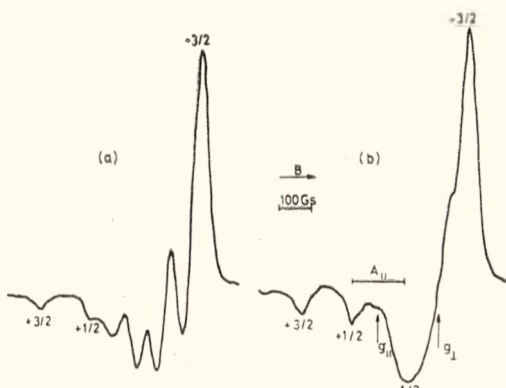
Fig. 3. Efectul deshidratării asupra spectrelor RES ale [Cu (trien) SCN]+ adsorbit pe SiO₂: (a)-probă B(∼ 2—3 monostraturi apă), (b)--probă C(∼ 1 monostrat).

mişcării de rostogolire a complexului, şi unul tipic fazei solide, cînd complexul este fixat de suprafaţă. Acest din urmă caz fiind obţinut (fig. 3b) printr-o deshidratare suplimentară la ∼ 1 monostrat de apă (probă C). Datorită cantităţii reduse de apă complexul de dimensiuni mari devine practic fixat pe suprafaţa de silicagel, nu mai poate executa mişcări de rostogolire, iar tensorii $\tilde{g}$ şi $\tilde{A}$ nu sînt astfel mediaţi încît spectrul RES devine analog cu cel din faza îngheţată la −15°C (fig. 2).

Aşa cum s-a remarcat anterior [9, 10], cantitatea de apă mobilă adsorbită pe SiO₂ poate fi modificată fie prin variaţia cantităţii totale de apă adsorbită, fie prin răcirea continuă a unei probe cu un conţinut mare de apă.

3. Discuţii şi concluzii. Deosebirea esenţială ce apare între spectrele RES din apă şi apă adsorbită pe SiO₂ în exces, este aceea a dispariţiei în primul caz a structurii hiperfine prin îngheţare. Acest fapt poate fi atribuit îngheţării sub formă policristalină a apei pure, şi a formării unor „aglomerări" ale moleculelor de complex în matricea îngheţată [11].

În cazul apei adsorbite pe SiO₂ aceasta îngheaţă sub formă vitroasă [10, 12], formîndu-se o reţea structurală puternică care nu mai permite formarea unor „aglomerării" ale moleculelor de complex.

Se obţin astfel spectre caracteristice ionilor „izolaţi" cu structură hiperfină bine rezolvată.

Dacă probele au un conţinut mare de apă (peste 10 monostraturi) la temperatura camerei complexul se comportă ca în soluţii de apă pură. Există suficientă apă (liberă) mobilă încît complexul se poate rostogoli liber, rezultînd astfel un spectru mediat destul de omogen (fig. 2).

Scăzînd cantitatea de apă adsorbită (2—3 monostraturi), aceasta devine mai legată de suprafaţă, viscozitatea sa creşte, iar mişcarea complexului este frînată încît nu mai are loc o mediere completă a tensorilor $\tilde{g}$ şi $\tilde{A}$. Putem considera de data aceasta coexistenţa a două tipuri de complecşi [13]. Unii

situați în apropierea suprafeței, legați puternic de aceasta, care dau un spectru caracteristic fazei solide, înghețate. Alții, care pătrund în porii sau cavitățile silicagelului unde rămîne apă în exces, pot efectua încă mișcări de rostogolire, dînd astfel un spectru caracteristic fazei lichide. Prin suprapunerea acestor două tipuri de spectre rezultă cel din fig. 3a.

Cînd cantitatea de apă adsorbită este redusă la ~1 monostrat, aceasta este puternic legată de suprafață și la fel moleculele de complex încît putem vorbi de o fază solidă, inertă, chiar la temperatura camerei. Forma acestui spectru rămîne neschimbată prin înghețare la 77 K, ceea ce indică că structura complecșilor și a matricei nu se mai modifică semnificativ. Acest lucru este demonstrat și de valorile tensorilor $\bar{g}$ și $\bar{A}$ care rămîn practic constante (tabel 1).

Tabel 1

Parametrii RES și coeficienții MO pentru [Cu(trien)SCN]⁺ adsorbit pe SiO₂

Proba	T	$g_{||}$	$g_\perp$	$\dfrac{\|A_{||}\|}{(10^{-4}\mathrm{cm}^{-1})}$	α^2	β^2	δ^2
A	−15°C	2,169	2,055	168,4	0,65	0,55	0,86
C	+21°C	2,180	2,047	182,2	0,74	0,52	0,64
C	−196°C	2,183	2,047	183,3	0,74	0,52	0,64

Menționăm de asemenea că în cazul probelor deshidratate C prin înghețare la 77 K are loc o ,,clusterizare'' a moleculelor de complex, fapt dovedit în spectrele RES prin suprapunerea peste spectrul ionilor ,,izolați'' a unei linii largi, aceasta datorîndu-se interacțiilor dipolare dintre doi sau mai mulți ioni Cu²⁺[14].

Situațiile anterioare pot fi obținute și prin scăderea temperaturii pe o probă cu apă în exces, aceasta conducînd la formarea în imediata vecinătate a cationului a ,,liquid cage''-ului înconjurat de ghiață [12]. Aici complexul mai are încă o oarecare posibilitate de rostogolire, dar datorită dimensiunilor mari ale complexului înghețarea completă se produce destul de repede (la —15°C) față de cazul complexului [Cu(H₂O)₆]²⁺ cînd înghețarea completă are loc abia la −40°C [10].

Coeficienții MO caracteristici complexului pot fi evaluați după procedeul descris în lucrarea [8]. Starea fundamentală și principalele stări excitate caracteristice electronului paramagnetic sînt :

$$|B_{1g}\rangle = \alpha d_{xy} - \alpha' \Phi_\sigma(xy) \tag{1}$$

$$|A_g\rangle = \beta d_{x^2-y^2} - (1 - \beta^2)^{1/2} \Phi_\pi(x^2 - y^2) \tag{2}$$

$$|B_{2g}\rangle = \delta_1 d_{xz} - (1 - \delta_1^2)^{1/2} \Phi_\pi(xz) \tag{3}$$

$$|B_{3g}\rangle = \delta_2 d_{yz} - (1 - \delta_2^2)^{1/2} \Phi_\pi(yz) \tag{4}$$

Presupunînd în continuare că $\delta_1 = \delta_2 = \delta$, $g_z = g_{||}$ și $g_x = g_y = g_\perp$, coeficienții α^2, β^2, δ^2 pot fi calculați din relațiile :

$$\alpha^2 = \frac{4}{7}\left[\frac{|A_{||}|}{P} - \frac{|A|}{P} + \frac{3}{2}g_{||} - \frac{5}{21}g_\perp - \frac{6}{7}\right] \tag{5}$$

$$g_{||} = 2,002 - \frac{8\lambda}{\Delta_{x^2-y^2}}\alpha^2\beta^2 \tag{6}$$

$$g_\perp = 2,002 - \frac{2\lambda}{\Delta_{xz}}\alpha^2\delta^2 \tag{7}$$

unde : $\lambda = -828\,cm^{-1}$, $P = 0,036\,cm^{-1}$, $\Delta_{x^2-y^2} = 14.100\,cm^{-1}$ și $\Delta_{xz} = 16.800\,cm^{-1}$.

Analizînd rezultatele din tabelul 1 se constată o covalență mai puternică a legăturii σ pentru probele $A(\alpha^2 = 0,65)$ decît pentru cele deshidratate $C(\alpha^2 = 0,74)$. Acest fapt poate fi atribuit unei extensii în cel de al doilea caz a distanței interatomice metal-ligand. Datorită cantității reduse de apă, moleculele de complex sînt puternic fixate de suprafață, aceasta manifestînd o tendință de „întindere" asupra lor. Moleculele de complex sînt astfel fixate în poziții rigide care nu se mai modifică aproape deloc prin înghețare la 77 K, gradul de covalență al legăturii σ rămînînd același ($\alpha^2 = 0,74$).

Spre deosebire de aceasta, covalența legăturilor π crește odată cu scăderea cantității de apă adsorbită.

Creșterea covalenței legăturii π în afara planului prin scăderea lui δ^2 de la 0,86 (proba A) la 0,64 (proba C) poate fi explicată prin lipsa moleculelor de apă care să coordineze pe direcția Oz, în mod analog cu situația din amestecurile apă-etanol [8].

BIBLIOGRAFIE

1. F. B a s a l o, R. L. B u r w e l l J r., *Catalysis Progress in Research*, Plenum, New York, 1973.
2. H. T o m i n a g a, Y. O n o, T. K e i i, J. Catal., **40**, 197 (1975).
3. B.J. H a t h a w a y, C. E. L e w i s, J. Chem. Soc., **A 2295** (1969).
4. J. H. A n d e r s o n J r., J. Ctatal., **28**, 76 (1973).
5. V. A. B o g d a n o v, V. A. S v e ț, V. B. K a z a n s k i, Kinet. i Katal., **15**, 176 (1974).
6. P. A. B e r g e r, J. F. R o t h, J. P h y s. Chem., **71**, 4307 (1967).
7. S. T s u r u y a, T. Y o n e z a w a, H. K a t o, J. Phys. Chem, **78**, 811 (1974).
8. O. C o z a r, V. Z n a m i r o v s c h i, I. H a i d u c, J. Molec. Struct., **31**, 153 (1976).
9. R. T. P e a r s o n, W. D e r b y s h i r e, J. Coll. Inter. Sci., **46**, 232 (1974).
10. O. C o z a r, V. Z n a m i r o v s c h i, V. V. M o r a r i u, Rev. Roum. Phys., **21**, 579 (1976).
11. S. F u j u w a r a, S. K a t s u m a t a, T. S e k i, J. Phys. Chem., **71**, 115 (1967).
12. L. B u r l a m a c c h i, J. Chem. Soc. Faraday II, 54 (1975).
13. O. C o z a r, V. Z n a m i r o v s c h i, V. V. M o r a r i u, Proc. Congr. Ampere Tallin-U.R.S.S. (1978).
14. R. D e e n, P. I. Th. S c h e l t u s, G. d e V r i e s, J. Catal., **41**, 218 (1976).

E.S.R. STUDY OF [Cu(trien)SCN]SCN IN ADSORBED WATER ON SiO₂

(S u m m a r y)

It has been found that the amount of adsorbed water on silica surface is responsible for the shape of the ESR spectrum of [Cu(trien) SCN] SCN.

Also, with the diminution of the adsorbed water amount on the silica surface the covalency degree of the σ — bond decreases.

By freezing at 77 K a clustering effect of the complexes was noticed.

HIGH TEMPERATURE PHASE TRANSITION OF KH_2PO_4 STUDIED BY N.M.R.

AL. NICULA, M. PETEANU, C. HĂGAN

In 1965, I m r y, P e l a h and W i e n e r [1] conclude theoretically the existence of two phase transition points in KDP, which correlate each other. They identified these points as being the Curie point (T = 123 K) and the melting, or dissociation, point. The theory suggest the rise of the dielectric constant near the melting point, corresponding to the Curie-Weiss behaviour in the Curie point vicinity.

Important theoretical contribution concerning the hydrogen bonds is due to R e i d [2] which showed that the double minimum potential asymmetry is monotone rising with the O—O distance.

Grindberg and L e v i n [3] reported the experimental identification of a high temperature phase transition in KDP and DKDP, according to the theory. The transition point is distinct from the melting point and it precedes this one. At this transition point sharp changes in the dielectric constant and I.R. spectra were oberved. This transition takes place at about 180°, and it is followed by the substance decomposition.

B l i n c, D i m i c and K o l a r [4] verify the existence of a high temperature transition preceding the melting point, by means of thermogravimetrical measurements (TGA) and differential thermal analysis (DTA). The DTA data reveal two endothermal reactions. The first endothermal maximum corresponds to a structural change resulting from a specific heat anomaly, in the same temperature range as the dielectric anomaly reported by P e l a h [1], while the second, much stronger, extends over the thermal decomposition range, according to TGA data. From their experiments, using a heating rate of 300°C/ hour, Blinc measured the average temperature at the beginning of this change as being 171°C, and the endothermal minimum at 188°C. The DTA and TGA combined data demonstrate that the high temperature phase transition in KDP takes place before the thermal decomposition.

This paper refers to our studies by means of proton resonance of the high temperature phase transition in KDP, trying to obtain information about the molecular motions and their changes when passing through the transition point. The nuclear spin of the proton is $I = 1/2$ but it has no quadrupol electric moment, so the information obtained using the proton resonance in solid are more limitated compared with those given by the deuteron magnetic resonance. The parameters measured by means of proton resonance are the shape and the moments of the line, and the spin-lattice relaxation time, T_1.

Using a broad band spectrometer we studied the temperature dependence of the line width. Our sample was powdered KH_2PO_4 having crystallites of about 0.1—0.2 mm. The spectra were recorded at 23 Mc/sec, over a temperature range of 29—210°C. The temperature dependence of line width (plotted as ratio of the actual line width against the width of the signal recorded at
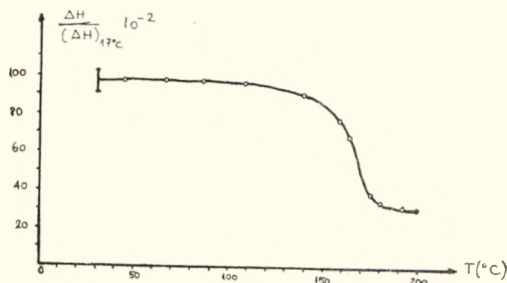
F i g. 1. Temperature dependence of the line width for the proton resonance signal of powdered KDP.

room temperature) with the temperature, is given in figure 1. One can see, that at small temperatures the line width is almost constant, the $\dfrac{\Delta H}{(\Delta H)_{R.T.}}$ ratio tending to unity. At room temperature the line width is 2.8 gauss. The signal begins to narrow at about 90°C, showing a slow protonic movement of high amplitude caused probably by the thermal excited tetrahedra rotation about one of their axes. At about 154°C the line width is 1.5 gauss and up to this temperature a visible narrowing of the signal takes place, the line width reducing to 0.8 gauss. From our temperature dependence (fig. 1) one can approximate that the transition is centered at about 170 ± 3°C. The concordance with already reported data, obtained as resulting from different experimental methods, is evident. The transition takes place, as we attempted, before the thermal decomposition point of the sample (at 210°C). The line narrows when the correlation frequency of the local field fluctuations becomes of the same order as the line width corresponding to the ,,rigid'' lattice, given in frequency units. The only type of movement which can produce an averaging in the dipolar broadening is the hydrogen autodiffusion. The line narrowing domain depends on the movement rate, as can be seen from the BPP [5] and K u b o, T o m i t a [6] theories. The movement rate described by the correlation frequency ν_c, which can be estimated from the line width δH partially narrowed, using the formula derived from the BPP equation :

$$\nu_c = 2(2ln2)^{1/2} \, \Delta\nu/\tan[\pi(\delta H/\delta H_0)^2/2]$$

where $\Delta\nu$ is the observed line width, in frequency units (c/sec), and δH_0 is the line width for the rigid lattice, in gauss. This equation is applicable only for gaussian shapes of line in the low temperatures limit. For τ estimation, the equation becomes :

$$\tau = \left| \frac{4ln2}{\pi\gamma\Delta H} \right| \tan\left[\frac{\pi}{2} \left(\frac{\Delta H}{\Delta H_0} \right)^2 \right]$$

where $\gamma = \gamma_{proton} = 2.6753 \times 10^4$ Hz/gauss (or sec^{-1}/gauss). From the temperature dependence of the line width experimentally otained, we can obtain the τ_c temperature dependence, using the above equation.

Writing $\tau = \tau_0 \exp (E_a/kT)$

where E_a is the activation energy, and logarithmating the relation we obtain

$$\ln\tau = \ln\tau_0 + E_a/kT$$

or $\ln\tau = \ln\tau_0 + E_a/RT$

where $R = kN_0 = 8.31 \dfrac{J}{mol \cdot K} = 8.31 \times 0.24 \dfrac{Cal}{mol \cdot K}$

Plotting $\ln \tau = f(1/T)$ we obtain (fig. 2) in the transition region, a linear dependence, the slope being

$$\tan \alpha = \frac{E_a}{R}$$

The activation energy thus obtained is $E_a = 15.363$ kcal/mol in agreement with the values calculated by spin-lattice relaxation and electric conductivity.

The line moments of protonic absorption may be calculated using the Van Vleck's results concerning the dipolar broadening of a rigid lattice.

For a powdered sample, the relation for the second moment is

$$M_2 = \frac{3}{5} \gamma^2 \hbar^2 I(I+1) \sum_{i>k} r_{ik}^{-6}$$

where I is the protonic spin, and r_{ik} the separation between the protons i and k.

F i g. 2. Plot of $\ln \tau$ versus $1/T$.

The moments of our signal, corresponding to the lowest value of temperature, that is in the rigid lattice approximation are

$$M_2 = 1.3216$$

$$M_4 = 5.4250$$

and their ratio : $M_4/M_2^2 = 3.1061$, which confirm the gaussian character of the line shape.

By substituting in the second moment expression the experimental values of M_2, we can estimate the structural parameter r. Supposing that the interaction concerns two OH groups, that is $N = 2$, by using the approximation

$$M_2 = 720 \frac{1}{N} \sum_{j>k} r_{ik}^{-6}$$

we obtain for r the value of 2.546 Å, representing the proton-proton distance.

REFERENCES
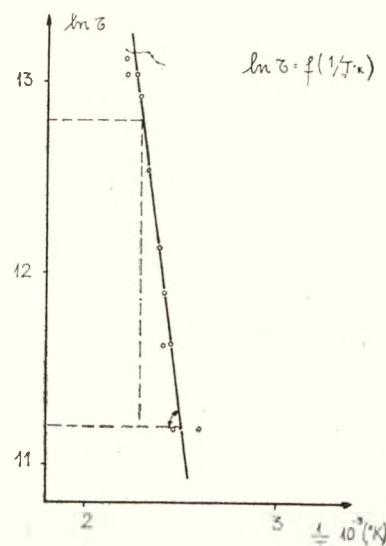
1. Y. I m r y, I. P e l a h, E. W i e n e r, J. Chem. Phys., **43,** 2332 (1965).
2. C. R e i d, J. Chem. Phys., **30,** 182 (1959).
3. J. G r i n d b e r g, S. L e v i n, Solid State Commun., **5,** 863 (1967).
4. R. B l i n c, V. D i m i c, D. K o l a r, J. Chem. Phys., **11,** 4996 (1968).
5. N. B l o e m b e r g e n, E. M. P u r c e l l, R. V. P o u n d, Phys. Rev., **73,** 679 (1948).
6. R. K u b o, K. T o m i t a, J. Phys. Soc. Japan, **9,** 888 (1954).

TRANZIȚII DE FAZĂ LA TEMPERATURĂ ÎNALTĂ ÎN KH_2PO_4
STUDIATE PRIN R.M.N.

(R e z u m a t)

Lucrarea reprezintă un studiu asupra tranziției de fază de la temperatură înaltă caracteristică KDP, folosind rezonanța protonică. Datele experimentale (dependența de temperatură a lărgimii liniei, de exemplu) oferă informații asupra mișcărilor moleculare și modificărilor structurale la trecerea prin punctul de tranziție.

IRRADIATION CENTERS IN K.D.P. SINGLE CRYSTALS

M. PETEANU, AL. NICULA and C. HĂGAN

The ESR study of electrons irradiated KH_2PO_4 single crystals performed by J e f f e r s et al [1] evidenced eight anisotrope resonant lines which may be associated in four pairs, each having 50 gauss splitting. This spectrum structure was explained by means of hiperfine interactions with phosphorous nuclei and protons. K o h i n [2] and later H u g h e s [3] proposed a radical OPO_3H^- resulting by one hydrogen atom losing from the $H_2PO_4^-$ ion. They consider the unpaired electron as having a small spin density on phosphorous atom, most of its orbital overlapping the p oxygen orbital. They reported a deviation of about 14° of the g tensor maximum eigenvalue from the P—O bond.

A more unitary explanation of the experimental results was done by T s u c h i d a et al [4] which studied the ESR spectra of irradiated KDP both in X and K band. By comparing the signal amplitudes in these two bands they concluded a line anisotropy due to the g tensor anisotropy and not to the hyperfine coupling with hydrogen atoms.

Our samples were grown by slow vaporisation from an aqueous KDP solution. The resulting single crystals showed all the qualities required by an ESR study : transparence, purity, suitable dimensions. The irradiation centers were induced in the crystal lattice by means of γ irradiation of the samples in the ^{60}Co source, during 3 hours. Because of the relatively short life-time of these centers, that is their instability, the irradiation was performed at liquid nitrogen temperature. The ESR spectra were recorded in ferroelectric phase (liquid nitrogen temperature) using the JES—3B spectrometer. The angular dependence of these spectra with respect of the static magnetic field axis was also performed.

When the magnetic field is lying in the ab plane the ESR spectrum consists of four doublets, the doublet splitting being of about 40 Gauss (fig. 1), while for the case when the magnetic field is parallel with the c axis the spectrum re-
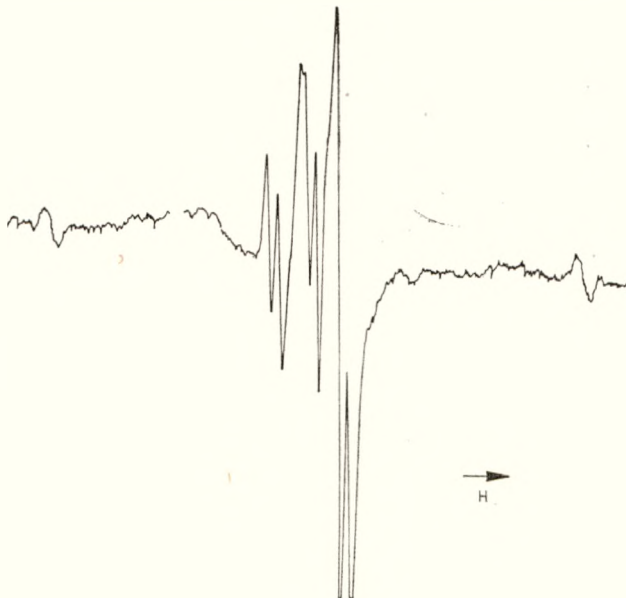
F i g. 1. ESR spectrum of KDP γ irradiated, when $H//a$.

duces to one doublet. Having in view the lattice structure of the KDP single crystal, one may explain the spectrum structure by means of the four spatial orientations of the P—O bond implied in the paramagnetic radical. It results the four doublets of the spectrum, the „doublet" character being a result of the hyperfine interaction of the unpaired electron and the phosphorous nuclear spin $(I = 1/2)$. The hyperfine splitting, and the hyperfine coupling constant reflects the covalent character of the P—O bond and the fact that the unpaired electron is located mainly on the oxygen ions. This explains the anisotropic character of the A tensor reported in [5].

As previously mentioned, the signals anisotropy is a consequence of the g tensor anisotropy. This results from the superposition of Zeeman and spin-orbit interactions. If an unpaired electron is located on a certain oxygen, this has five electrons and a hole in the 2p orbits. By forming the Slater determinant of the five electronic wave functions as total wave function, and using the second order perturbation theory, one obtains the principal values of the g tensor:

$$g_{xx} = 2; \; g_{yy} = 2 + \frac{2\lambda}{E_2 - E_0}; \; g_{zz} = 2 + \frac{2\lambda}{E_1 - E_0}$$

where λ is the spin-orbit coupling coefficient of the electron, and E_0, E_1, E_2 represent the energy levels of the five electrons and a hole in the orbitals φ_x, φ_y, φ_z of the oxygen, respectively.

Because $E_2 > E_1 > E_0$ and λ is positive, it follows $g_{zz} > g_{yy} > g_{xx} > 2$. The experimental values of our spectra recorded for H//a, respectively H//b verify the above inequalities; in fact $g_{xx} = 2.0207 \pm 0.005$ and $g_{yy} = 2.022 \pm \pm 0.005$.

Another feature of the angular dependence (fig. 2) is the deviation of the maximum extent directions of the resonance spectra (that is the g tensor axes) with 13° from the crystallographic axes a and b. That is due to the rotation of PO$_4$ tetrahedron with approx. 13° about the c axis.

In a polar coordinates system in which the polar axis coincides with c, the P—O bond direction after γ irradiation, was determined to be $\theta = 55°$ and $\varphi = 77°$ [4]. Because the P—O bond direction before irradiation is $\theta = 55°$, $\varphi = 61°$, the above-mentioned rotation is concludent. The PO$_4$ tetrahedron keeps its shape nonaltered. In fig. 3 is presented the atoms position in (001) plane after γ irradiation [5].

Besides the signals already discussed, there are

Fig. 2. Angular dependence of the ESR spectrum of γ irradiated KDP.
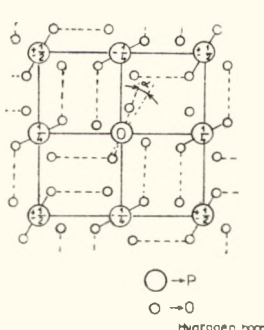
Fig. 3. Relative position of KDP atoms in a (001) plane, after irradiation.

two extreme placed peaks in the resonance spectrum, symmetrically placed with respect to the center (fig. 1). The separation between these extra peaks being of about 480 gauss, we may account these signals to the hyperfine interaction between the irradiation induced electron and the nuclear spin of hydrogen ($I = 1/2$). The fact that the ESR signals corresponding to this last type of centers do not show angular dependence (at least in the ab plane in which our measurements were made) indicates the occupancy of sites insensible to orientation.

REFERENCES

1. F. J e f e r s, P. E. W i g e n, J. A. C o w e n, Bull. Am. Phys. Soc., **6**, 118 (1961).
2. R. P. K o h i n, D. W. O v e n a l l, Bull. Am. Phys. Soc., **8**, 343 (1963).
3. W. E. H u g h e s, W. G. M u o l t o n, J. Chem. Phys., **39**, 1359 (1963).
4. K. T s u c h i d a, J. Phys. Soc. Japan, **35**, 2 (1973).
5. K. T s u c h i d a, R. A b e, J. Phys. Soc. Japan, **38**, 6 (1975).

CENTRII DE IRADIERE ÎN MONOCRISTALE K.D.P.

(R e z u m a t)

Lucrarea se referă la identificarea prin rezonanță electronică de spin a centrilor de iradiere de diferite varietăți produse în rețeaua cristalină a KDP în urma acțiunii radiației gamma asupra acesteia.

ON INSTABILITY OF CIRCULARLY POLARIZED ELECTROMAGNETIC WAVES IN THE RELATIVISTIC ELECTRON BEAM-PLASMA SYSTEM

J. KARÁCSONY

In a previous paper [1] we deduced the conditions under which circularly polarized electromagnetic waves may become unstable in the relativistic electron beam-plasma system. It was shown that a relativistic electron beam may excite a right-handed circularly polarized electromagnetic wave if:

a, the beam and the wave propagate in the opposite direction to that of the external magnetic field, and

b, there is a resonance between the cyclotron frequency of the electrons in the beam and the frequency of plasma waves [1].

In the present paper we will discuss the implications of the resonance condition.

Mathematically the resonance condition can be written as:

$$F_p(\omega, \ k) = 0 \tag{1}$$

and

$$\omega = k v_0 + \omega_c \gamma_0 \tag{2}$$

where

$$F_p(\omega, \ k) \equiv \omega^2 - k^2 c^2 - \frac{\omega_p^2 \ (\omega + k v_1)}{\omega + k v_1 - \omega_c} \tag{3}$$

Here we used identical notations to that of ref. [1].

The equation (1) requires that ω to be the root of the plasma dispersion equation, but, on the other hand, ω must vary with k in accordance with the expression (2).

Our aim is to find the ω frequencies which satisfy these requirements and, in addition, make $\partial F_p/\partial \omega$ negative. (The negative sign for $\partial F_p/\partial \omega$ is prescribed by condition a, [1].) For this purpose, we have to write k from (2) as:

$$k = \frac{\omega - \omega_c \gamma_0}{v_0} \tag{4}$$

Substituting this value of k in (3) we obtain the following equation to determine the frequencies of resonant waves:

$$F_p(\omega) \equiv -\frac{c^2 \gamma_0^2}{v_0^2} \omega^2 + 2 \frac{c^2 \gamma_0}{v_0^2} \omega_c \omega - \frac{c^2 \gamma_0^2}{v_0^2} \omega_c^2 - \omega_p^2 \frac{\omega (1 + \varepsilon) - \varepsilon \gamma_0 \omega_c}{\omega(1 + \varepsilon) - \omega_c(1 + \varepsilon \gamma_0)} = 0 \tag{5}$$

Now, it is convenient to introduce the dimensionless parameters:

$$x = \frac{\omega}{\omega_c} \ ; \quad \beta = \frac{v_0}{c} \quad \text{and} \ \alpha = \frac{\omega_p}{\omega_c}$$

The equation (5) then takes the form:

$$-\frac{\gamma_0^2}{\beta^2} x^2 + 2 \frac{\gamma_0}{\beta^2} x - \frac{\gamma_0^2}{\beta^2} - \alpha^2 \frac{x(1 + \varepsilon) - \varepsilon \gamma_0}{x (1 + \varepsilon) - (1 + \varepsilon \gamma_0)} = 0 \tag{6}$$

The analysis of eq. (6) is most readily effected by means of a graphical procedure. Thus the quantity

$$y \equiv f(x) = -\frac{\gamma_0^2}{\beta^2} x^2 + 2\frac{\gamma_0}{\beta^2} x -$$

$$\tag{7}$$

$$-\frac{\gamma_0^2}{\beta^2} - \alpha^2 \frac{x(1 + \varepsilon) - \varepsilon\gamma_0}{x(1 + \varepsilon) - (1 + \varepsilon\gamma_0)}$$

was plotted schematically in fig. 1. (Depending on the values of the parameters of the system, one may obtain a graph as given in fig. 1. or a similar graph — not shown here — where the branch to the right of the asymptote $y = (1 + \varepsilon\gamma_0)/(1 + \varepsilon)$ does not intersect the axis of abscissas).


F i g. 1.

The zeros of the function $f(x)$ satisfy the equation (6). It is clear from the figure that equation (6) has not negative roots. Therefore a relativistic electron beam cannot excite a right-handed circularly polarized electromagnetic wave in an electron plasma.

A similar graphical procedure could be given for the left-handed circularly polarized electromagnetic waves. In the latter case the corresponding graph would be obtained by reflecting the curve in fig. 1. about the vertical axis. The instability condition $\partial F_p/\partial\omega > 0$ for these waves [1] requires the existence of positive roots of the plasma dispersion equation. Because there are not such roots, a relativistic electron beam cannot excite left-handed circularly polarized electromagnetic waves in an electron plasma.

Consequently, a relativistic electron beam cannot excite high frequency circularly polarized electromagnetic waves, since one cannot obtain a resonance between an electron plasma wave and the electron gyrofrequency of the beam electrons. The instability of these waves needs, probably, the inclusion in the treatment of the ion motion.

R E F E R E N C E S

1. J. K a r á c s o n y, Studia Univ. Babeş-Bolyai, Phys., 2, 20 (1968).

DESPRE INSTABILITATEA UNDELOR ELECTROMAGNETICE CIRCULAR POLARIZATE ÎN SISTEMUL FASCICUL DE ELECTRONI RELATIVIŞTI-PLASMA

(R e z u m a t)

Se studiază condiţia de rezonanţă necesară exercitării undelor electromagnetice circular polarizate de către un fascicul de electroni relativişti şi se constată că în cazul oscilaţiilor de frecvenţă ridicată (oscilaţiile plasmei electronice) această condiţie nu este satisfăcută.
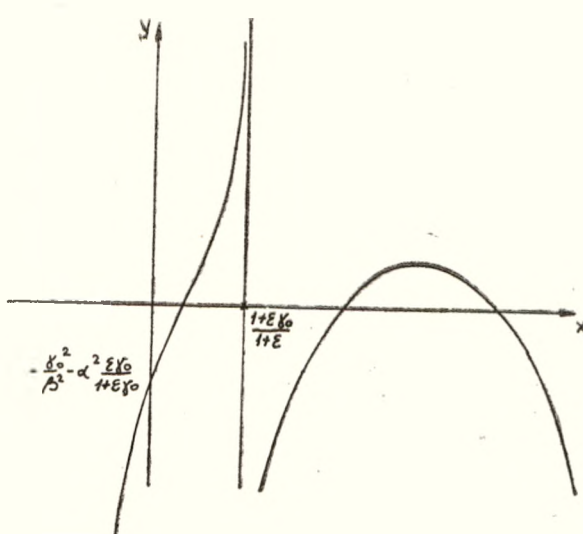
SUR L'ÉQUATION DE DISPERSION D'UN MODÈLE DE PLASMA COMPOSÉ (I)

MIRCEA VASIU

1. **Introduction.** Dans le présent mémoire nous voulons déduire l'équation de dispersion d'un modèle de plasma cosmique constitué d'un *composant ionique*, compressible, visqueux, en *mouvement de rotation*, doué d'une conductivité électrique finie et d'une pression anisotrope, sous l'action d'un champ magnétique uniforme et de son propre champ gravifique et d'un *composant neutre*, compressible, visqueux et sous l'action du même champ gravifique. On suppose que les vitesses du composant ionique et du composant neutre, dans l'état d'équilibre, sont nules $(\vec{v_0} = 0, \ \vec{v_{n_0}} = 0)$.

Nous choisirons comme système de référence le système de coordonnées cartésiennes Oxyz. Le composant ionique possède une vitesse angulaire $\vec{\Omega}$ dirigée d'après l'axe Oz $(\vec{\Omega}\ (0, 0, \Omega))$. À l'intérieur du plasma le champ magnétique a une seule composante dirigée d'après l'axe Ox $(\vec{B_0}(B_0, 0, 0))$. En même temps, nous admettons des variations de type adiabatique pour la pression cinétique du plasma.

Nous utilisons les résultats obtenus par B h a t i a [1], H e r r n e g g e r [2], C h h o n k a r, B h a t i a [3]. À la différence des travaux cités nous prenons en considération l'action de la vitesse angulaire sur le comportement du plasma étudié, mais en l'absence du courant Hall.

2. **Equations fondamentales pour l'état perturbé du plasma.** Pour le modèle de plasma considéré, le système d'équations magnéto-hydrodynamiques pour l'état perturbé du plasma s'écrit de la manière suivante :

$$\rho_0 \frac{\partial \vec{u}}{\partial t} = - \nabla(\delta \overleftrightarrow{P}) - \rho_0 \nabla(\delta V) + 2\rho_0 \vec{u} \times \vec{\Omega} +$$

$$\rho_0 \nu_c\ (\vec{u_n} - \vec{u}) + \frac{\tilde{\mu}}{3} \nabla(\nabla \cdot \vec{u}) + \tilde{\mu}\Delta\vec{u} + \frac{1}{4\pi}\ (\nabla \times \delta\vec{B}) \times \vec{B_0}, \tag{1}$$

$$\rho_{n_0} \frac{\partial \vec{u_n}}{\partial t} = - \nabla(\delta p_n) - \rho_{n_0}\nabla(\delta V) - \rho_0\nu_c(\vec{u_n} - \vec{u}) + \tilde{\mu}_n\Delta\vec{u_n} + \frac{\tilde{\mu}_n}{3} \nabla(\nabla \cdot \vec{u_n}), \tag{2}$$

$$\frac{\partial(\delta\rho)}{\partial t} = - \rho_0\nabla \cdot \vec{u}, \tag{3}$$

$$\frac{\partial(\delta\rho_n)}{\partial t} = - \rho_{n_0}\nabla \cdot \vec{u_n}, \tag{4}$$

$$\frac{\partial(\delta\vec{B})}{\partial t} = \nabla \times (\vec{u} \times \vec{B_0}) + \nu_m\Delta(\delta\vec{B}), \tag{5}$$

$$\Delta(\delta V) = 4\pi G(\delta\rho + \delta\rho_n). \tag{6}$$

où ρ_0 est la densité massique du composant ionique, $\vec{u}$ est la perturbation de la vitesse du composant ionique, $\delta \overleftrightarrow{P}$ est la perturbation du tenseur de pression du plasma, δV est la perturbation du potentiel gravifique, ν_c est la fréquence des collisions entre les ions et les atomes, $\vec{u}_n$ est la perturbation de la vitesse du composant neutre du plasma, $\tilde{\mu}$ est le coefficient de viscosité dynamique du composant ionique, $\delta \vec{B}$ est la perturbation du champ magnétique, δp_n est la perturbation de la pression du composant neutre, ρ_{n_0} est la densité massique du composant neutre, $\tilde{\mu}_n$ est le coefficient de viscosité dynamique du composant neutre, ν_m est le coefficient de viscosité magnétique du plasma, G est la constante gravitationnelle, ∇ est l'opérateur *nabla*, Δ est l'opérateur de Laplace.

Admettons que de petites perturbations se propagent dans le plasma sous la forme des ondes planes

$$\delta \varphi = \varphi^* \; exp[i(kz - \omega t)], \tag{7}$$

où $\delta \varphi$ est la perturbation d'une grandeur physique du plasma, φ^* est l'amplitude de la perturbation, $k = k_z$ est le nombre d'onde (le vecteur nombre d'onde $\vec{k}$ est dirige d'après l'axe Oz), ω est la pulsation. Les perturbations étant supposées petites, leurs carrés et leurs produits peuvent être négligés dans les calculs.

En tenant compte des égalités vectorielles

$$(\nabla \times \delta \vec{B}) \times \vec{B}_0 = (\vec{B}_0 \cdot \nabla)\delta \vec{B} - \nabla(\vec{B}_0 \cdot \delta \vec{B}) =$$

$$= B_0 \frac{\partial(\delta \vec{B})}{\partial x} - B_0 \nabla(\delta B_x),$$

$$\tag{8}$$

$$\nabla \times (\vec{u} \times \vec{B}_0) = (\vec{B}_0 \cdot \nabla)\vec{u} - \vec{B}_0 \nabla \cdot \vec{u},$$

$$\vec{u} \times \vec{\Omega} = \vec{\varepsilon}_x u_y \, \Omega - \vec{\varepsilon}_y u_x \Omega,$$

de la forme (7) pour les perturbations, introduisant les vecteurs de déplacement infinitésimal ξ et ξ_n de sorte que

$$\vec{u} = \frac{\partial \vec{\xi}}{\partial t} = -i\omega \vec{\xi} \tag{9}$$

et

$$\vec{u}_n = \frac{\partial \vec{\xi}_n}{\partial t} = -i\omega \vec{\xi}_n, \tag{10}$$

le système des équations (1) — (6), en projection sur les axes Ox, Oy, Oz, prend la forme

$$[\omega^2 + i\omega(\nu_c + k^2 \tilde{\nu})]\xi_x - 2i\omega\Omega\xi_y = \frac{1}{\rho_0} \frac{\partial(\delta P_{13})}{\partial z} + i\omega\nu_c \xi_{nx}, \tag{11}$$

$$2i\omega\Omega\xi_x + [\omega^2 + i\omega(\nu_c + k^2\tilde{\nu})]\xi_y = \frac{1}{\rho_0}\frac{\partial(\delta P_{23})}{\partial z} + i\omega\nu_c\xi_{ny}, \tag{12}$$

$$\left[\omega^2 + i\omega\left(\nu_c + \frac{3}{4}k^2\tilde{\nu}\right)\right]\xi_z = \frac{ikv_s^2}{\rho_0}\delta\rho + ik\delta V + \frac{1}{\rho_0}\frac{\partial(\delta P_{33})}{\partial z} +$$

$$+ \frac{ikB_0}{4\pi\rho_0}\delta B_x + i\omega\nu_c\xi_{nz}, \tag{13}$$

où $\delta p = v_s^2\delta\rho$, $v_s^2 = \gamma p_0/\rho_0$ est la vitesse du son dans le composant ionique, $\tilde{\nu} = \tilde{\mu}/\rho_0$ et

$$[\bar{\rho}_n\omega^2 + i\omega(\nu_c + k^2\tilde{\nu}_n)]\xi_{nx} = i\nu_c\omega\xi_x, \tag{14}$$

$$[\bar{\rho}_n\omega^2 + i\omega(\nu_c + k^2\tilde{\nu}_n)]\xi_{ny} = i\nu_c\omega\xi_y, \tag{15}$$

$$\left[\bar{\rho}_n\omega^2 + i\omega\left(\nu_c + \frac{4}{3}k^2\tilde{\nu}_n\right)\right]\xi_{nz} = i\nu_c\omega\xi_z + i\bar{\rho}_n k\delta V + \frac{ik}{\rho_0}v_{ns}^2\delta\rho_n, \tag{16}$$

où $\bar{\rho}_n = \rho_{n_0}/\rho_0$, $\tilde{\nu}_n = \tilde{\mu}_n/\rho_0$, $v_{ns}^2 = \gamma p_{n_0}/\rho_{n_0}$ est la vitesse du son dans le composant neutre du plasma et

$$i\delta\rho = k\,\rho_0\xi_z, \tag{17}$$

$$i\delta\rho_n = k\,\rho_{n_0}\xi_{nz}, \tag{18}$$

$$(\nu_m k^2 - i\omega)\,\delta B_x = -\,B_0\,k\omega\xi_z, \tag{19}$$

$$\delta B_y = 0, \tag{20}$$

$$\delta B_z = 0, \tag{21}$$

$$\delta V = -\,\frac{4\pi G}{k^2}(\delta\rho + \delta\rho_n). \tag{22}$$

Il est a remarquer que les composants de la perturbation du tenseur $\delta\overleftrightarrow{P}$ s'écrivent sous la forme [3]

$$\delta P_{11} = \delta p;\ \ \delta P_{12} = \delta P_{21} = -2\rho_0\nu\left(\frac{\partial u_x}{\partial z} + \frac{\partial u_z}{\partial x}\right);$$

$$\delta P_{13} = \delta P_{31} = 2\rho_0\nu\left(\frac{\partial u_x}{\partial y} + \frac{\partial u_y}{\partial x}\right);\ \ \delta P_{22} = \delta p - \rho_0\nu\left(\frac{\partial u_z}{\partial y} + \frac{\partial u_y}{\partial z}\right); \tag{23}$$

$$\delta P_{23} = \delta P_{32} = \rho_0\nu\left(\frac{\partial u_y}{\partial y} - \frac{\partial u_z}{\partial z}\right);\ \ \delta P_{33} = \delta p + \rho_0\nu\left(\frac{\partial u_z}{\partial y} + \frac{\partial u_y}{\partial z}\right)$$

ν est la gyroviscosité du composant ionique du plasma.
Tenant compte de (7), de (17) — (23), les égalités (11) — (13) et (16) deviennent

$$[\omega^2 + i\omega(\nu_c + k^2\tilde{\nu})]\xi_x - 2i\omega\Omega\xi_y = i\nu_c\omega\xi_{nx}, \tag{24}$$

$$2i\omega\Omega\xi_x + [\omega^2 + i\omega(\nu_c + k^2\tilde{\nu})]\xi_y + i\nu k^2\omega\xi_z = i\nu_c\omega\xi_{ny}, \tag{25}$$

$$- i\nu k^2\omega\xi_y + \left[\omega^2 + i\omega\left(\nu_c + \frac{4}{3}k^2\tilde{\nu}\right) - (k^2v_s^2 - 4\pi G\rho_0) + \frac{ik^2v_A^2\omega}{\nu_m k^2 - i\omega}\right]\xi_z =$$

$$= (i\nu_c\omega - 4\pi G\rho_{n_s})\xi_{ns}$$

$$\left[\tilde{\rho}_n\omega^2 + i\omega\left(\nu_c + \frac{4}{3}k^2\tilde{\nu}_n\right) - \tilde{\rho}_n(k^2v_{ns}^2 - 4\pi G\tilde{\rho}_n\rho_0)\right]\xi_{nz} = (i\omega\nu_c - 4\pi G\rho_{n_s})\xi_z. \tag{27}$$

Introduisons maintenant les notations suivantes

$$A = 2i\Omega\omega, \ \ C = i\nu k^2\omega \ ; \ \ D^2 = \omega^2 + i\omega(\nu_c + k^2\tilde{\nu}),$$

$$D_n^2 = \tilde{\rho}_n\omega^2 + i\omega(\nu_c + k^2\tilde{\nu}_n) \ ; \ \ E^2 = \omega^2 + i\omega\left(\nu_c + \frac{4}{3}k^2\tilde{\nu}\right),$$

$$E_n^2 = \tilde{\rho}_n\omega^2 + i\omega\left(\nu_c + \frac{4}{3}k^2\tilde{\nu}_n\right) \ ; \ \ \Omega_c = i\nu_c\omega, \tag{28}$$

$$\Omega_J^2 = k^2v_s^2 - 4\pi G\rho_0 \ ; \ \ \Omega_{Jn}^2 = \rho_n(k^2v_{sn}^2 - 4\pi G\rho_{n_s})$$

$$\Omega_G = i\nu_c\omega - 4\pi G\rho_{n_s} \ ; \ \ \Omega_{in}^2 = \nu_m k^2 - i\omega,$$

$$\Omega_A^2 = \frac{ik^2v_A^2}{\Omega_m^2} \ ; \ \ v_A^2 = \frac{B_0^2}{4\pi\rho_0}$$

où v_A est la vitesse Alfvén, les équations (24) — (27) et (14) — (15) s'écrivent sous la forme

$$D^2\xi_x - A\xi_y = \Omega_c\xi_{nx}, \tag{29}$$

$$A\xi_x + D^2\xi_y + C\xi_z = \Omega_c\xi_{ny}, \tag{30}$$

$$- C\xi_y + (E^2 - \Omega_J^2 + \Omega_A^2)\xi_z = \Omega_G\xi_{nz}, \tag{31}$$

$$(E_n^2 - \Omega_{Jn}^2)\xi_{nz} = \Omega_G\xi_z, \tag{32}$$

$$D_n^2\xi_{nx} = \Omega_c\xi_x, \tag{33}$$

$$D_n^2\xi_{ny} = \Omega_c\xi_y. \tag{34}$$

En tenant compte des égalités (32) — (34), le système des équations (29) — (31) s'écrit sous la forme

$$\left(D^2 - \frac{\Omega_c^2}{D_n^2}\right)\xi_x - A\xi_y = 0, \tag{35}$$

$$A\xi_x + \left(D^2 - \frac{\Omega_c^2}{D_n^2}\right)\xi_y + C\xi_z = 0, \tag{36}$$

$$- C\xi_y + \left(E^2 - \Omega_J^2 + \Omega_A^2 - \frac{\Omega_G^2}{E_n^2 - \Omega_{Jn}^2}\right)\xi_z = 0. \tag{37}$$

3. L'équation de dispersion. L'équation de dispersion pour le modèle de plasma étudié s'obtient par l'annulation du déterminant formé par les coefficients des grandeurs ξ_x, ξ_y, ξ_z

$$\begin{vmatrix} D^2D_n^2 - \Omega_c^2 & -AD_n^2 & 0 \\ AD_n^2 & D^2D_n^2 - \Omega_c^2 & CD_n^2 \\ 0 & -C(E_n^2 - \Omega_{Jn}^2) & K^2(E_n^2 - \Omega_{Jn}^2) \end{vmatrix} = 0 \tag{38}$$

où $K^2 = E^2 - \Omega_J^2 + \Omega_A^2 - \dfrac{\Omega_G^2}{E_n^2 - \Omega_{Jn}^2}$. Faisant les calculs on obtient l'égalité

$$[(E^2 - \Omega_J^2 + \Omega_A^2)(E_n^2 - \Omega_{Jn}^2) - \Omega_G^2][(D^2D_n^2 - \Omega_c^2)^2 + A^2D_n^4] +$$
$$+ (D^2D_n^2 - \Omega_c^2)(E_n^2 - \Omega_{Jn}^2)C^2D_n^2 = 0 \tag{39}$$

Cette égalité représente l'équation de dispersion cherchée.

Cas particulier. En l'absence du mouvement de rotation ($A = 0$; $\Omega = 0$) l'équation de dispersion (39) se réduit à l'équation de dispersion obtenue par C h h o n k a r, B h a t i a [3] (pour le cas de la propagation transversale des perturbations).

BIBLIOGRAPHIE

1. P. B h a t i a, Astron. a. Astrophys., **1**, 399 (1969).
2. F. H e r r n e g g e r, J. Plasma Phys., **8**, 393 (1972).
3. R. C h h o n k a r, P. B h a t i a, J. Plasma Phys., **18**, 273 (1977).

ASUPRA ECUAŢIEI DE DISPERSIE A UNUI MODEL DE PLASMĂ COMPUSĂ (I)

(R e z u m a t)

În această lucrare autorul îşi propune să stabilească ecuaţia de dispersie pentru un model de plasmă constituită : dintr-o *componentă ionică*, compresibilă, vîscoasă, în *mişcare de rotaţie*, cu conductivitate electrică finită şi cu presiune anizotropă, sub acţiunea unui cîmp magnetic uniform şi a propriului său cîmp gravitaţional şi dintr-o *componentă neutră* (atomi neionizaţi), compresibilă, vîscoasă, sub acţiunea aceluiaşi cîmp gravific.

Aplicînd metoda micilor perturbaţii şi un procedeu de calcul analog cu cel utilizat de Chhonkar, Bhatia, autorul stabileşte ecuaţia de dispersie pentru modelul de plasmă analizat.

În cazul particular, al absenţei mişcării de rotaţie, ecuaţia de dispersie obţinută de autor se reduce la ecuaţia de dispersie obţinută de Chhlonkar, Bhatia (pentru cazul propagării transversale a perturbaţiilor din plasma analizată).

MEASUREMENT OF THERMAL CONDUCTIVITY OF HEAT INSULATORS BY A VARIABLE STATE METHOD

F. KELEMEN

Theoretical considerations. Ina previous paper [1] we have described a transient heating and cooling method which is suitable to determine the thermal conductivity on samples with small dimensions (approximately $1.5 \times 0.8 \times 0.8$ cm³) and with thermal conductivity of 10^{-1} to 10^{-3}Wcm^{-1}K^{-1}, in the temperature range from 100 to 450 K. According to this method the rectangular prism- or cylinder-like sample is fixed between two copper blocks. The lower block is continuously heated or cooled and the upper block is applied as a heat capacity standard. We have shown that in order to obtain the real value for thermal conductivity it is necessary to know or to determine the thermal resistance of the contacts between the sample and copper blocks, too.

Our present study of the thermal conductivity of some heat insulators (vitreous materials) indicates that the below specified heat losses of the heat capacity standard should also be taken into consideration (fig. 1):

a) dQ_2/dt, the heat current produced by the thermal conduction of the air surrounding the sample, when the pressure (p) in the device is higher than 10^{-3} torr; this heat loss is defined by

$$\frac{dQ_2}{dt} = K_a(S_0 - S) \cdot \frac{T_1 - T_2}{L},\qquad(1)$$

where K_a is the thermal conductivity of the air, S_0 the cross-sectional area of the block B_1, L the length of the sample P and S its cross-sectional area, T_1 and T_2 the temperatures of the blocks B_1 and B_2, respectively, at time t;

F i g. 1 *Heat losses of the heat capacity standard*
P — sample; B_1 — heat capacity standard (copperblock); B_2 — copper block; D — glass rod.

b) dQ_3/dt, the heat transmission per time unit caused by convection and radiation, defined by

$$\frac{dQ_3}{dt} = \alpha(S_0 + S_L - S_C) \cdot (T_1 - T_S),\qquad(2)$$

where α is the heat transfer coefficient, S_L the lateral surface of the block B_1, S_C the contact surface between B_1 and the glass rod D, and T_S the temperature of the surrounding air;

c) dQ_4/dt, the heat current flowing through the contact surface S_C, and defined by

$$\frac{dQ_4}{dt} = K_C S_C \cdot \frac{T_1 - T_D}{L_C},\qquad(3)$$

where K_C, S_C and L_C are the thermal conductivity, the cross-sectional area and the thickness, respectively, of contact layer between the

block B_1 and glass rod D, and T_D the temperature of the rod D at time t.

Taking into account these heat losses, the heat current flowing through the sample P is given by the equation:

$$\frac{dQ}{dt} = C_1 \cdot \frac{dT_1}{dt} \cdot \left(1 + \frac{C}{2C_1} \cdot \frac{dT_1 + dT_2}{dT_1}\right) - \left(\frac{dQ_2}{dt} + \frac{dQ_3}{dt} + \frac{dQ_4}{dt}\right), \qquad (4)$$

where C_1 and C signify the heat capacity of the block B_1 and the sample P, respectively, and dT_1 and dT_2 the temperature variations of the blocks B_1 and B_2, respectively, in the time dt [1].

From the equations (1) to (4) results that the thermal conductivity of the sample P is defined by

$$K = K_m - \left\{K_a \cdot \frac{S_0 - S}{S} + \left[\alpha(S_0 + S - S_C) \cdot \frac{T_1 - T_S}{T_1 - T_2} + K_C \cdot \frac{S_C}{L_C} \cdot \frac{T_1 - T_C}{T_1 - T_2}\right] \cdot \frac{L}{S}\right\}, \qquad (5)$$

where

$$K_m = \frac{LC_1}{S(T_1 - T_2)} \cdot \frac{dT_1}{dt} \cdot \left(1 + \frac{C}{2C_1} \cdot \frac{dT_1 + dT_2}{dT_1}\right). \qquad (6)$$

The equation (6) gives the thermal conductivity measured in the case when heat losses defined by equations (1) to (3) are neglected. If the pressure is lower than 10^{-3} torr, the thermal conductivity of the air is very reduced and, therefore, the first term in the bracket of equation (5) is negligible. The second term — mainly at low temperatures — is also negligible, because the heat transfer coefficient α at low pressures is proportional to the thermal conductivity of the air: $\alpha = \frac{Ka}{2d}$, where d means the diameter of the block B_1 [2]. Otherwise, if the cross-sectional area of the sample P and the block B_1 are comparable, i.e. $S \simeq S_0$, the sum of the terms in the bracket becomes proportional to the ratio $\frac{L}{S}$. Therefore, the measured thermal conductivity K_m, according to (5), may be written in the form

$$K_m = K_{m0} + A(T) \cdot \frac{L}{S}, \qquad (7)$$

where $A(T)$ is a quantity depending on the temperature $T = \frac{1}{2} \cdot (T_1 + T_2)$. In the limiting case, when the ratio $\frac{L}{S} = 0$, then $K_m = K_{m0}$. The quantity K_{m0} can be calculated from the equation (7), if measurements are made at least for two values of the ratio $\frac{L}{S}$, at temperature T. For amorphous materials or cubic crystals, these measurements can be carried out at two or three different positions of a rectangular prism-shaped sample, if its linear dimensions are different.
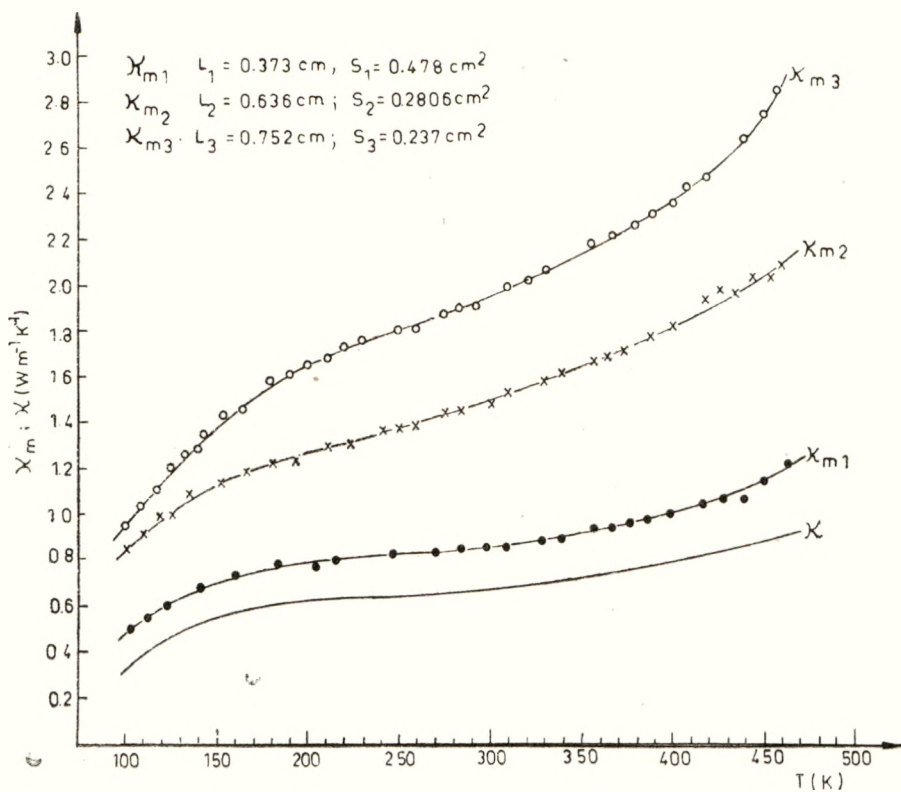
F i g. 2 *Measured and calculated thermal conductivity of the sample 1 of composition*
$3B_2O_3 \cdot PbO$ *versus temperature*
χ_{m_1}, χ_{m_2}, χ_{m_3} — the measured thermal conductivity for the three positions of the sample;
χ — the thermal conductivity calculated from equation (8).

Controlling measurements. The controlling measurements were performed on several glass samples, by means of the device already described [1]. The glass samples had the compositions: $x \cdot Fe_2O_3 + (1-x) \cdot (3B_2O_3 \cdot PbO)$ and the values of x for samples 1, 2, 3 and 4 were 0, 0.25, 0.35 and 0.50, respectively.

The coefficient K_m, measured at three positions of a rectangular prism-shaped sample of composition $3B_2O_3 \cdot PbO$ (sample 1) is represented as a function of temperature T in fig. 2. The linear dimensions of this sample are indicated in the figure.

Fig. 3 shows the variation of K_m as a function of the ratio $\dfrac{L}{S}$ for the mentioned sample. The points indicated in this figure are determined from the data of fig. 2. One can see that there is a linear relationship between K_m and $\dfrac{L}{S}$ for $T =$ constant.
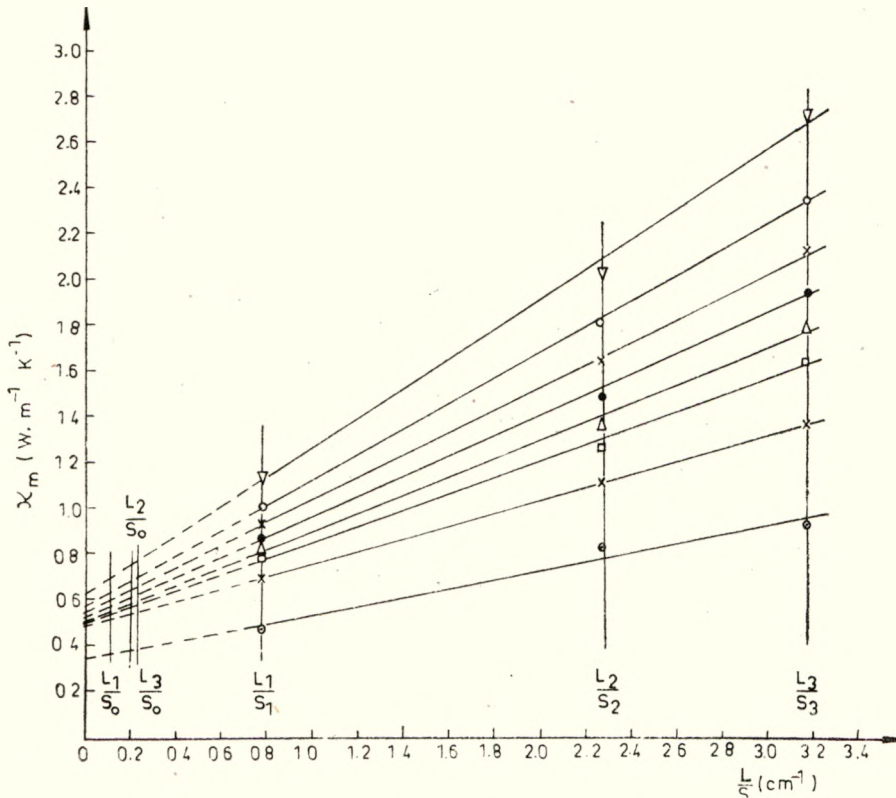
F i g. 3 *Variation of the measured thermal conductivity of the sample 1 versus the ratio*
$\frac{L}{S}$, *for different temperatures.*

The variation of the quantity $A(T)$ versus temperature T, for the four samples of different dimensions and compositions, is plotted in fig. 4. It is evident that $A(T)$ depends on the thermal conductivity of the samples.

Knowing the ratios $\frac{L_1}{S_0}$, $\frac{L_2}{S_0}$ and $\frac{L_3}{S_0}$, we can calculate the corresponding values of $K_m(K_{m01}, K_{m02}$ and $K_{m03})$ from equation (7). In this manner, from equation

$$K = \frac{L_j - L_i}{\dfrac{L_j}{K_{m0j}} - \dfrac{L_i}{K_{m0i}}} ,$$

(8)

proved in [1], by using the corresponding values of L_j, L_i, K_{m0j} and K_{m0i} (where $i = 1, 2$; $j = 2, 3$ and $i \neq j$), we can calculate the real value K of the thermal conductivity. This refers to the case, when the thermal resistance between the sample P and the block B_1, respectively B_2, is eliminated.
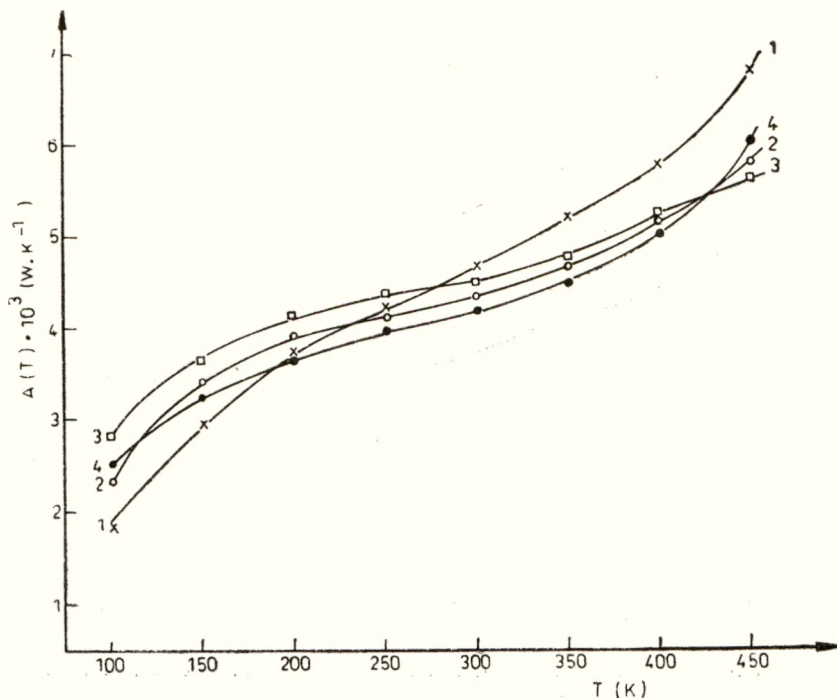
Fig. 4. *Variation of the quantity $A(T)$ versus temperature for four samples of different compositions and dimensions*

Compositions of samples: $x.Fe_2O_3 + (1-x) \cdot (3B_2O_3 \cdot PbO)$;
$1 - x = 0$; $2 - x = 0.25$; $3 - x = 0.35$; $4 - x = 0.50$;
Dimensions of samples:
$1 - L_{l_1} = 0.373$ cm; $L_{l_2} = 0.636$ cm; $L_{l_3} = 0.752$ cm;
$2 - L_{l_1} = 0.240$ cm; $L_{l_2} = 0.545$ cm; $L_{l_3} = 0.663$ cm;
$3 - L_{l_1} = 0.393$ cm; $L_{l_2} = 0.403$ cm; $L_{l_3} = 0.700$ cm;
$4 - L_{l_1} = 0.406$ cm; $L_{l_2} = 0.408$ cm; $L_{l_3} = 0.611$ cm.

The curve K in fig. 2 is drawn on the basis of the data calculated from equation (8), by using the measured values of (K_{m1}, K_{m2}, K_{m3}). The measurements show that the smaller is the ratio $\frac{L_1}{S_1}$, the slighter is the difference between K and K_{m1}.

Fig. 5 shows the temperature dependence of the thermal resistance $W_{c,0}$ per surface unity of the contact between the sample P and the blocks B_1 and B_2, respectively. The values of $W_{c,0}$ are calculated from equation (9a) or (9b) stated in [1]. The curves in this figure refer to the four samples studied. It should be mentioned that vacuum grease was used to improve the contacts.
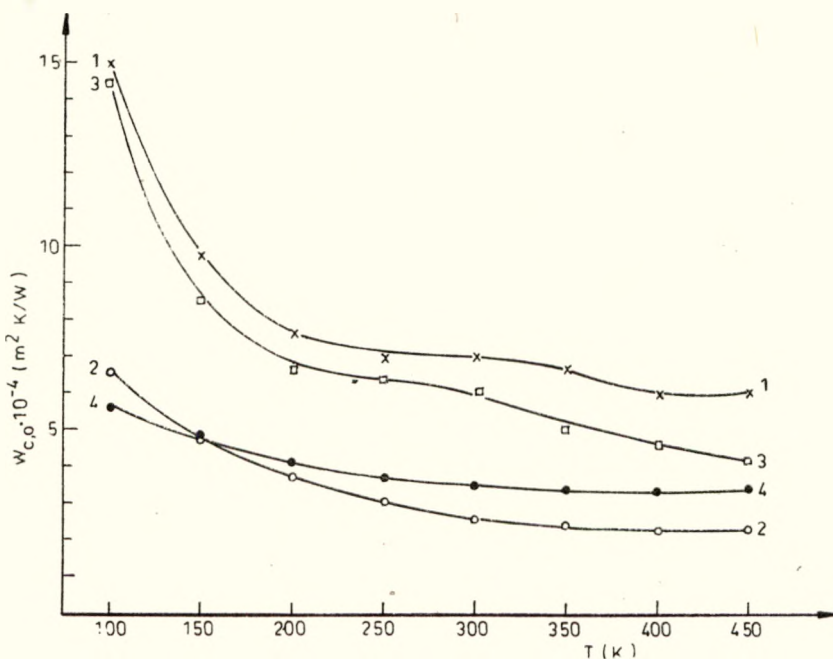
F i g. 5 *Variation of the thermal resistance per surface unity ˌversus temperature for the four samples studied.*

It is interesting to note that the thermal resistance $W_{c,0}$, and its dependence on temperature are different for different samples. Consequently, the thermal resistance also depends, to a certain extent, on the nature and dimensions of the bodies which are in contact.

REFERENCES

1. F. K e l e m e n, Studia Univ. Babeş-Bolyai, Phys., 2, 56 (1978).
2. M. A. M i h e j e v, *A hőátadás gyakorlati számításának alapjai* (translated from Russian), Tankönyvkiadó, Budapest, 1963, p. 68.

MĂSURAREA CONDUCTIBILITĂŢII TERMICE A IZOLATOARELOR TERMICE PRINTR-O METODĂ NESTAŢIONARĂ

(R e z u m a t)

În lucrarea prezentă se discută aplicarea metodei nestaţionare, descrisă într-o lucrare anterioară [1], la măsurarea conductibilităţii termice a izolatoarelor termice. Se stabilesc erorile sistematice şi se arată că ele pot fi luate în consideraţie dacă se fac măsurători cel puţin la două poziţii diferite ale probelor de formă paralelipipedică dreptunghiulară. Coeficientul de conductibilitate termică măsurat este cu atît mai apropiat de cel real, cu cît este mai mică lungimea probei faţă de secţiunea ei transversală. Se determină şi rezistenţa termică a contactelor între proba şi blocurile de cupru între care este montată proba.

COMPORTAREA MAGNETICĂ A UNOR STICLE DIN SISTEMUL
xFe$_2$O$_3$ · (1−x)[0,95TeO$_2$ · 0,05PbO]

I. ARDELEAN, GH. ILONCA, M. PETEANU şi I. LUCA

Introducere. Studiile privind obţinerea ordonării magnetice în materialele vitroase omogene cu ioni ai metalelor de tranziţie au stîrnit interes odată cu elaborarea teoriei lui G u b a n o v [1]. S i m p s o n [2], G o b e şi H a n d r i c h [3] şi H a s e g a w a [4] au dezvoltat această teorie folosind metodele cunoscute pentru materialele cristaline. S-a demonstrat că în sticlele diluate dependenţa de temperatură a susceptibilităţii magnetice urmează legea Curie, iar în cazul celor cu concentraţie mai mare de ioni ai metalelor de tranziţie, legea Curie-Weiss, cu temperatura Curie paramagnetică

$$\theta_p = \frac{\mu_0}{k} |\bar{\gamma}| \cdot \bar{Z},$$

unde μ_0 — moment magnetic dipolar, k — constanta lui Boltzmann, $|\bar{\gamma}|$ — reprezintă coeficientul cîmpului efectiv mediu al perechii şi Z — numărul mediu al vecinilor care interacţionează cu un ion oarecare.

O serie de lucrări experimentale au demonstrat existenţa unei ordini antiferomagnetice în sticle oxidice omogene cu ioni de fier [5, 6]. Explicaţia acesteia se bazează pe apariţia interacţiunii de superschimb între ionii Fe^{3+}, între ionii Fe^{2+} şi respectiv între ionii Fe^{3+} şi Fe^{2+}.

În lucrarea de faţă ne-am propus să efectuăm un studiu al proprietăţilor magnetice la sticlele din sistemul TeO$_2$—PbO cu ioni de fier.

Tehnica experimentală. S-a ales matricea din sistemul TeO$_2$—PbO care formează sticle într-un larg domeniu de concentraţie [7]. În matricea de compoziţie 95% mol TeO$_2$—5% mol PbO s-a introdus Fe$_2$O$_3$ în proporţie de la 1 la 20% mol.

Probele au fost preparate prin topirea concomitentă a TeO$_2$, PbO şi Fe$_2$O$_3$ de puritate p.a. în creuzete de sintercorund la 1 000 °C timp de o oră şi răcite la temperatura camerei prin turnarea pe o placă de oţel inoxidabil.

Măsurătorile magnetice au fost efectuate între 80 K şi 300 K folosindu-se o balanţă de tip Faraday.

Rezultate şi discuţii. Variaţia inversului susceptibilităţii magnetice cu temperatura este reprezentată în fig. 1.

În tot domeniul de concentraţii susceptibilitatea sticlelor studiate satisface legea Curie-Weiss, cu temperatura Curie paramagnetică negativă. Dependenţa de concentraţie a temperaturii Curie paramagnetice θ este reprezentată în fig. 2.
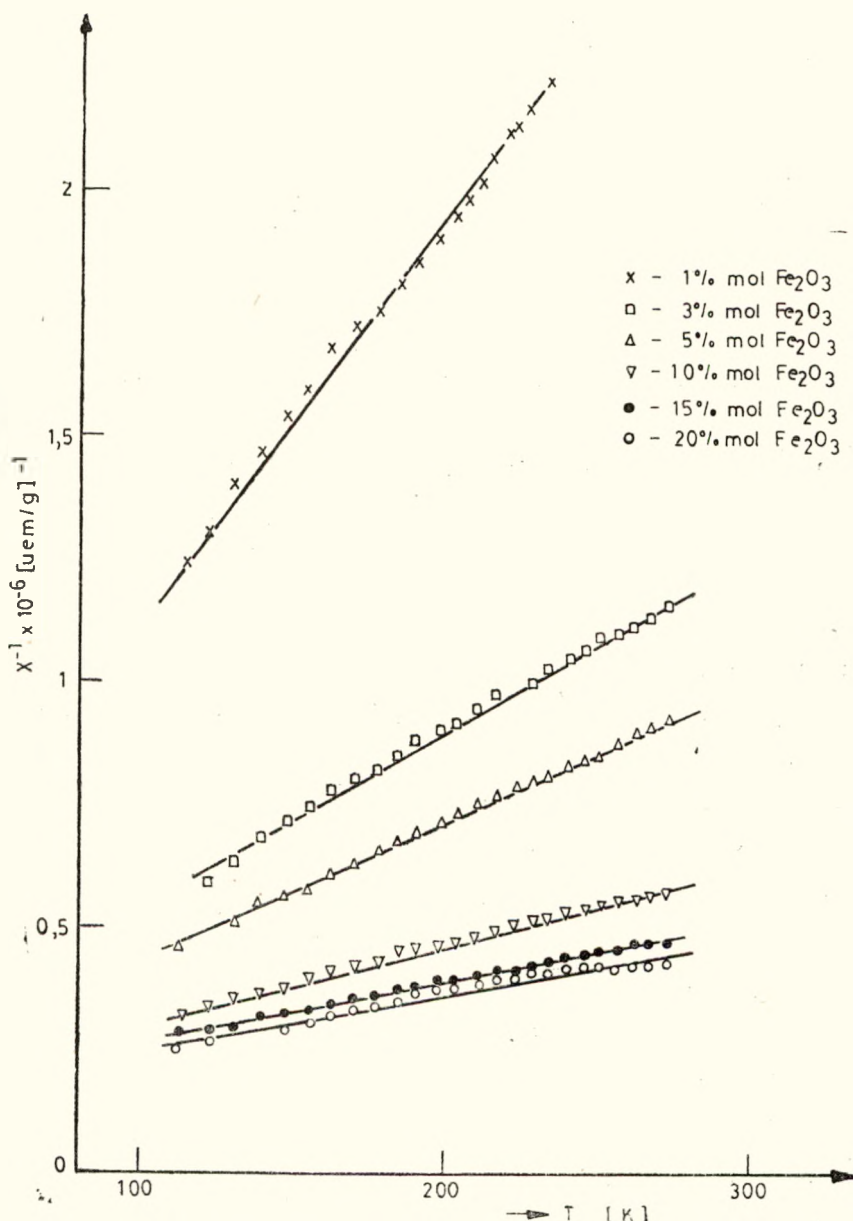
Fig. 1. Dependența inversului susceptibilității magnetice funcție de temperatură.
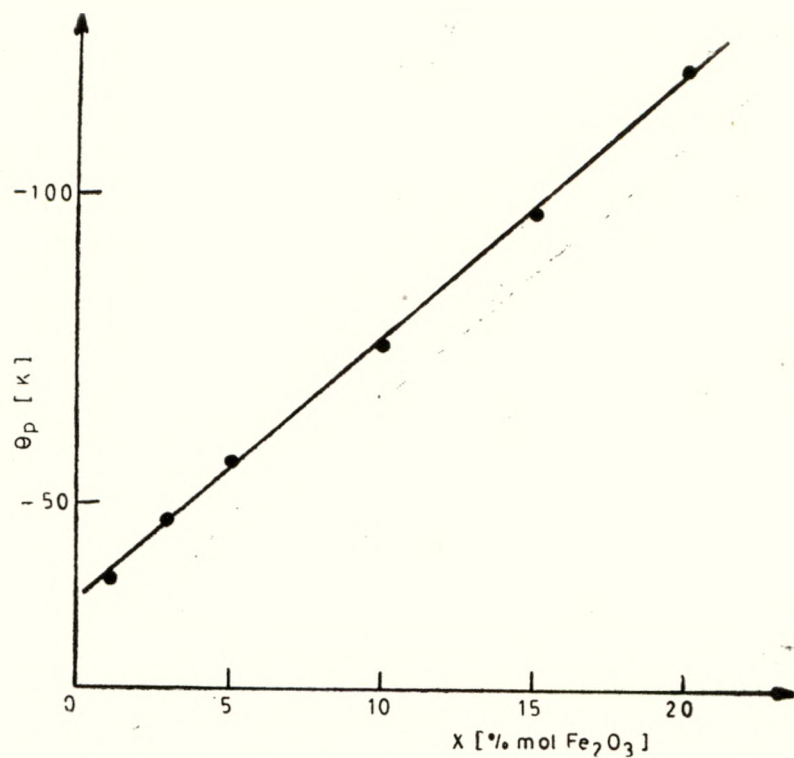
Fig. 2. Dependența temperaturii Curie paramagnetice de conținutul de Fe_2O_3.
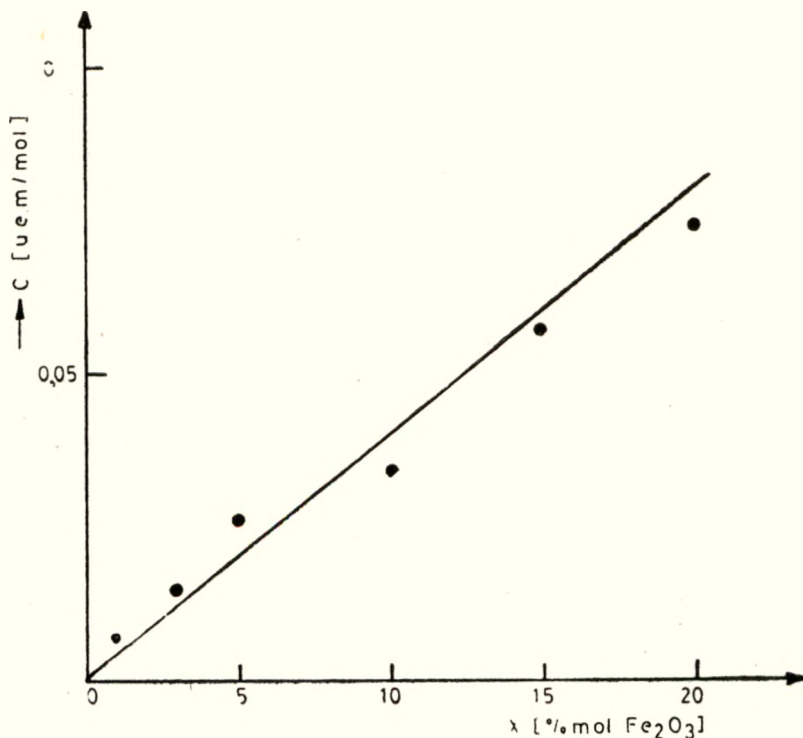
Fig. 3. Dependența constantei Curie de conținutul de Fe_2O_3.

Se constată că valoarea lui θ_p scade liniar cu creşterea concentraţiei de Fe_2O_3. Aceste rezultate sugerează prezenţa unei ordini magnetice la temperaturi mai joase de 80 K. Temperatura de tranziţie magnetică se găseşte la temperaturi foarte joase, întrucît în domeniul de temperatură studiat dependenţa inversului susceptibilităţii de temperatură este o linie dreaptă.

Pentru determinarea corectă a constantelor Curie, C, am făcut corecţii la susceptibilitatea magnetică pentru contribuţiile diamagnetice ale elementelor componente. Rezultatele obţinute pentru C funcţie de compoziţie sînt redate în fig. 3.

Se observă o dependenţă liniară a constantelor Curie funcţie de conţinutul de Fe_2O_3. Dependenţa pentru constantele Curie obţinute din măsurătorile de susceptibilitate magnetică se plasează între cele două extreme, cînd s-ar considera că toţi ionii de fier sînt fie Fe^{3+}, fie Fe^{2+}. Avînd în vedere faptul că nu se cunoaşte exact raportul numărului de ioni Fe^{3+}/Fe^{2+} în aceste sticle, este greu de stabilit contribuţia efectivă a acestor ioni la constantele Curie. Prezenţa acestor ioni este însă responsabilă pentru comportarea magnetică a sticlelor studiate.

Aceste rezultate arată că sticlele studiate sînt paramagnetice în domeniul de temperatură studiat. Prezenţa unei ordini magnetice la temperaturi joase trebuie, însă, să aibă un caracter local, caracteristic structurii sticlelor.

Concluzii. Inversul susceptibilităţii magnetice funcţie de temperatură pentru sticlele din sistemul $xFe_2O_3 \cdot (1-x)[0,95TeO_2 \cdot 0,05PbO]$ variază conform legii Curie-Weiss. Temperatura Curie paramagnetică θ şi constanta Curie, C variază liniar cu conţinutul de Fe_2O_3.

BIBLIOGRAFIE

1. A. I. Gubanov, Fiz. Tverd. Tela, **2**, 502 (1960).
2. A. W. Simpson, Phys. Stat. Solidi, **40**, 207 (1970).
3. S. Kobe and K. Handrich, Phys. Stat. Solidi, **42**, K 69 (1970).
4. R. Hasegawa, Phys. Stat. Solidi, b **44**, 613 (1971).
5. E. J. Friebele, L. K. Wilson, A. W. Dozier and D. L. Kinser, Phys. Stat. Solidi, b **45**, 323 (1971).
6. O. Horie, Y. Syono, Y. Nakagawa, A. Ito, K. Okamura and S. Yajiwa, Solid State Comm., **25**, 423 (1978).
7. H. Rawson, *Inorganic Glass — formig System*, Londra—New York, Academic Press, 1967, p. 11—223.

MAGNETIC BEHAVIOUR OF $xFe_2O_3 \cdot (1-x)[0,95TeO_2 \cdot 0,05PbO]$ GLASSES

(S u m m a r y)

Magnetic susceptibility measurements of $xFe_2O_3 \cdot (1-x)$ $[0,95TeO_2 \cdot 0,05PbO]$ glasses with x varying from 1 to 20 mol% revealed that the Curie-Weiss law holds above the magneticordering temperature, giving negative paramagnetic Curie temperature. Curie constants and paramagnetic Curie temperature vary linearly with Fe_2O_3 contents.

DISPERSING ACTION OF ULTRASOUND UPON SOME SUSPENSIONS OF DYES

AURELIA CIUPE, D. AUSLÄNDER

Introduction. The mechanism of ultrasonic dispersion [1, 2, 3] having at its origin the essential contribution of cavitation was studied, in the case of ZnO in water system.

The samples were prepared by 10 minutes ultrasonic irradiation at 25 °C temperature, under different conditions regarding the frequency and intensity of the ultrasonic field ; as a control a suspension dispersed with a magnetic stirrer was used, under the same conditions of time, concentration and temperature.

In order to determine the size distribution of solid particles in suspension, the gravitational cumulative technique was used :

$$r = \frac{9}{2} \left[\frac{\eta H}{t(\rho_1 - \rho_2)g} \right]^{1/2} \tag{1}$$

where : r — radius of the particle settled in t time,

H — distance covered by the particle in the liquid,

ρ_1, ρ_2 — density of solid and respectively liquid substance,

η — viscosity of the liquid,

g — acceleration of gravity.

The mass of the substance settled in t time at H distance below the level of the fluid is given by [4] :

$$W = \int_{r_1}^{r_{max}} f(r)dr + \int_{r_{min}}^{r_1} \frac{vt}{H} f(r)dr \tag{2}$$

where : r_1 — radius of the particle corresponding to the t sedimentation time,

$f(r)$ — occurence frequency of the particles of r_1 radius,

r_{min} and r_{max} — minimum and respectively maximum radius of particles,

v — velocity for a particle with : $r < r_1$.

The mass of sediment was measured with a torsion balance adapted for that purpose. Based on the obtained data, the integral and differential distributions for both the control and irradiated suspensions were calculated.

Experimental results. The differential distribution data are represented in fig. 1 where curve 1 correponds to the control and 2, 3 and 4 concern the samples irradiated at 1 MHz and at intensities of 2.16 W/cm², 2.68 W/cm² and 3.42 W/cm², respectively, $\Delta w/\Delta r = f(r)$ being the occurence frequency in weight percentage of the particles having sizes between an interval of $\Delta r = 1\mu$. While the control displays a heteropolar distribution, the principal maximum being placed in the field of $0-1\mu$ and the secondary one at $12-13\mu$, after the ultrasonic irradiation the suspensions tend to become homogeneous, being characterized by one maximum only, placed between 0 and 1μ. The increase
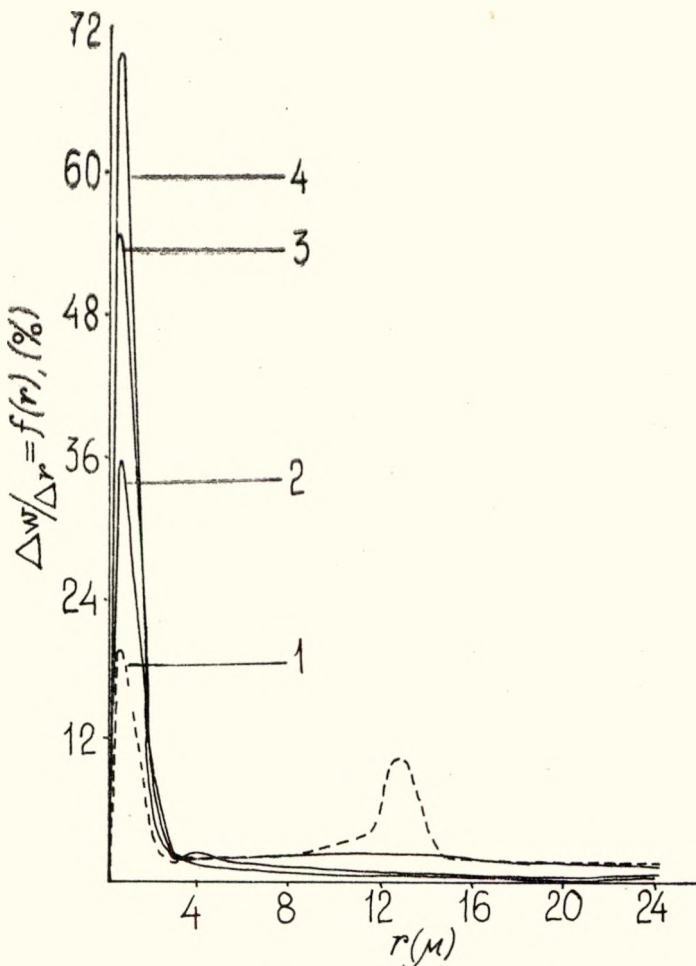
Fig. 1. Differential distribution of ZnO — water suspensions at different intensities of the 1 MH ultrasonic field.

of ultrasonic field intensity shifts the value of distribution maximum in the same direction, without altering its location. Thus, the increase of maximum value from 35% to 70% corresponds to the intensity variation from 2.16 W/cm² to 3.42 W/cm², simultaneously observing the decrease of bigger particles weight.

The change of dispersion degree depending on frequency is shown in fig. 2. Curve 1 represents the control, curves 2 and 3 are the differential distributions of the suspensions obtained at 1 MHz and 2.16 W/cm² and 2.68 W/cm² intensities respectively, curve 4 corresponds to the frequency of 0.5 MHz and I = 2.15 W/cm², and curve 5 to the frequency of 20 KHz and I = 1.17 W/cm².
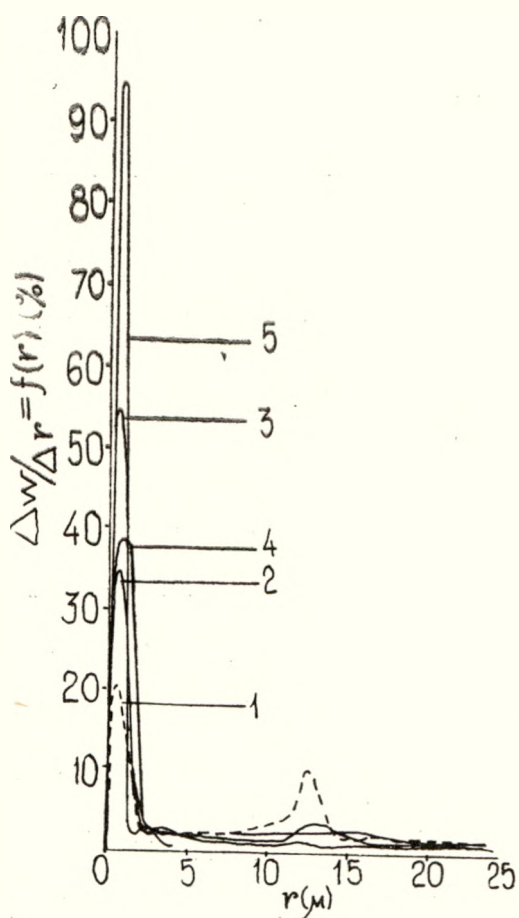
F i g. 2. Differential distribution of ZnO — water suspensions at different frequencies.

It is found that at all the mentioned frequencies the suspension becomes homogeneous, loosing its initial heteropolar character ; in this direction one can observe the stronger action of the 20 KHz ultrasonic field.

The suspension exposed to 20 KHz ultrasound is characterized by a marked dispersion, over 90% of the solid particles having the radius between 0 and 1μ ; practically, the particles bigger than 5μ do no more exist. In the field of MHz the homogenizing action of ultrasounds is apparently more advanced at the frequency of f=1 MHz and I=2.68 W/cm² than at f = 0.5 MHz and I = 2.15 W/cm². At this latter frequency the secondary maximum of the 12—13μ range still persists, but it is more attenuated (3.3%) than in the control (10.5%), and the principal maximum is wider (0—2μ) than in the suspensions obtained at 1 MHz (0—1μ). The dispersing action upon the particles bigger than 18μ is more marked at 0.5 MHz frequency than at 1 MHz.

Discussions. In a suspension submitted to the action of an ultrasonic field of high intensity a series of phenomena take place, some of them having a dispersing character, others an agglomeration effect.

At the basis of the dispersion process there if a mechanism of a cavitational nature. In their motion in ultrasonic field the small solid particles have an insufficient potential energy to overcome the potential barrier in the vicinity of cavity wall, remaining to oscillate at some distance from it [5]. The big particles, with a high potential energy, can overcome the above-mentioned rejection and they will reach the cavity surface. The shock wave produced at the cavitation implosion has a very strong destroying effect upon the big particles, but it does not affect the small ones.

In this way, in the ultrasonic field opposite phenomena can simultaneously take place : dispersion and agglomeration ones. During the ultrasonic irradiation the suspension evolves towards a more uniform distribution, the ultrasounds intensity not influencing the final preferential dimension to which the particles are reduced, but only the dispersion velocity. The results shown in the figures 1 and 2 agree with these conclusions.

On the other hand, the intensity of the process of cavitation, for which a theoretical criterium was defined [6] according to the relation:

$$\chi = \frac{R_{max}^3}{R_{min}^3 \cdot \Delta t \cdot f} \tag{3}$$

depends on the experimental conditions and the characteristic parameters of the liquid, the increase succession of their influence upon χ being:

$$\sigma, \quad R_0, \quad \rho, \quad P_A, \quad f, \quad \eta, \quad p_v, \quad P_0 \tag{4}$$

where: R_{max} = maximum radius reached by cavity during the growing pro-
cess,
R_{min} = minimum radius of cavity at compression,
Δt = duration of implosion,
f = frequency of ultrasound,
σ = surface tension of the liquid,
P = amplitude of sound pressure,
η = dynamical viscosity,
p = pressure of saturated vapours of the liquid,
P_0 = statical pressure.

Thus, the differentiation of the experimental results upon the frequency demonstrate the preponderant role played by intensity, in the case of the relatively close, frequencies 0.5 MHz and 1 MHz respectively, while for the much different frequencies of 20 KHz the determining factor in the dispersion phenomenon through the process of cavitation becomes the frequency.

The agglomeration of the particles in the ultrasonic field probably proceeds from the collision effects resulting from the superposition of several actions, like: hydrodynamical flows with different velocities depending on the dimensions, shiftings in the currents occured under the action of the shock waves produced at the cavitational implosion of bubbles — and which have different directions, disturb the relatively regular motion of the particles due to the previous mechanism, — the participation to the oscillatory motion of the liquid, the brownian motion, etc.

The participation of the disperse phase particles to the oscillatory motion of the fluid is described by the relations:

$$\frac{x_p}{x_1} = \frac{1}{\left[\left(\frac{4\pi\rho \ r^2 f^2}{9\eta} \right)^2 + 1 \right]^{1/2}} \tag{5}$$

where: x_p — amplitude of solid particle motion,
x_1 — amplitude of fluid particle motion.
For a given suspension this relationship depends on $1/r^2 f$; at constant ultrasonic intensity and frequency, the solid particle amplitude becomes a function of $1/r^2$ only, which shows a higher probability of collision for the smaller particles.

In this way, in an ultrasonic field the superposition of the dispersion and respectively agglomeration effects finally leads to a critical dimension of

particles, according to the dynamical equilibrium between the two opposite effects, also characterized by a distribution with a monodisperse tendency, in agreement with the experimental data.

REFERENCES

1. M. Y a K a ţ, Akust. Jurn., **1**, 47 (1961).
2. F. A. B r o n i n, *Issledovanie cavitationnogo razruşenija i dispergirovanija tverdîh tel v ul'trazvukovom pole vîsokoi intensivnosti*, Avtoreferat disertaţia, Moskva, 1967.
3. A. P i o t r o v s k a, H. G o r s k a, I. Z i e n i u c, Proc. of 2-nd Conf. on Ultrasonic Technology, P.W.N., Warsawa, 1957.
4. R. R. I r a n i, C. F. C a l l i s, *Particle size measurement interpretation and application*, John Wiley & Sons. Inc., New York, London, 1963.
5. V. M. F r i d m a n, Ultrasonics, July, 162 (1972).
6. B. A. A g r a n a t, V. I. B a s k i r o v, Dokl Akad. Nauk SSSR, 179, 821 (1968).

ACŢIUNEA DISPERSANTĂ A ULTRASUNETULUI ASUPRA UNOR SUSPENSII DE COLORANŢI

(R e z u m a t)

Lucrarea prezintă rezultatele cu privire la efectul dispersant al cîmpurilor ultrasonice cavitaţionale asupra suspensiei de ZnO în apă. Fenomenul este urmărit în funcţie de intensitatea şi frecvenţa cîmpului aplicat. Distribuţia de dimensiuni a sistemului dispers este determinată experimental printr-o tehnică gravitaţională de sedimentare.

NOTE

ON THE Yb CONTENT DETERMINATION IN Cr—Yb ALLOYS BY THERMAL NEUTRON ACTIVATION

V. ZNAMIROVSCHI, L. DĂRĂBAN and T. FIAT

It is well-known that neutron bombardment of a given element can lead, by means of a nuclear reaction, to the establishment of a gamma radioactivity specific for the isotope which is formed.

Measuring this induced radioactivity by gamma spectrometry method it is possible to determine, qualitatively and quantitatively, the elements [1—3]. The activation analysis is the most sensible means from the non-destructive analysis methods. It is particularly suited for rare-earth elements [4].

At the present time there are few works [5—6] devoted to the analysis of Yb content. In this work we have studied a range of Cr-Yb alloys which have been previously used in magnetical studies [7].

The samples have been irradiated is VVR—S reactor of the Atomic Institute of Bucharest, for 43 hours, with an average flux of thermal neutrons of 4.10^9n/s.cm^2.

From the nuclear reactions produced in this experiment we get : $^{50}\text{Cr}(n,\gamma)$ $^{51}\text{Cr}(T_{1/2} = 27.8$ day, $\sigma_{act} = 15 \cdot 5 \pm 1. \cdot 6$ barns), $^{168}\text{Yb}(n,\gamma)$ $^{169}\text{Yb}_{1/2}(T_{1/2} = 31$ day, $\sigma_{act} = 11000 \pm 3000$ barns but isotope abundance is only 0.14%) and $^{174}\text{Yb}(n,\gamma)$ $^{175}\text{Yb}(T_{1/2} = 4.2$ day, $\sigma_{act} = 60 \pm 40$ barns, the isotope abundance being 31.84%). Because of the great activity of ^{51}Cr in alloys the Yb activity has not been measured immediately after neutron irradiation.

The alloys have been analysed by means of gamma spectrometry after a ,,cooling'' period of one week. Considering that the Yb activity is lower than of ^{51}Cr, we have determined the Cr content as compared the activity with a standard sample. The analysis has been performed with a multi-channel analyser KFKI-Budapest having 4096 channels, equipped with a NaI (T1) scintillation sonde.

The energy scale has been previously gauged with $32.1 \pm 0,1$ keV and $661.635 \pm 0,076$ keV lines of standard ^{137}Cs source (Fig. 1).

Then the 320 keV line ^{51}Cr has been identified and used for analysis.

In fig. 2 the standard sample (100% Cr) and alloy (Cr—Yb) spectra for 2048 chanels, are shown accumulated in the same period.

As the peak area (P) is proportional to the quantity of element (m) the following relation between standard sample (s) and alloy (a) has been applied :

$$\frac{m_s}{m_a} = \frac{P_s}{P_a} \qquad (1)$$

Using relation (1) the Cr quantity in the measured sample has been determined.
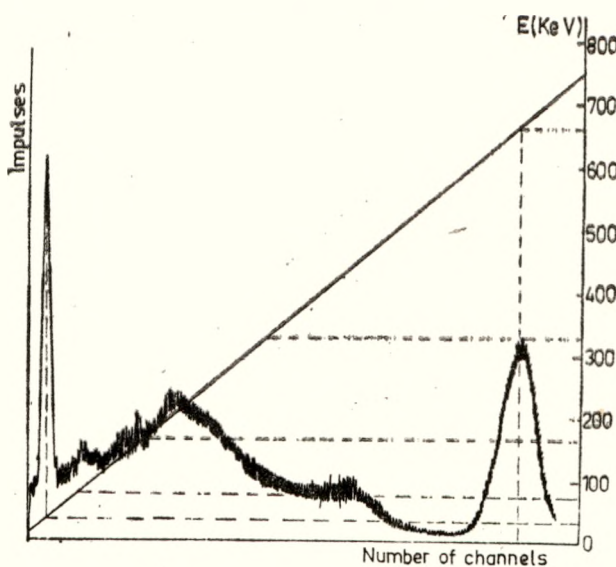
F i g . 1. Standard line of gamma spectrum.
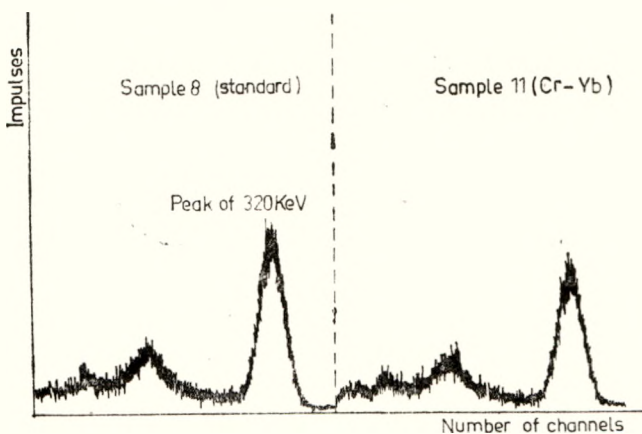
F i g . 2. Gamma spectrum of Cr standard sample and
Cr — Yb alloy.

For the same purpose another method, in which the peak area measurement is not necessary, has been used. The analyser was monitored so as to stop when 10^{12} impulses have been tracked and thus the standard alloy sample spectrum has been registered. The stocking time (t) was also measured. We have

observed that two peaks have perfectly matched one another and so we conclude that the peaks area is identical. In this case the following relation has been used :

$$\frac{m_s}{m_a} = \frac{t_a}{t_s} \tag{2}$$

and we have obtained the same results. Thus using the Cr content determination we have computed the Yb contents in binary alloys.

REFERENCES

1. T. Născuțiu, C. Pencea, Rev. Roum. Chim., **13**, 1359 (1968).
2. V. P. Guin, *Modern Trends. in Activation Analysis*, vol. I, 93, 1969.
3. L. C. Bate, S. E. Lindberg, A. W. Andrew, J. Rad. Chem., **32**, 125 (1976).
4. L. B. Garmann et al., Chem. Geol., **15**, 103 (1975).
5. G. M. Kolesov, J. Rad. Chem., **30**, 553 (1976).
6. L. A. Haskin et al., Geochim., Cosmochim., Acta, Supl. 1, 343 (1970).
7. I. Pop et al. (to be published).

ASUPRA DETERMINĂRII CONȚINUTULUI DE Yb ÎN ALIAJELE Cr—Yb PRIN ACTIVARE CU NEUTRONI TERMICI

(R e z u m a t)

În notă sînt prezentate două metode complementare de identificare a cromului prin activare cu neutroni în vederea dozării yterbiului în aliajele binare Cr—Yb.

THE INFLUENCE OF MANGANESE AND GADOLINIUM IONS ON THE STRUCTURE OF SOME BORATE GLASSES

S. SIMON, V. SIMON, AL. NICULA

Taking into account that a great number of physical properties of borate glasses are determined by the ratio between the four-coordinated and three-coordinated boron atoms, we have examined the manner in which different paramagnetic ions influence this ratio. In this way it was observed the effect of increasing concentration of paramagnetic ions on the shape of ^{11}B—NMR spectra in several borate glasses.

The use of ^{11}B—NMR spectra in order to obtain information about the boron atoms coordination in different matrices was described in detail especially by Taylor, Bray et al [1—4] which used computer techniques to interpret the ^{11}B—NMR spectra.
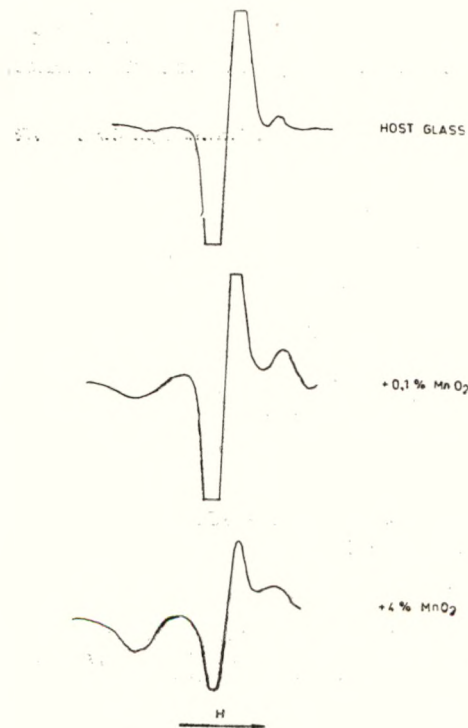

F i g. 1. The effect of MnO_2 concentration on the ^{11}B-NMR spectra for the $59\% B_2O_3 - 10\% Li_2O - 23,5\% Bi_2O_3 - 2,5\% SiO_2 - 5\% As_2O_3$ glass.
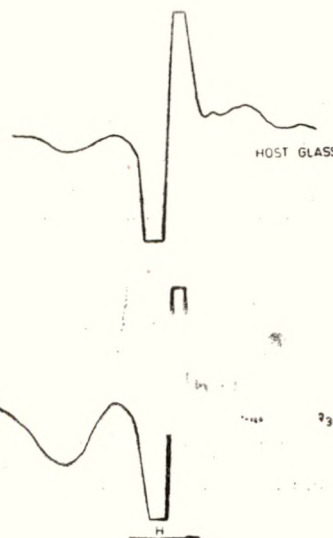
F i g. 2. The effect of Gd_2O_3 content on the ^{11}B-NMR spectra for the $80\% B_2O_3 - 15\% Li_2O - 5\% SiO_2$ glass.

Our spectra are recorded on a JEOL NMR-Spectrometer, at 9,212 MHz, on powder samples, at room temperature.

As it can be seen in fig. 1, the increase of MnO_2 concentration in $59\% B_2O_3$ $-10\% Li_2O - 23,5\% Bi_2O_3 - 2,5\% SiO_2 - 5\% As_2O_3$ glass determines a significant increase of three-coordinated boron atoms, while the number of four-coordinated boron atoms decreases. A similar effect, but more pronounced, is observed (fig. 2) in the case of spectra recorded on $80\% B_2O_3 - 15\% Li_2O - - 5\% SiO_2$ glasses impurified with Gd_2O_3. More non-equivalent sites were evidenced for the three-coordinated boron atoms, characterized by different quadrupol interactions.

These results correlated with those obtained from the analysis of EPR spectra for the same paramagnetic ions [5—6], permit to consider that in these glasses, wherein more than one phase was proved, the paramagnetic ions are arranged in the phase-separation regions, and determine a size diminuation of the phase in which the boron atoms are preponderantly four-coordinated, a fact illustrated by the results obtained from the electronic microscopies as well.

Therefore one can conclude that the paramagnetic ions generally used to obtain glasses with certain colours or other special properties, have a considerable influence not only on their immediate vicinity, but also on the glassy matrix structure, which determines changes in the physical and mechanical properties of the respective glasses.

REFERENCES

1. P. C. T a y l o r, P. Y. B r a y, J. Magn. Resonance, **2**, 305 (1970).
2. P. C. T a y l o r, P. J. B r a y, Amer. Ceram. Soc. Bull. **51**, 3, 234 (1972).
3. P. C. T a y l o r, E. J. F r i e b e l e, J. of Non-Cryst. Solid, **16**, 375 (1974).
4. P. C. T a y l o r, J. F. B a u g h e r, H. M. K r i z, Chem. Rev., **75**, 2, 203 (1975).
5. S. S i m o n, F. T o l e a, I. D u c a, Al. N i c u l a, Studia Univ. Babeş-Bolyai, Phys., **1**, 37 (1979).
6. A. N i c u l a, M. P e t e a n u, Studia Univ. Babeş-Bolyai, Phys., 42 (1976).

INFLUENŢA IONILOR DE MANGAN ŞI GADOLINIU ASUPRA STRUCTURII UNOR STICLE BORICE

(R e z u m a t)

În această notă sînt prezentate calitativ efectele ionilor paramagnetici asupra structurii matricei unor sticle pe bază de bor, rezultate din spectrele RMN ale nucleului ^{11}B. Concluziile desprinse sînt corelate cu cele rezultate din analiza spectrelor RES ale ionilor paramagnetici respectivi.

STUDIUL OPTIC AL MONOCRISTALELOR DE
LiNbO$_3$, Bi$_{12}$GeO$_{20}$ şi AgGaS$_2$

I. MILEA, GH. ILONCA, L. GILĂU, W. MIESKES, D. STĂNILĂ

Cristalele studiate au fost obţinute prin metodele clasice de creştere [1], [2], [3].

Spectrele de absorbţie la temperatura camerei au fost efectuate cu un spectrofotometru U.V. Vis produs de firma Karl Zeiss din Jena, iar spectrele la temperatura de 80 K au fost efectuate cu instalaţia descrisă în [4], cuplată cu un monocromator, un fotomultiplicator şi un înregistrator. Spectrele de reflexie s-au făcut cu un spectrofotometru VSU—2P producţie Zeiss Jena.

S-a determinat lărgimea zonelor interzise ale acestor cristale. Rezultatele obţinute din spectrele de absorbţie înfăţişate în fig. 1 sînt prezentate în tabelul 1.

Se observă că pentru cristalul de AgGaS$_2$ absorbţia este bruscă, deci se presupune că în apropierea nivelului de energie corespunzător bandei de conducţie nu există nivele cu probabilitate de tranziţie mai mică.

Tabel 1
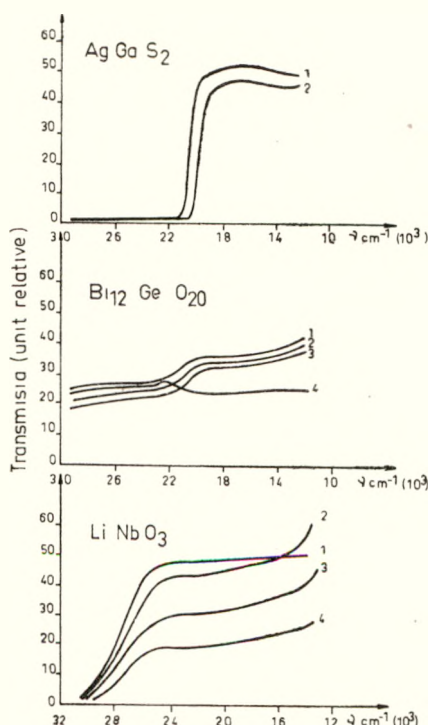
F i g. 1.

Cristalul	Nr. pe grafic	λ(nm.)	E(ev)	Timp de iradiere (minute)	Temperat. (K)
LiNbO$_3$	1	335,5	3,75	0	293
	2	335,5	3,75	30	293
	3	336,1	3,74	60	293
	4	338,9	3,71	120	293
Bi$_{12}$GeO$_{20}$	1	312,5	4,03	0	293
	2	312,5	4,03	30	293
	3	370,3	3,40	60	293
	4	inversare benzi		120	293
AgGeS$_2$	1	476,0	2,64	0	293
	2	383,0	2,61	0	80

Iradierea cu raze γ nu duce la o schimbare a spectrului cristalului de AgGaS$_2$, în schimb pentru cristalul de LiNbO$_3$ odată cu creşterea timpului de iradiere valoarea zonei interzise se micşorează, iar de la un timp de peste 120 minute valoarea ei rămîne constantă. Pentru cristalul de Bi$_{12}$GeO$_{20}$, odată cu creşterea timpului de iradiere pe lîngă micşorarea zonei interzise, la o iradiere de peste 120 minute se pare că are loc o suprapu-

nere a benzilor de conducție și valență, fapt care urmează să fie confirmat prin măsurători de conductibilitate. Culoarea cristalelor de $Bi_{12}GeO_{20}$ și $AgGaS_2$ nu s-a schimbat la iradiere, în schimb cristalul de $LiNbO_3$ s-a colorat în roșu maroniu, colorație care se manifestă prin apariția a două benzi de absorbție la 488 și 757 nm.

Rezultatele obținute au fost verificate și prin spectrele de reflexie difuză. Coincidența lor cu cele de absorbție confirmă faptul că, pentru substanțe solide fără o absorbție optică intensă, culoarea reflectată de pulberea acestei substanțe reprezintă de obicei culoarea luminii transmise prin cristal [5], [6].

Studiul dependenței zonei interzise cu temperatura la cristalul de $AgGaS_2$ arată o creștere a valorii acesteia de la 2,61 eV la 2,68 eV, cînd temperatura scade de la 293 K la 80 K (fig. 1, grafic 2).

(Intrat în redacție la 30 septembrie 1978)

BIBLIOGRAFIE

1. O. R a d u, Studii și cercetări chimice, **19,** 1199 (1971).
2. A. A. B e l l m a n, J. Cryst. Growth, **1,** 37 (1967).
3. A. K e m i n o v, V. T u r n e r, Appl. Optics, **5,** 1612 (1966).
4. I. M i l e a, W. M i e s k e s, Studia Univ. Babeș-Bolyai, Phys., 2, 20 (1977).
5. S. P. T a n d o m and N. G u p t a, Phys. Stat. Sol., **38,** 363 (1970).
6. P. D. F o c h s, Proc. Phys. Soc., **B 69,** 76 (1956).

OPTICAL STUDY OF $LiNbO_3$, $Bi_{12}GeO_{20}$ AND
$AgGaS_2$ MONOCRYSTALS

(S u m m a r y)

The values of the forbidden bands for $LiNbO_3$, $BiGeO_{20}$ and $AgGaS_2$ crystals have been measured at the temperature of 77K and 293K. These values have changed very much after the crystals were irradiated with γ rays.

În cel de al XXIV-lea an (1979) *Studia Universitatis Babeş-Bolyai* apare semestrial în specialităţile :

matematică

fizică

chimie

geologie-geografie

biologie

filozofie

ştiinţe economice

ştiinţe juridice

istorie

filologie

На XXIV году издания (1979) *Studia Universitatis Babeş-Bolyai* выходит два раза в год со следующими специальностями :

математика

физика

химия

геология-география

биология

философия

экономические науки

юридические науки

история

филология

Dans sa XXIV-e année (1979) *Studia Universitatis Babeş-Bolyai* paraît semestriellement dans les spécialités :

mathématiques

physique

chimie

géologie-géographie

biologie

philosophie

sciences économiques

sciences juridiques

histoire

philologie

43 904

Lei 10